MOLECULAR ENGINEERING OF CATALYTIC NUCLEIC ACID PROBES FOR BIOANALYTICAL AND BIOMEDICAL APPLICATIONS

By

HUI WANG

A DISSERTATION PRESENTED TO THE GRADUATE SCHOOL
OF THE UNIVERSITY OF FLORIDA IN PARTIAL FULFILLMENT
OF THE REQUIREMENTS FOR THE DEGREE OF
DOCTOR OF PHILOSOPHY

UNIVERSITY OF FLORIDA

2011

To my family

ACKNOWLEDGMENTS

I am deeply indebted to a long list of people who made this dissertation possible. First, I wish to express my gratitude to my advisor, Dr. Weihong Tan. His advice, suggestions, and encouragement were greatly helpful for advancing and progressing projects and were the driving sources that kept me challenging to be a better scientist every day. In addition, I thank Dr. Gail Fanucci, Dr. Kenneth Merz, Dr. David Powell and Dr. Chen Liu on my graduate committee. The advice, assistance, and encouragement from my committee are highly appreciated.

This dissertation is a result of successful collaborations with scientists in different areas. I would like to thank Dr Youngmi Kim for guiding me when I started the very first research project. I greatly appreciate Dr. Kim for initiating the unimolecular nucleic acid sensor project and trained me the experimental skills. I appreciate Dr. Haipeng Liu and Liu Yang for the critical comments and help in development of unimolecular nucleic acid sensor project. I appreciate Dr. Yufen Huang for helping me with my rotation project while I was a first year graduate student. I am very thankful for Dr. Ling Meng's generous help on the catalytic nucleic acid sensor for telomerase activity monitoring project. I also would like to thank Suwussa Bamrungsap and Dr. Zhi Zhu for their special friendship.

The Tan research group is a special place to work. The help and friendship from former and current group members make my memory of Gainesville enjoyable and unforgettable. I would like to thank Dr. Ronghua Yang, Dr. Kwame Sefan, Dr. Zhiwen Tang, Dr Prabodhika Mallikaratchy, Dr. Carmen Maria Estevez , Dr. Xiaoling Zhang, Karen Martinez, Dr. Hui Chen, Dr. Parag Parekh, Dr. Yanrong Wu, Dr. Huaizhi Kang, Dr. Yan Chen, Dr. Xu Ye, Megan O'Donoghue, Dalia Lopez-Colon, Xiaolan Chen,

Dimitri Simaeys Van , Basri Gulbakan, Elizabeth Jimenez, Xiangling Xiong, Lu Peng, Tao Chen, Mingxu You, Da Han, Yunfei Zhang for their friendship, encouragement, and help.

I am deeply indebted to my parents for their unconditional love, support, guidance and strong spirit. I am grateful to my husband, Yue Yang for being a wonderful friend, helpful colleague, and supportive spouse who enable me to succeed. I thank my lovely daughter, Amelia Yang, for being such a great daughter and bringing every kind of joy to my life every moment.

TABLE OF CONTENTS

page

LIST OF TABLES

LIST OF FIGURES

Abstract of Dissertation Presented to the Graduate School
of the University of Florida in Partial Fulfillment of the
Requirements for the Degree of Doctor of Philosophy

MOLECULAR ENGINEERING OF CATALYTIC NUCLEIC ACID PROBES FOR BIOANALYTICAL AND BIOMEDICAL APPLICATIONS

By

Hui Wang

August 2011

Chair: Weihong Tan
Major: Chemistry

Over the past few decades, the role of nucleic acids including deoxyribonucleic acids and ribonucleic acids in purely biological systems has been defined, and these versatile compounds have also been integrated into nanoscience. The overall goal of this doctoral research is dedicated to engineering these biomolecular components with the objective of building novel molecular tools and devices for biological studies, biomedical research and therapeutic applications.

DNAzymes are ideal for metal sensor design, because most DNAzymes require metal ions as cofactors for their catalytic activities. A catalytic molecular beacon Pb^{2+} sensor based on a Pb^{2+} specific DNAzyme was designed previously. The sensor was highly sensitive and selective at 4 °C; while high background fluorescence was observed at room temperature. In this paper, we take advantage of DNA molecular engineering to improve the properties of DNAzymes by designing a unimolecular probe for lead ion (Pb^{2+})-catalyzed reaction, achieving in turn, the ability to monitor a single Pb^{2+} in solution by fluorescence microscopy.

The second phase of this research has involved the development of catalytic nucleic acid probe for telomerase activity monitoring, in which telomeric primer was linked to a DNAzyme which will be able to cleave telomeric elongation product, producing amplified signal that reporting telomerase overexpression. Since telomerase have been found highly expressed in cancer cells, this work is essential for early cancer diagnosis.

The third phase of this research has involved the molecular assembly of DNAzymes as micelle for cancer therapeutic application. To emphasize previous work on telomerase activity monitoring, the telomerase inhibition concept has been applied to engineer 10-23 DNAzyme with high affinity and specificity for a given telomerase RNA fragment. The process involves assembly covalent conjugation between a hydrophobic diacyllipid tail and DNAzyme micelle onto cell surface by cell membrane anchoring, followed by cell uptaking of lipid conjugated 10-23 DNAzyme complex, resulted in a silencing of telomerase hTERT RNA. After 96 hours, the cell viability assay shows an 80% cell death.

In summary, this research has focused on the design, synthesis and investigation of multifunctional and advanced nucleic acid probes, with the ultimate goal of increasing the understanding of biological processes and the development of advanced molecules for nucleic acid-based detection and therapy.

CHAPTER 1
INTRODUCTION

Review of Nucleic Acids

Nucleic Acid Structure

The molecular building blocks for DNA and RNA polymers are shown in Figures 1-1 and 1-2. The monomer units, called nucleotides, which contain a sugar (2-deoxyribose in DNA and ribose in RNA) are esterified to a phosphate. The sugar is also linked to a cyclic base via a β-N-glycosidic bond. The nucleotides are bonded by phosphate linkages between the 3′ and 5′ carbons on the sugar rings.

The chemistry of DNA has been studied since 1868. By the 1940s, it was known that DNA is made up of individual units called nucleotides that are linked to each other to form long chains. In 1950s, Rosalind Franklin, James Watson and Francis Crick using X-ray diffraction analysis of crystallized DNA discovered the double helix formation of DNA. (Figure 1-3).[1] In 1953, Watson and Crick proposed an ingenious double helix model for DNAs, in which complementary bases (C and G; A and T) on each strand are linked by hydrogen bonds (3 H-bonds for C-G; 2 H-bonds for A-T). The two polynucleotide chains of DNA align anti-parallel to each other in the coil, leading to a double helix structure. For DNA molecules with thousands or millions of base pairs, the designations are kilo base pairs and mega base pairs, respectively. For example, the DNA of human chromosome 1 is one double-stranded helix that has about 263 mega base pairs (Mb). This high molecular weight nucleic acid (109 Daltons or greater) is found primarily in the nuclei of complex cells, known as eukaryotic cells, or in the nucleotide regions of prokaryotic cells, such as bacteria.

Genetic information is encoded in the DNA polymers via successive groups of three nucleotides. Each 3-base code corresponds to a certain amino acid in the coded protein. To access this information the pattern is transcribed to RNA templates, a lower molecular weight, but much more abundant nucleic acids. Three kinds of RNAs have been identified. The largest subgroup (85 to 90%) is ribosomal RNAs (rRNAs), the major component of ribosomes, guiding the translation of mRNA into a protein. The sizes of rRNA molecules vary, but they are generally smaller than DNAs. The other forms of RNAs are messenger RNAs (mRNAs), which carry genetic information from the nucleus to the cytoplasm, and transfer RNAs (tRNAs), which bring amino acid corresponding to the 3-base code to ribosome during protein synthesis. Both mRNAs and tRNAs have transient lifetimes. Recently, regulatory RNAs, such as microRNAs and siRNAs, were newly discovered.

Chemical Synthesis of Nucleic Acid

After complete structures of nucleic acids were clearly elucidated, the phosphoramidite method was developed to synthesize artificial nucleic acids by an automated system. Thus, nucleic acids have become popular building blocks for designing molecular probes due not only to their capability for selective recognition against a wide range of targets but also automated DNA synthesis technology for highly efficient and reproducible synthesis with a variety of modifications for numerous applications in biological studies. The basis of the synthetic chemistry is solid-support synthesis of oligonucleotide via phosphoramidite chemistry. In nature, the formation of the phosphate linkages in DNA was catalyzed enzymatically in a reversible reaction:

$$dNTP + (dNMP)_n \leftrightarrow (dNMP)_{n+1} + pp_i$$

That is, a deoxynucleotide triphosphate was added to a growing deoxynucleotide monophosphate polymer by a polymerase in the presence of Mg^{2+} and the forward reaction resulted in the n+1 polymer and a pyrophosphate.

Phosphoramidites are composed of different functional groups (Figure 1-4). To eliminate side reactions during the synthesis of nucleic acids, appropriate protecting groups that are vulnerable to basic condition, such that they can be effectively removed by strong bases block primary amines of bases. 5'-O is capped by dimethoxytrityl (DMT) group to selectively activate 5'OH under strong acidic condition. The phosphate is also protected by diisopropylamino and 2-cyanoethyl groups for selective activation under appropriate condition. Any modifiers, such as fluorophore, biotin, amine, and polyethylene glycol linker, share the same strategy to design functional phosphoramidites.

The synthesis is carried out in a column containing a solid controlled-pore glass (CPG) support, where the 3'-hydroxyl of the first nucleotide or modified functional group is attached through a long spacer arm. This support allows excess reagents to be removed by washing and eliminates the need for tedious purification steps during the synthesis process. The synthesis requires four chemical reaction steps: 1) detritylation, 2) coupling, 3) capping and 4) oxidation (Figure 1-5). In the first step, detritylation is to remove the trityl protecting group on the 5′ oxygen to activate the 5' hydroxyl on the growing oligonucleotide attached to CPG, by adding strong acidic reagents, either 3% of dichloroacetic acid (DCA) or trichloroacetic acid (TCA) in dichloromethane (DCM) to the column. After deprotection and removal of excess acid with acetonitrile, coupling takes place (step 2) by adding a phosphoramidite derivative of the next nucleotide in the

presence of tetrazole, a weak acid. The tetrazole plays two important roles in conjugating the monomers. It protonates the nitrogen of the diisopropylamine group on the 3'- phosphorous of the incoming nucleotide to produce a tetrazolyl phosphoramidite, which is susceptible to nucleophilic attack by the activated 5’ hydroxyl group to form a phosphate linkage. After coupling, the column is washed to remove any extra tetrazole followed by the capping step. Since the coupling yield cannot reach 100%, there are always a small percentage of failure sequences, which must be capped to prevent further coupling and the need to remove DNAs having one or more sequences missing. Capping (step 3) is accomplished by adding acetic anhydride and N-methylimidazole in tetrahydrofuran to the reaction column. Only residual bare 5’-hydroxyl groups are acetylated, but not the DMT-protected 5’ hydroxyl groups. Capping is followed by oxidation (step 4), in which the less stable phosphate is oxidized to the stable pentavalent phosphate tri-ester using iodine as the oxidizing agent and water as the oxygen donor. After completion of these four steps, one nucleotide has been added to the chain, which is now ready for the next round of conjugation.

Following the complete synthesis, post-treatment cleaves the product from the solid support and deprotects the nitrogen bases by reaction with ammonium hydroxide at high temperature, normally above 50 °C. However, if fragile modifiers are present, this procedure is changed to avoid such a harsh condition. For example, 1-[3-(4-monomethoxytrityloxy) propyl]- 1'-[3-[(2-cyanoethyl)-(N, N-diisopropyl phosphoramidityl] propyl]-3,3,3', 3’- tetramethylindodicarbocyanine chloride (Cy5 phosphoramidite) and 6-(4- monomethoxytritylamino) hexyl- (2-cyanoethyl)-(N, N-diisopropyl)-phosphoramidite (MMT-NH_2 modifier) are vulnerable to strong basic conditions and often decompose or

lose the 5'-protecting group. After the completion of cleavage and base deprotection, the oligonucleotide is precipitated in ethanol/NaCl. After incubation at -20 ^{o}C for 30 minutes, the precipitated solid is obtained with high-speed centrifugation.

The solid is re-dissolved in 0.1 M triethylammonium acetate (TEAA), pH 7, for the further high-performance liquid chromatography (HPLC) purification. HPLC purification strongly relies on the hydrophobic protecting group (generally DMT) remains on the 5′ position after successful synthesis of the desired oligonucleotide. The typical mobile phase for oligonucleotide purification for HPLC is 0.1 M TEAA, pH 7, and acetonitrile. After the purified oligonucleotide is dried, the DMT group is removed by incubation with 80% acetic acid. The reaction is quenched with ethanol followed by vacuum drying. Pure oligonucleotide is then quantified by UV measuring absorption at 260 nm.

Fluorescence and Signal Transduction

Fluorescence can be easily incorporated into other signaling mechanisms, such as fluorescence resonance energy transfer (FRET), fluorescence quenching, fluorescence lifetime and fluorescence anisotropy to monitor a molecular recognition event. Thus, nucleic acid probes modification with fluorescent molecules and incorporation of various signaling transductions has been the most popular approaches in the design of nucleic acid probes. Fluorescence measurement has been widely used for a variety of investigations in bioanalytical, biochemical, and chemical research due to its nondestructive nature, high sensitivity, and multiplexing capabilities.

Fluorescence Mechanism

Fluorescence is one of the relaxation mechanisms for electronically excited molecules.[2, 3] There are a number of pathways by which the excited molecules can return to ground state, and Figure 1-6, termed a Jablonski diagram, shows a few of

these processes. The singlet (no unpaired electrons) ground state is labeled S0, with S1 and S2 as singlet excited states. The labels T1 and T2 refer to triplet excited states (2 unpaired electrons). When exposed to electromagnetic radiation (EMR), the chromophore is excited to an upper vibration level in S1 (or in S2). Then, the excited molecule drops to the ground vibration level of the S1 state via vibration relaxation. If conditions are favorable, the molecule returns to an upper vibration level in S_0 by emission of visible EMR. This process, called fluorescence, occurs in the 10^{-9} to 10^{-5} seconds of the time range. The energy lost through vibration relaxation causes the red shift (longer wavelength), which allows the clear differentiation of the emission signal from the excitation signal. Besides this fluorescence emission, there are several other pathways for returning to the ground state from the excited singlet state, including non-radioactive decays (generally thermal relaxation) and intersystem crossing to a triplet excited state (phosphorescence).

Fluorescence Quenching Mechanism

Quenching refers to any process that decreases the fluorescence intensity of a given substance, which occurs via two major mechanisms: collisional quenching and static quenching. Collisional quenching occurs when the excited fluorophore experiences contact with an atom or molecule that can facilitate non-radioactive transitions to the ground state. Common quenchers include O_2, I^-, Cs^+ and acrylamide. The decay of fluorescence intensity caused by collisional quenching can be described using the Stern-Volmer equation:

$$\frac{F_0}{F} = 1 + K[Q] = 1 + k_q \tau_0 [Q] \qquad (1\text{-}1)$$

in which

F_0 = Initial fluorescence intensity without quencher
F = Fluorescence intensity with quencher
K = Stern-Volmer quenching constant (M^{-1})
k_q = Bimolecular quenching rate constant ($M^{-1}s^{-1}$)
τ_0 = Fluorescence lifetime in the absence of the quencher (s)
$[Q]$ = quencher concentration (M)

In aqueous solutions at room temperature, a fluorophore with a lifetime, τ_0, of 1 ns generally has a Stern-Volmer quenching constant of about 10 M^{-1} for a typical quencher. This estimation suggests that, for quencher concentrations in the millimolar range, the effect of quenching is not significant. However, when the fluorophore and the quencher are covalently linked to each other, the collision rate can be dramatically elevated due to the close proximity, and not thereby depending on diffusion, which results in significant quenching.

In some cases, the fluorophore can form a stable complex (FQ) with another molecule. If this ground state is non-fluorescent then we say that the fluorophore has been statically quenched. The relationship between the fluorescence decrease and the quencher concentration is given by:

$$\frac{F_0}{F} = 1 + K_f[Q] = 1 + \frac{[FQ]}{[F]} \qquad (1\text{-}2)$$

in which

K_f = Formation constant for FQ
[FQ] = Concentration of the dark complex
[F]: Concentration of fluorophore
[Q]: Concentration of quencher.

Unlike dynamic quenching, the lifetime of the sample will not be reduced since those fluorophores, which are not complexed – and hence are able to emit after excitation – will have normal excited state properties. The fluorescence of the sample is

reduced since the quencher is essentially reducing the number of fluorophores, which can emit. In contrast, dynamic quenching causes the lifetime to decrease by the same factor as the fluorescence intensity. In addition, the effect of temperature is different for the two types of quenching. In static quenching, elevated temperature causes the quenching efficiency to decrease due to dissociation of the weakly bound FQ complex. On the other hand, accelerated diffusion rate at elevated temperature increases the collisional quenching rate, resulting in a significant decrease of fluorescence. Static quenching can be incorporated into the design of molecular probes for studying molecular recognition. The typical example is the molecular beacon, which is described later in this Chapter.

Fluorescence Resonance Energy Transfer (FRET)

FRET is a distance-dependent dipole-dipole interaction between the electronic excited states of two dye molecules in which excitation is transferred from a donor molecule to an acceptor molecule without emission of a photon. [3] Efficient FRET generally requires: a) Proximity: the donor and acceptor molecules must be close to each other (approx. 10 – 100 Å). b) Spectral overlap: the absorption spectrum of the acceptor must overlap with the emission spectrum of the donor. c) Relative donor-quencher orientation: in most assays with fluorescent probes, it is assumed that the relative orientation of the dyes is random (Figure 1-7). The FRET efficiency, E, also depends strongly on the distance between the two molecules, as described in the following equation:

$$E = \frac{R_0^6}{R_0^6 + r^6} \qquad (1\text{-}3)$$

In which

R^0 = Forester radius where energy transfer is 50% efficient
r = distance between the donor and the acceptor

The strong distance dependency of FRET efficiency has been widely exploited in molecular structure and dynamics studies, intermolecular association detection, intermolecular binding assays, as well as molecular probe design.

Molecular Beacons

Molecular beacons (MBs) shown in Figure 1-8 are single-stranded DNA probes composed of three different functional domains: stem, loop, and fluorophore/quencher pair.[4] The stem sequences (4-7 base pairs) are complementary to each other, and the loop is complementary to the target. The fluorophore/quencher (F/Q) signaling element, switches between the on and off 28states, depending on the conformational state of the MBs. In the absence of targets, the energy absorbed by F is transferred via FRET to Q, which is spatially very close to F due to stem hybridization, and fluorescence is not observed (off state). When the target is present, the loop and target hybridize (generally 15 to 25 base pairs), and the distance between F and Q greatly increases (approximately longer than 10nm). Thus, FRET no longer occurs, and strong fluorescence is observed (on state).

The unique hairpin structure and on/off signaling mechanism endow the MBs with several advantages. First of all, the light-up signaling mechanism allows it to perform highly sensitive detections for nucleic acid monitoring in real time. Because the unbound MBs stay in the off state, fluorescence is produced only when target is added, and the intensity is proportional to the target concentration. Such a detection-without-separation property is particularly useful for the MBs in situations where it is either impossible or undesirable to extract the probe/target hybrids from an excess of the unbound probes.

Another advantage of the MBs is their relatively high signal-to-background ratio (S/B), which provides high sensitivity. Upon hybridization of its target, a well designed MB can generate a fluorescence enhancement as high as 200-fold under optimal conditions.[5] This provides the MBs with a significant advantage over other fluorescent probes in ultra-sensitive analysis. In addition to its sensitivity, the MBs offer excellent selectivity. They are extraordinarily target-specific and are able to differentiate changes as small as single-mismatched sequences. The selectivity of the MBs is a direct result of its hairpin conformation because the stem hybrid acts as an activation energy barrier to the loop-target hybrid. The remarkable selectivity has been demonstrated in a variety of biological environments where a large number of different non-target nucleic acid sequences are present. Since they were first created in 1996, the MBs have been utilized in many research fields and applications, including intracellular monitoring, biosensor development and clinical diagnosis.

DNAzyme

RNA and DNA molecules, like proteins, have complex three-dimensional structures that depend on the sequence of their building blocks - though whereas proteins have twenty amino acids, RNA or DNA molecules have only four types of nucleotide to play with. Still, this variety, together with single-stranded and double-stranded domains, can give complex structures that, much like enzymes, can selectively bind substrates and catalyze useful chemical reactions. Such nucleic acid based catalysts are called DNAzymes and ribozymes and hold great promise as chemical sensors; tools to construct nanostructures; and molecular machines and computing systems.

Nucleic Acid as catalyst for DNA/RNA cleavage

Deoxyribozyme was reported by Breaker and Joyce in 1994 and catalyzes cleavage of a single ribonucleotide linkage embedded within a strand of DNA nucleotides.[6] It has now been found to catalyze many reactions that include ligation,[7-9] phosphorylation,[10] oxidative DNA cleavage,[11] RNA cleavage,[12] porphyrin metallation,[13] and depurination[14] to name a few. Most DNAzymes are metalloenzymes and, quite commonly, the activity for which they have been selected involves cleavage of a complementary oligonucleotide substrate by virtue of a divalent metal ion cofactor. Via attack of the 2'-hydroxy group at the adjacent phosphodiester linkage (Figure 1-9), the cleavage reaction occurs by transesterification. In last decade, many DNAzymes were found recruiting divalent metal ion such as Pb^{2+}, Mg^{2+}, Ca^{2+}, or Zn^{2+}(Figure 1-9) as cofactors.[15] All of these deoxyribozymes were identified using in vitro selection, for which a brief overview is given in next section. In many cases, substrates that are made entirely from RNA—rather than having only a single RNA linkage—are cleaved efficiently. This cleavage is often achieved with the additional feature of relatively broad RNA sequence generality, meaning that by ensuring Watson–Crick complementarity between the RNA substrate and DNA enzyme, many different RNA substrate sequences may be cleaved merely.[16] For most substrates, only the nucleotides near the cleavage site have restrictions on their sequence identities, and sets of DNAzymes have been developed allow practical cleavage of almost any RNA sequence.[16]

In Vitro Selection of DNAzyme

The idea of designing structures that act as catalytic enzyme-like DNA strands, became practical in the 1990s, following the development of the Systematic Evolution of Ligands by Exponential Enrichment (SELEX) process. Here, nucleic acids with specific

binding properties, or affinities towards a particular transition-state analogue, are fished out of a library of 10^{15} nucleic acids and amplified by the polymerase chain reaction (PCR). The catalytic nucleic acids made this way are, in effect, man-made analogues of protein-based enzymes. But the nucleic acid enzymes have advantages over their protein analogues: DNAzyme is chemically very stable; It can be efficiently automated-synthesized by PCR; and the timeline for generating DNAzyme is less than that of protein.

Besides binding-based target recognition elements, there are also target recognition elements utilizing catalytic reactions. Protein enzymes have been widely used, as they possess very high substrate specificity and detection signal can be amplified through catalytic turnovers. Primary examples are glucose sensors based on glucose oxidases.[17] In the realm of enzyme, protein has long been thought to be the only player until the discovery RNAzyme (ribozyme) in 1982. [18] Since then, many naturally occurring RNAzymes have been found, [19] and many more RNAzymes with customizable functions and properties have been generated with in vitro selections. [20] Although no DNAzymes were found in nature, the same in vitro selection technique has been used to isolate DNAzymes, with the first DNAzyme obtained in 1994. From then on, many DNAzymes have been selected to catalyze many of the same reactions as seen for protein enzymes and RNAzymes. (Table 1-1)[8, 20-22]

Secondary structures of three metal-specific DNAzymes are shown in Figure 1-10 lower part, all the three DNAzymes contains a substrate strand (upper strands) and an enzyme strand (lower strands). The one in Figure 1-10A is known as the 8-17 DNAzyme, [12, 23-25] which will be discussed in detail later. The second DNAzyme (Figure

1-10B) has 100-fold selectivity for Zn^{2+} over Cd^{2+} and more than 500-fold selectivity over any other divalent metal ions.[26] The third one (Figure 1-10C) is a Cu^{2+}-dependent DNAzyme.[11, 27, 28] Only Cu^{2+} can activate the DNAzyme.

Among the many protocols applied to select DNAzymes, the one used to isolate the first DNAzyme with endonuclease activity is presented here as an example to illustrate the selection process.[6] As shown in the Figure 1-11 the initial pool, contained single-stranded DNA with a 40 nucleotides random region (shown as a bar) flanked by two conserved primer-binding regions. The number of DNA sequences in the pool can be as high as 10^{15}. In a first PCR, the pool was amplified and the DNA molecules were present as double-stranded. In a second PCR, one of the primers contained a biotin on the 5'-end, and an adenine ribonucleotide (rA) on the 3'-end. Therefore, after the second PCR, one strand contained rA and biotin. The rA was introduced to be the cleavage site, as it is easier to be hydrolyzed. The conserved sequence of the strand containing rA and biotin is presented in Figure 1-10A. The pool was then incubated in an avidin column for immobilization. NaOH was added to denature the double-stranded DNA, and the strand without biotin was washed away. At this step, a metal ion of choice was added and incubated with the pool. If some sequences self-cleaved in the presence of the added metal cofactor, the cleaved products were collected and amplified by PCR to seed the next round of selection. To obtain DNAzymes with higher activity and cofactor binding ability, the concentration of cofactor and the time for incubation can be gradually decrease. The selection process was performed until the activity o the pool stopped increasing, and the surviving DNA molecules ere cloned and sequenced. Negative selections can be performed to eliminate populations that are also active in the

presence of competing metal ions. The as selected DNAzymes are called self-cleaving, or cis-cleaving DNAzymes, because both the enzyme and the substrate part of the enzyme are in the same single-stranded sequence (Figure 1-10A).

Truncation studies can be performed to obtain trans-cleaving DNAzymes to separate the substrate and the enzyme part. The DNAzyme is therefore a true catalyst as it can perform multiple turnover reactions.

Advantage of DNAzyme-Based Sensors

There are many advantages to employ DNAzymes as the target recognition element for metal sensing.[8, 21, 29] First, the in vitro selection technique allows isolation of DNAzymes with promising metal selectivity. Second, the initial pool for the selection can contain as many as 10^{15} DNA molecules with random sequences, which is much bigger than a peptide selection pool.[30] Third, DNAzyme in vitro selection can be performed in relatively short time (1-2 day per round). Fourth, after knowing the sequence (primary structure) of a DNAzyme, its secondary structure could be conveniently predicted from algorithms like mfold.[31] Although tertiary interactions would be important for the activities of DNAzyme, most chemical modifications can be designed solely based on the secondary structure of a DNAzyme. Fifth, DNA molecules are stable. For practical applications, high stability is a crucial, as it allows the designed sensors to be used under rather harsh conditions and have a long shelf time. Because of these properties, DNAzymes have already found applications not only in biosensor development, but also as anti-viral agents,[12] DNA-based logic gate design,[32, 33] and components for nanomotors.[34, 35]

Table 1-1 DNAzymes isolated from in vitro selection.

Reaction	Cofactor	$K_{max}(min^{-1})$	K_{cat}/K_{unmax}	Ref.
RNA Cleavage	Ca^{2+}	0.08	10^5	36
	Mg^{2+}	10	10^5	12
	Pb^{2+}	1	10^5	6
	Zn^{2+}	40	$>10^5$	24
	Co^{2+}	7		37
	Cd^{2+}, Ca^{2+},	~1		38
	Ca^{2+}			
	L-histine	0.2	10^6	39
DNA cleavage	Cu^{2+}	0.2	$>10^6$	27, 11
RNA ligation	Mn^{2+}	2.2	$>10^6$	40
	Mg^{2+}	0.1	450	9
	Zn^{2+}	0.5	1.7×10^4	41
DNA ligation	Cu^{2+}, Zn^{2+}	0.07	10^5	7
	Mn^{2+}	10^{-5}	$>10^5$	42
DNA phosphorylation	Ca^{2+}	0.01	10^9	10
Thymine dimer cleavage	None	4.5	2.5×10^4	43
DNA adenylation	Cu^{2+}	0.003	$>10^{10}$	44
Porphyrin metallation	None	1.3	10^3	13
Phosphoramidae bond	Mg^{2+}	$\sim5\times10^{-4}$	$>10^3$	45
cleavage				

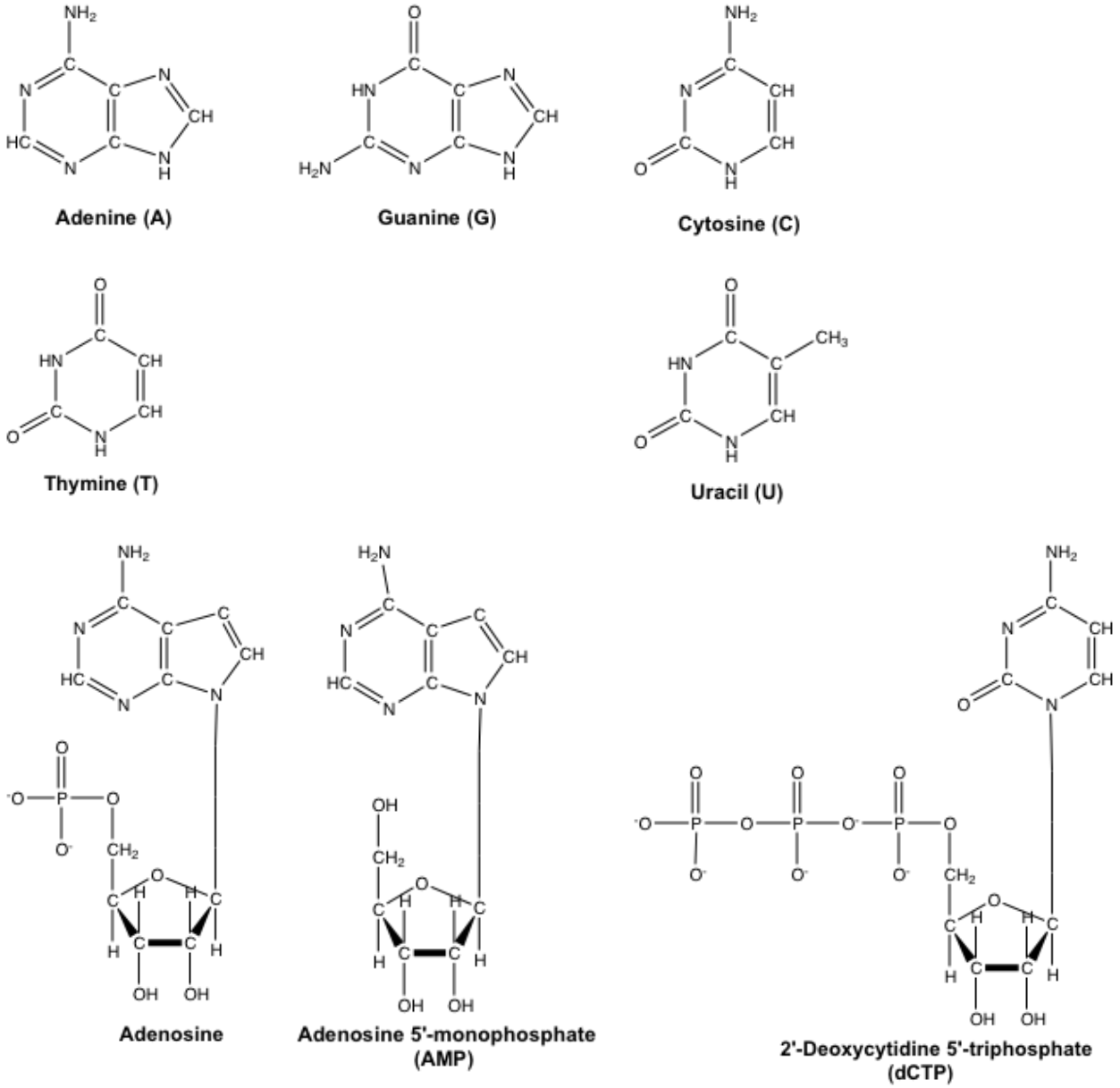

Figure 1-1 Structure of bases, nucleosides and nucleotides. The bold lines at the bottom of the sugar rings are meant to indicate that The bold lines at the bottom of the sugar rings are meant to indicate that the plane of the ring is set at an angle of 90° with respect to the plane of the corresponding base (i.e. if the plane of a base is represented as lying on the surface of the page, carbon atoms 2′ and 3′ of the sugar can be viewed as projecting upwards out of the page and the oxygen atom as projecting down below the surface of the page).

Table 1-2. Comparisons between aptamer and antibody.

Feature	Aptamer	Antibody
Production	< 8 weeks (automated, *in vitro*)	>10 weeks (*in vivo*)
Specificity and affinity	High, Kd: pico to low nanomolar	High, Kd : pico to low nanomolar
Inhibitory potential	High	Low, 1 out of 200
Molecular weight	5-25 kDa	~150 kDa
Immunogenicity and toxicity	Not observed	Immune reaction observed
Target space	Extra- and intracellular proteins	Extracellular proteins only
Chemical modification	Easy	Difficult
Physicochemical stability	Stable	Labile

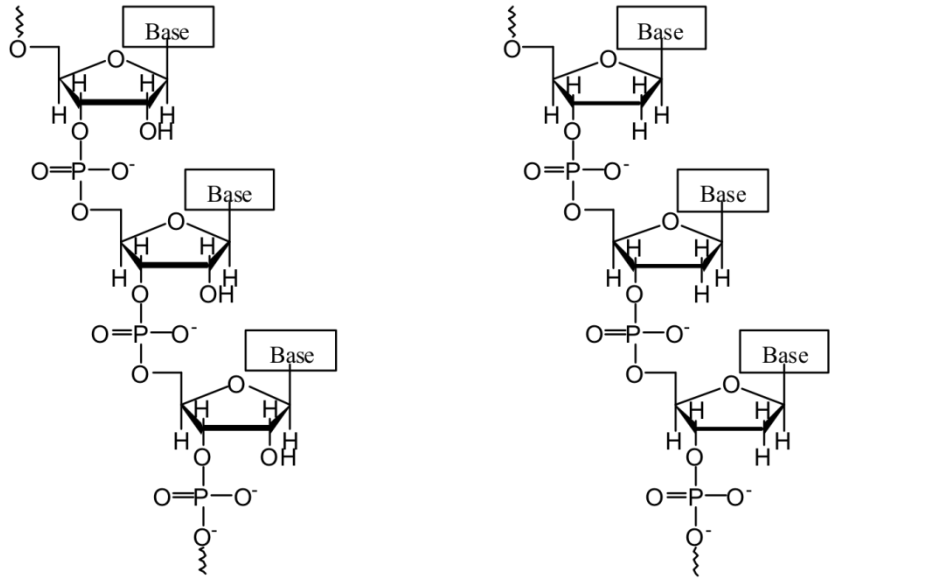

Figure 1-2. Nucleotide structure and linkage via phosphate groups.

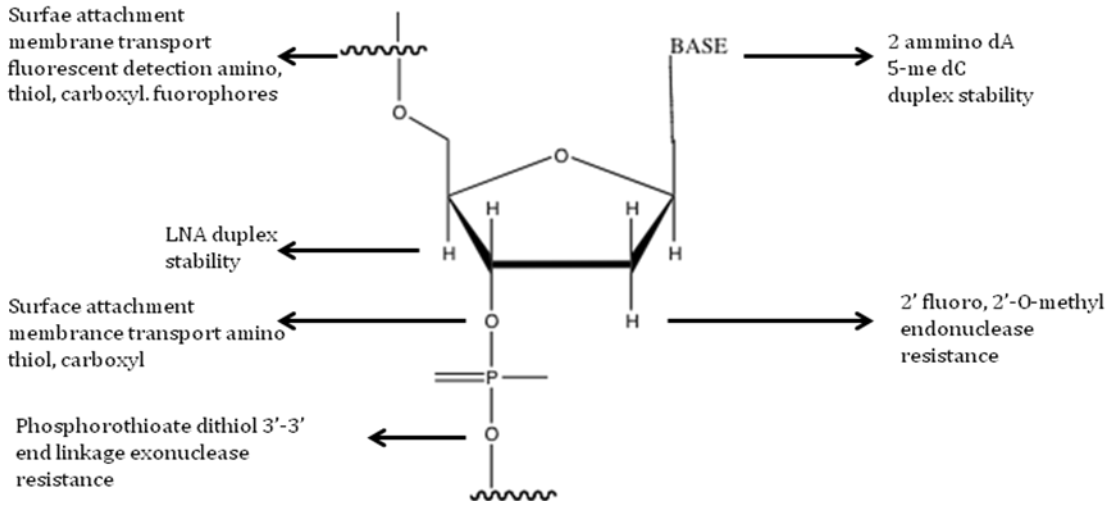

Figure 1-3. Bases modifications.

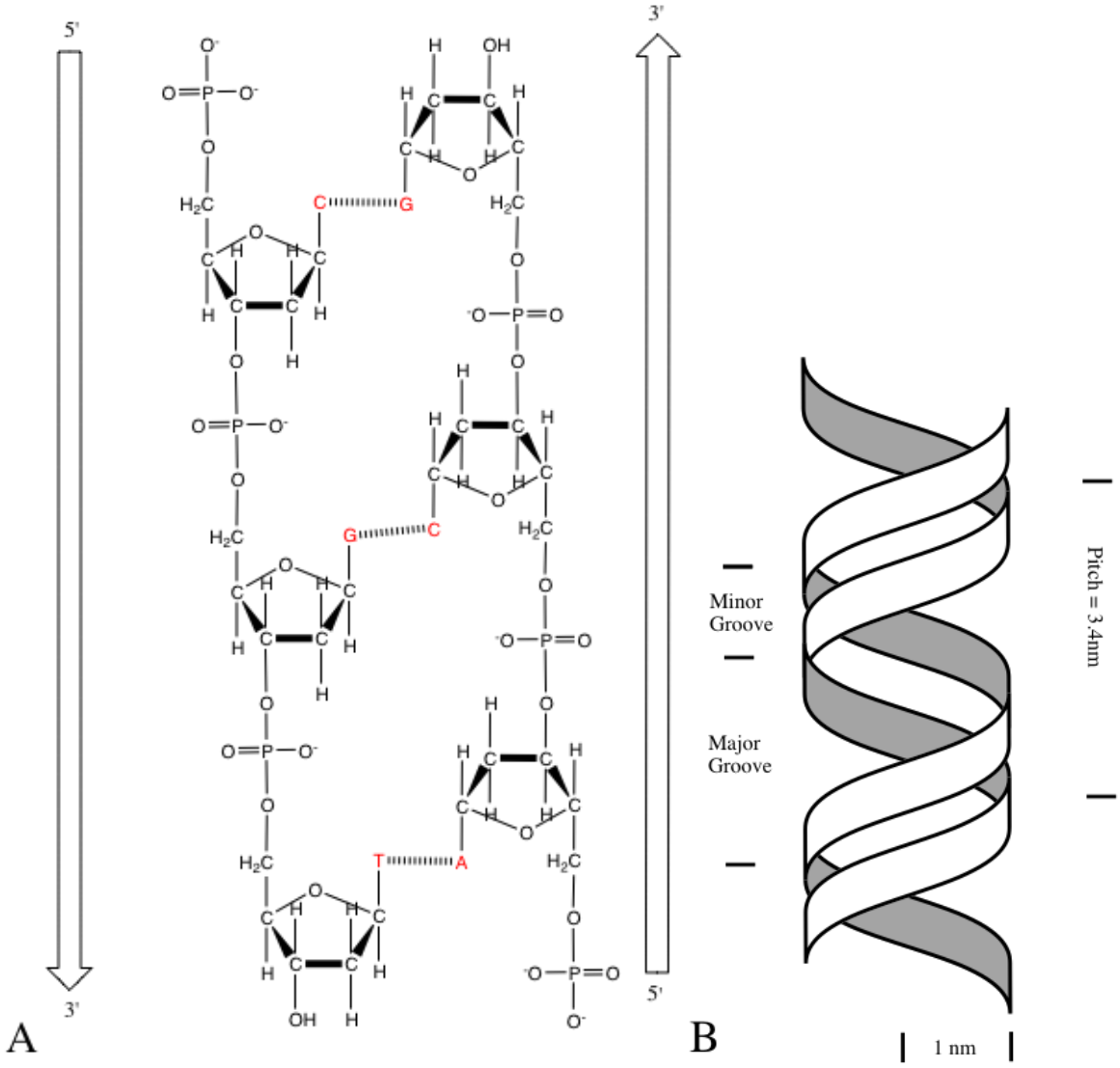

Figure 1-4. DNA structure is a double-stranded, antiparallel helix. A) Antiparallel nature of the two DNA strands. The two strands are antiparallel because they have opposite directions for linking of 3′ carbon atom to 5′ carbon atom. The structure shown is a double-stranded trinucleotide whose sequence can be represented as: 5′ pCpGpT-OH 3′ (DNA strand on left) / 5′ pApCpG-OH 3′ (DNA strand on right) (where p = phosphodiester bond and -OH = terminal OH group at 3′ end). This is normally abbreviated by deleting the ‘p’ *and* ‘OH’ symbols and giving the sequence on one strand only (e.g. the sequence could equally well be represented as 5′ CGT 3′ or 5′ ACG 3′). B) The double helical structure of DNA. *Note* that the two strands are wound round each other to form a *plectonemic* coil. The *pitch* of each helix represents the distance occupied by a single turn and accommodates 10 nucleotides in B-DNA.

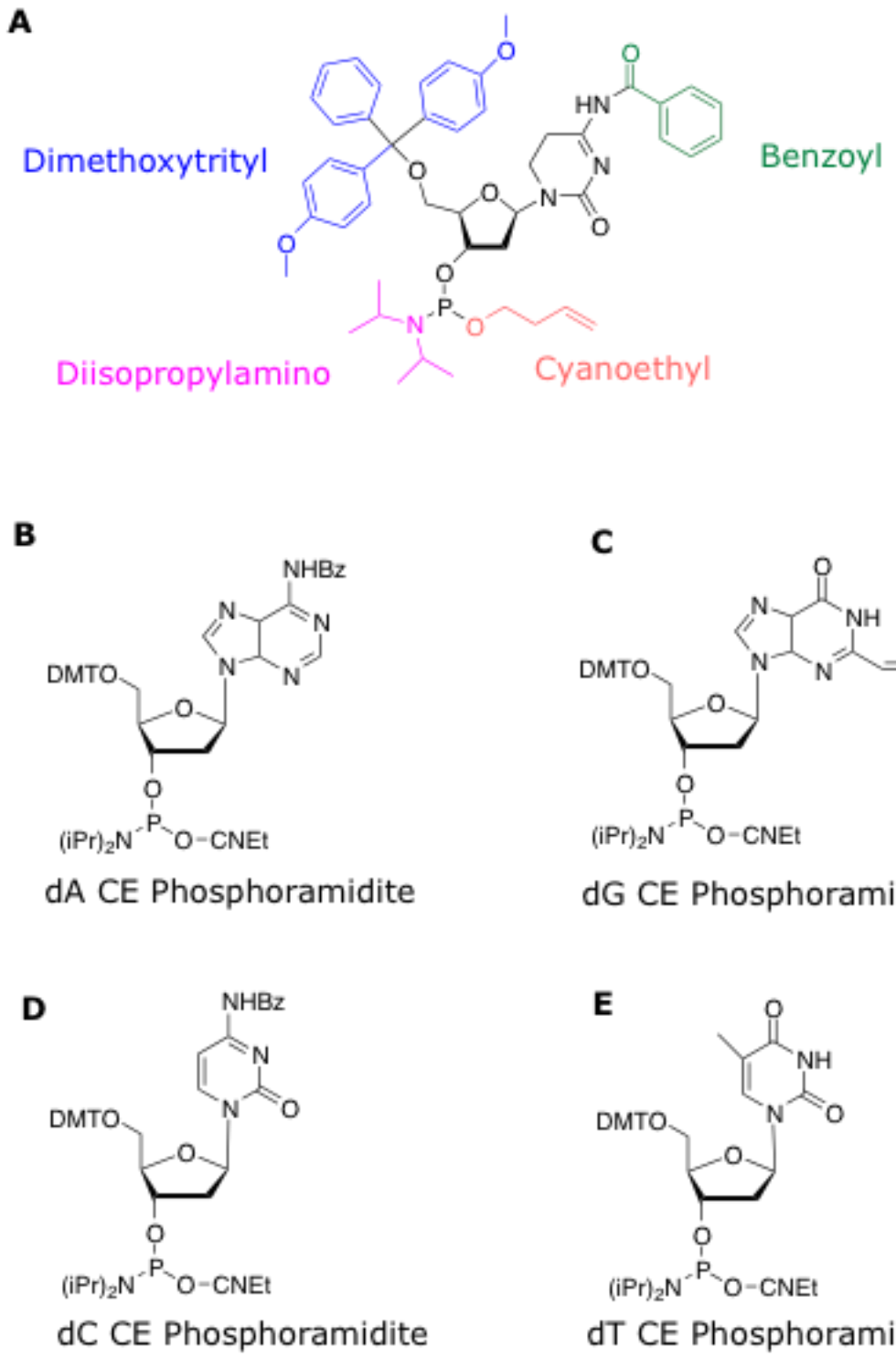

Figure 1-5. Structure of nucleic acid phosphoramidites. A) Cytosine phosphoramidite. B) dA CE phosphoramidite. C) dG CE phosphoramidite. D) dC CE phosphoramidite. E) dT CE phosphoramidite

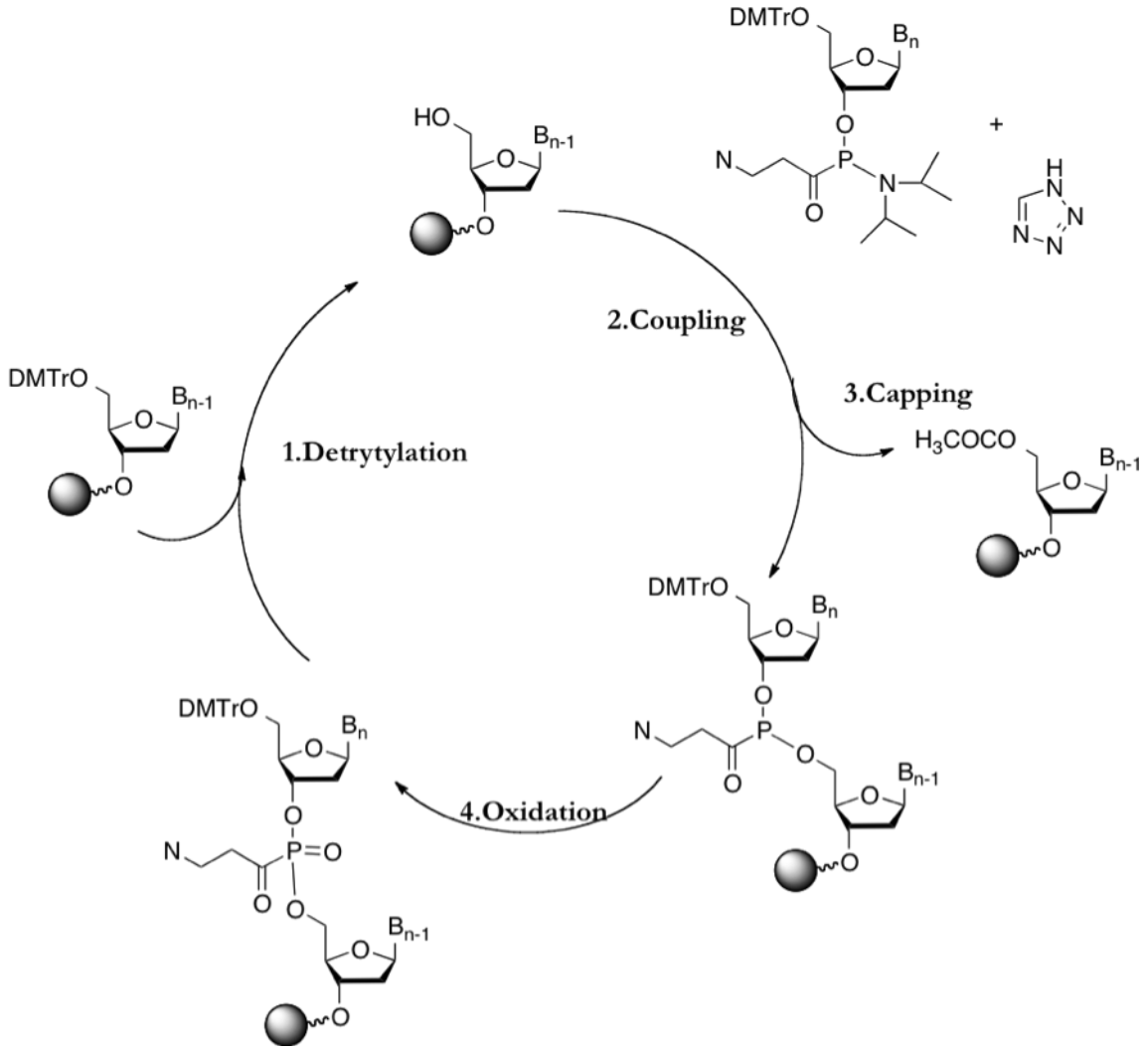

Figure 1-6. Automated oligonucleotide synthesis.There are four major steps involved in the synthesis of DNA: (1) Detritylation, (2) Coupling, (3) Capping/Coupling, and (4) Oxidation. This synthesis has been achieved through phosphoramidite chemistry.

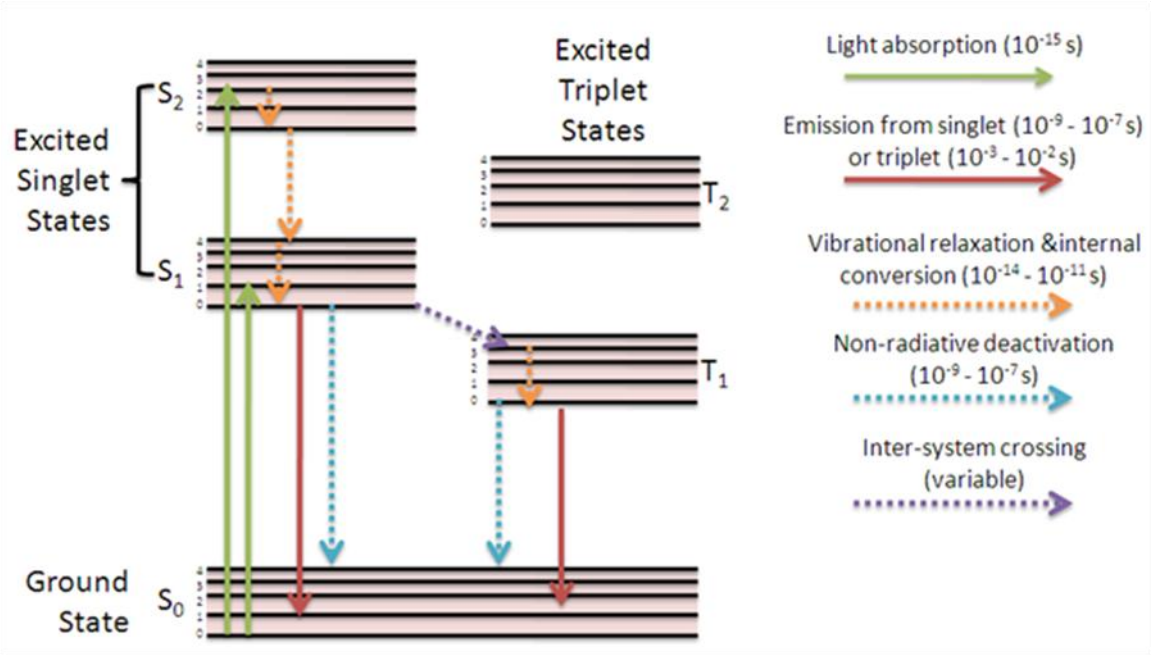

Figure 1-7. Jablonski diagram. Radioactive processes (those which are "vertical" in energy transfer) are shown in solid lines whereas non-radioactive processes ("horizontal" energy transfer) are shown using dotted lines. Indicative timescales are shown, although are molecule dependant.

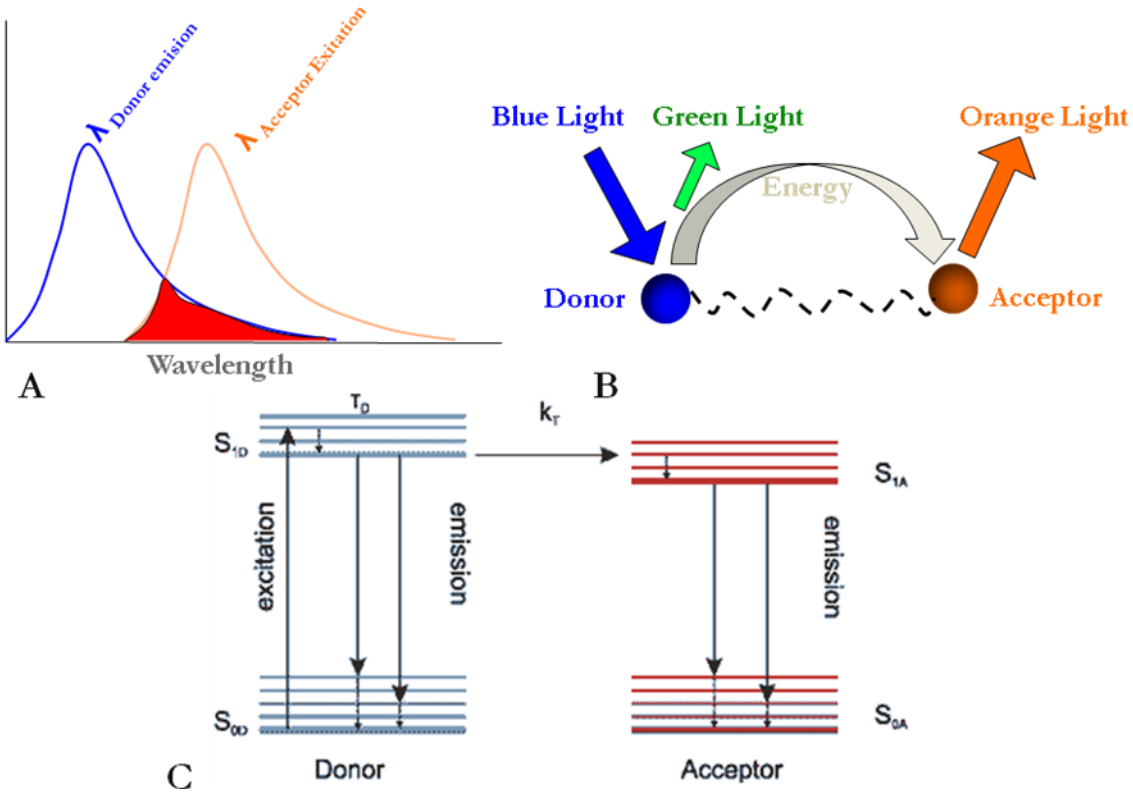

Figure 1-8. FRET description. A) Spectral overlap between donor's emission and acceptor's excitation. B) Fluorescence energy transfer scheme. C) Description of fluorescence resonance energy transfer.

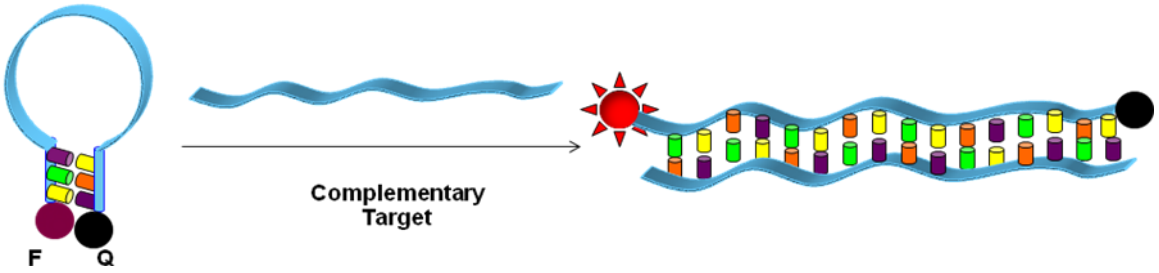

Figure 1-9. Working principle of molecular beacon. On their own, these molecules are non-fluorescent, because the stem hybrid keeps the fluorophore close to the quencher. When the probe sequence in the loop hybridizes to its target, forming a rigid double helix, a conformational reorganization occurs that separates the quencher from the fluorophore, restoring fluorescence.

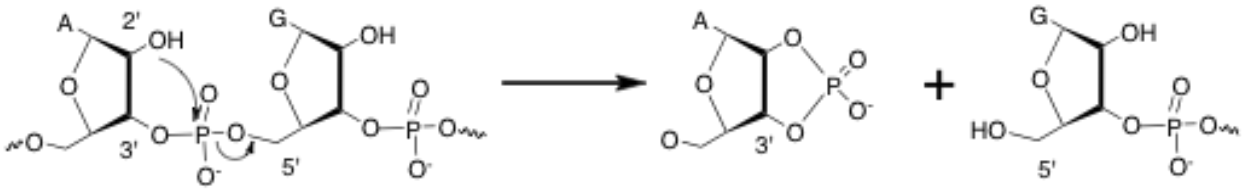

Figure 1-10. DNAzymes catalyzed RNA cleavage. Chemistry of the cleavage reaction: transesterification at phosphorus.

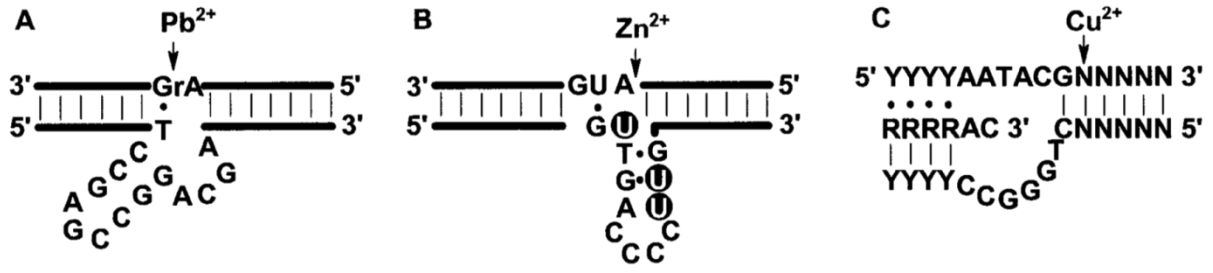

Figure 1-11. Three RNA-cleaving DNA enzymes. A) A Pb^{2+}-specific RNA cleaving 8-17 DNAzyme. B) A Zn+-specific RNA-cleaving DNAzyme. The Black dots with U present imidazole-modified deoxyuridines. (C) A Cu^{2+}-specfic DNA-cleaving DNAzyme.

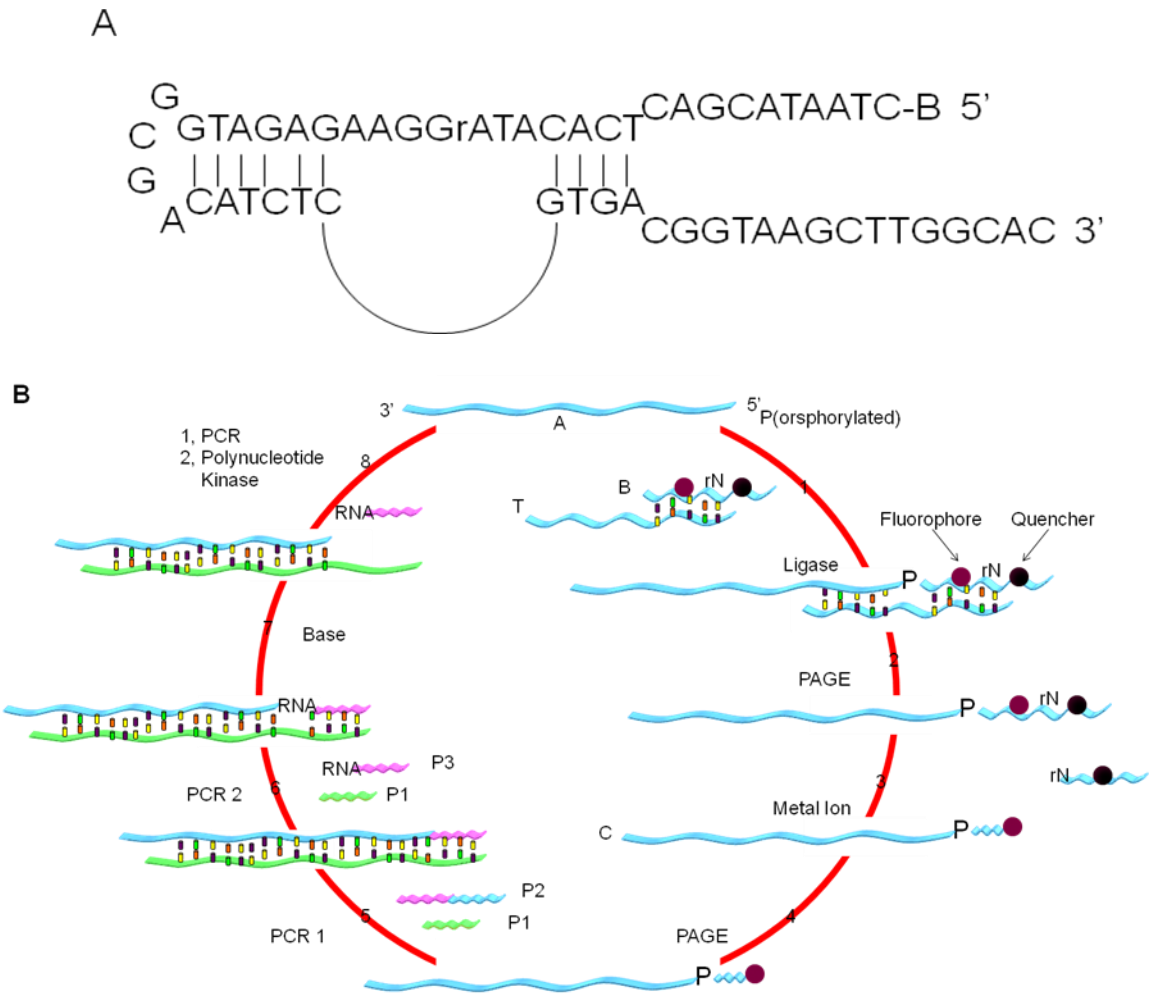

Figure 1-12. Schematic presentation of in vitro selection of DNAzymes. A) Secondary structure of starting DNA pool for selection of DNAzymes. B) Selection scheme of catalytic DNAzymes. (1) A DNA was ligated to acceptor DNA B; (2) the ligated DNA was isolated by polyacrylamide gel electrophoresis (PAGE); (3) purified DNA was incubated with metal ions to cleave the embedded RNA; (4) the cleavage fragment, C, was isolated by PAGE; (5) the recovered DNA was amplified by polymerase chain reaction (PCR) using primers P1 and P2; (6) the PCR product from the earlier cycle was reamplified using primers P1 and P3 to introduce a ribonucleotide linkage embedded within DNA; (7) the resulting double-stranded DNAs were treated with NaOH to cleave the RNA linkage; (8) the cleavage fragment is purified by PAGE, phosphorylated at the 5$_0$-end, and used to initiate the next round as a ssDNA.

CHAPTER 2
ENGINEERING A UNIMOLECULAR DNA-CATALYTIC PROBE FOR SINGLE LEAD ION MONITORING

Lead Toxicity

Lead toxicity can be due to acute or chronic exposure. Acute toxicity is frequently caused by pica syndrome; the symptoms can include abdominal pain, nausea and vomiting, hemolysis, renal failure, hepatotoxicity, seizures and coma. The symptoms of chronic lead poisoning are manifest in multiple organ systems, including the gastrointestinal tract, the hematopoietic process, the kidneys and the nervous system. The diverse clinical manifestations can be explained by the cellular mechanisms of lead toxicity that interfere with a variety of functions, including cell membrane integrity, neurotransmitter function, heme synthesis and mitochondrial oxidative phosphorylation. In the case of heme synthesis, for example, lead inhibits enzymes in the porphyrin pathway resulting in increases of substrates, which are subsequently eliminated and can be measured in urine. There is also inhibition of the ferrochelatase enzyme, resulting in failure to incorporate iron into the tetrapyrrole ring of heme.[46]

According to a very recent report by the Commission for Environmental Cooperation (CEC), lead is still the No.1 toxic substance released into environment that causes cancer, birth defects, and other developmental problems.[47] In 2002, the industry facilities in the US and Canada alone released 43.4 million kg of lead. With the phasing out of leaded paint in 1978 and leaded gasoline in 1980s, the current main source of lead contamination is from industry facilities, such as smelters and electric utilities.[47]

Lead poisoning is persistent and accumulative, which has posed serious health problems to human beings, especially to young children. For example, lead can cause

brain damages and developmental problems. In most cases, the damages are permanent.[48] The Center for Disease Control and Prevention (CDC) defined blood lead toxic level as 10ug/dL, which corresponds to a concentration of 480nM. The environmental Protection Agency (EPA) threshold for lead in drinking water is 75 nM and the federal threshold for lead in paint is 1mg/cm[248] or 0.5% by weight.[49]

Although detailed mechanism of lead poisoning is still unknown, Godwin and co-workers performed Pb^{2+} binding study on original Zn^{2+} or Ca^{2+}-binding peptides and proteins. The results suggested that the molecular origin of lead toxicity could be from lead competing with zinc and calcium binding sites in proteins.[50] In a recent report, spectroscopy results indicated that pb^{2+} binds in a three-coordinate mode in proteins containing Zn^{2+} binding sites; while Zn^{2+} binding in a four-coordination mode. Change of the coordination chemistry may contribute to the lost of activities of these proteins.[51]

Lead test results inform clinicians about exposure and therapy may be started if the concentration is sufficiently elevated. While a blood lead concentration of 10μg/dL is the current benchmark used to diagnose lead poisoning, there is ongoing research and some evidence that intellectual deficits may occur with lead concentrations as low as 7.5 μg/dL.[52]

Pb^{2+} Sensor Development

Instrumental analysis methods such as atomic absorption spectroscopy (AAS), [53, 54] inductive-coupled plasma mass spectroscopy (ICP-MS),[55, 56] and anodic stripping voltammetry[57] can detect Pb^{2+} with very high sensitivity.[58] However, these instruments are mostly equipped in analytical laboratories and it is hard for the instruments to be used on-site. For many other applications, such as the detection of leaded paint in old

housed, portable detection kits are desirable. Towards this goal, a number of chemical and biological sensing methods have been developed for lead detection, such as sensors based on fluorophore-coupled organic chelators,[59-63] peptides,[64] proteins,[65] antibodies,[66, 67] nanoparticles[68] and oligonucleotides.[69]

Most of Organic chelator-based Pb^{2+} sensors involve a macrocycle for Pb^{2+} recognition.[60, 62, 63] Upon Pb^{2+} binding, the attached fluorophore changes fluorescence properties either by shifting emission wavelength or by changing emission intensity. Several examples of such Pb^{2+} sensors are presented in Figure 2-1. For compound 1, the monoaza-15-crown-5 moiety recognized divalent metal ions with ionic diameters between 1.9-2.4 Å. As a result, most IIA and IIB group ions, particularly Hg^{2+} interfered with Pb^{2+} detection, Emission maximum shifted from 642 to 574 nm upon metal binding, and less than 1 μM of Pb^{2+} can be detected. Chen and cow-workers reported a structurally very similar compound 2, which contained the same crown ether structure. The difference was the presence of a keto bridge in compound 2 instead of an alkene bridge in compound 1. Surprisingly, the Pb^{2+} selectivity of compound 2 was much higher than that of compound 1, and more than 20-fold selectivity for Pb^{2+} was observed over other divalent metal ions, which could be resulted from a different Pb^{2+} binding mode.[60] It was proposed that compound 2 formed a 2:2 complex with Pb^{2+}. Besides the five coordinating atoms in the ring, the two keto oxygens from another molecule also involved in Pb^{2+} binding. Compound 3 contained a pseudo-18-crown-6 structure for Pb^{2+} recognition and the signal transduction relied on a pyrene fluorophore. In the presence of Pb^{2+}, two of the molecules sandwiched a Pb^{2+}. As a result, emission from pyrene dimmer was increased at the expense of pyrene monomer emission.[63]

Several non-macrocycle-based Pb^{2+} sensors were also reported.[61, 70, 71] Examples of these sensors are also given in Figure 2-1. Compound 4 chelated Pb^{2+} with the two nitrogen ligands,[70] and compound 5 coordinated with Pb^{2+} by the sulfur and the hydroxyl group.[71] One disadvantage associated with organic chelator-based sensors is the use of non-aqueous solvents.

Godwin and co-workers studied Pb^{2+} binding to cysteine-rich sites in proteins.[72] The results suggested that Pb^{2+} can bind tightly to Zn^{2+} binding sites in these proteins.[72] A fluorophore(dansyl)-conjugated tetrapeptide was designed to sense Pb^{2+}. Binding of Pb^{2+} changed the peptide conformation and thus changed the environment around dansyl, inducing a shift in fluorescence emission. The sensor can detect Pb^{2+} in a ratiometric manner. However, the dissociation constant between Pb^{2+} and the peptide was higher than 100 μM.[64]

Ralstonia tametallidurans is the only known bacterium to possess a Pb^{2+}-resistent pathway, and PbrR is its Pb^{2+}-regulatory protein. PbrR binds to the promoter region of a Pb^{2+}-regulatory gene. Binding of Pb^{2+} to the protein changes the DNA conformation. This is how the protein regulated gene behavior in the presence of Pb^{2+}. By incorporating fluorescent base analogous (e.g. 2-aminopurine for the adenine or pyrrolo-C for cytosine) to a 25-mer double-stranded DNA that mimics the PbrR-binding DNA, highly sensitive and selective fluorescent Pb^{2+} sensors were designed. The sensor showed a detection limit of 50nM and over 1000-fold selectivity for Pb^{2+} over other divalent metal ions. The same design strategy had been used to obtain a fluorescent Hg^{2+} sensor.[73]

Blake and co-workers developed competitive immunoassays for heavy metal ions, including Pb^{2+}.[66, 67] Using the Pb^{2+} assay as an example, first, monoclonal antibodies for a chelated Pb^{2+} complex were isolated. In such an assay, a sample to be detected was incubated with the Pb^{2+} chelator. The same solution was then incubated with the antibody in the presence of immobilized metal-chelator complex. As a result, the immobilized Pb^{2+} complex competed with dissolved Pb^{2+} complex for antibody binding. The final amount of antibody attached to surface was inversely proportional to the concentration of the Pb^{2+} complex in solution. The amount of immobilized antibodies was quantified by adding enzyme-labeled anti-species antibodies, which produced color signals in subsequent enzyme reactions. The method can in principle be used to detect a broad range of metal ions. However, the detection process is relatively tedious.

Hupp and co-workers functionalized gold nanoparticles with 11-mercaptoundecanoic acid (MUA). In the presence of Pb^{2+}, nanoparticles aggregated due to coordination of Pb^{2+} with MUA. The aggregation of nanoparticles resulted in a red-to-blue color change. However, Hg^{2+} and Cd^{2+} can also induce similar color changes. With the colorimetric detection method, a detection limit of 0.4mM was reported, which was improved to 25 μM by using hyper-Rayleigh scattering (RS) as a detection method.[68]

Pb^{2+} Sensing Based on Molecular Beacons

Nucleic acid probes represent a new class of detection tools that possess unique features.[74, 75] The targets of nucleic acids can range from ions to small organic and inorganic molecules,[37, 38, 76] other nucleic acids,[77] peptides,[78]proteins,[79]and even whole living cells.[80]The selected sequences are generally very specific with excellent binding affinity to targets.

Pb^{2+} Sensing Using Unimolecular DNAzyme Molecules

DNAzymes are DNA sequences, or deoxyribozymes, that catalyze chemical reactions, such as cleaving ribonucleic acid targets.[6] Among the DNAzymes attracting most attention are those that may be termed cation specific. Cation-specific DNAzymes are composed of two functional domains: a catalytic loop that recognizes specific ions employed as coenzyme and a binding arm that targets its complementary sequence, or substrate. When the DNAzyme is hybridized with its target substrate sequence and the desired cation binds to the catalytic loop, hydrolysis of the target substrate sequences is activated. Because of the lower affinity of the cleaved substrate, the DNAzyme can bind to yet another substrate so that it can be recycled for hydrolysis of multiple substrates in a manner similar to that of enzymes with their substrate target. Researchers have taken advantage of this unique enzyme-like feature of DNA probes by developing new classes of therapeutic agents to selectively down-regulate the translation of target mRNAs.[81] Still another application involves the development of 8-17 DNAzyme-based sensors for metal detection.[23]In fact, the design of fluorescent metal sensors and chemodosimeters has recently become one of the most active research areas because of the *in situ* and real-time information they provide in a variety of applications. Examples include monitoring environmental pollution, [82] metalloneurochemistry,[83] and biomedical diagnostics.[84] DNAzymes have also been shown to catalyze many of the same reactions as RNA or protein enzymes, but DNAzymes are relatively less expensive to produce and possess more stable hydrolysis than RNA and protein enzymes.[85] Exceeding the capability of protein enzymes, most DNAzymes can be denatured and renatured many times without losing binding ability or activity.

The development of lead ion sensors is an attractive research area, particularly since lead is an integral component of living systems and a common environmental contaminant.[86] Lead exposure can occur through a variety of sources, including air, bare soil, home remedies, drinking water, toy jewelry, and others.[87-89] Moreover, produce and other foods may be contaminated by dust exposure during growing or processing, and food containers add another source of contamination.[90] Low-level lead exposure is known to cause a number of adverse health effects.[91]For example, when exposed to lead, physical or mental development in infants and children might be delayed.[92] Furthermore, children can show slight deficits in attention span and learning abilities,[93] whereas adults may have kidney problems and high blood pressure.[94] As announced by the United States Environmental Protection Agency (EPA), the level of lead in the blood is considered toxic when it is ≥480 nM. In drinking water, lead is regulated by a treatment technique that requires systems to control the corrosiveness of their water. If more than 10% of tap water samples exceed the action level (0.015 mg/L),[95] water systems must take additional steps. Therefore, as a matter of public health, there is an urgent need to detect lead contaminants, either in solution *in situ* or in biological samples *in vivo*. To address this need, it has been reported that Pb^{2+}-specific 8-17 DNAzyme can be coupled to fluorescent signaling mechanisms to produce a metal biosensor with improved sensitivity and selectivity. However, it is also clear that such development still involves complicated modifications to 8-17 DNAzyme, with two problems posing particular challenges. First, as shown in Figure 2-1A, the 8-17 DNAzyme might not be close enough to its target substrate to achieve the best annealing of the DNAzyme and substrate strands. This results from the repulsive forces

of steric interactions that prevent straightforward bonding and, therefore, decrease the hybridization efficiency otherwise required of the DNAzyme and its target substrate by bringing those two strands close together. Second, as a consequence of the catalytic loop sequence, where the DNAzyme is flanked in the middle, these two pieces do not form a stable duplex, but rather a loose and unstable one. Together, these two problems cause lower hybridization efficiency, resulting in a limited amount of active DNAzymes and minimized hydrolysis reaction. Under these conditions, a simple quenching mechanism is not sensitive enough to detect low concentrations of Pb^{2+}, even though the selectivity is superior.

To address these problems, we proposed to covalently link the DNAzyme and leaving substrate fragment with polythymine to create a strong intramolecular interaction. Specifically, the leaving substrate fragment is labeled with a fluorophore, the conventional enzyme fragment is labeled with a quencher, and these two pieces are linked together with poly T. The resulting intra-molecular interaction tends to be strong enough to allow the hybridization of short base-paired sequences that could not otherwise form stable duplexes at room temperature via bimolecular interaction. By this intra-molecular assembly method, a new type of probe is developed which possesses four functional domains: (1) a catalytic sequence which is a DNAzyme sequence, (2) a leaving substrate fragment that can be hybridized with the catalytic sequence, (3) a linker that ties together the 8-17 DNAzyme fragment and the leaving substrate fragment sequences, and (4) a signaling domain composed of fluorophore and quencher. In the absence of Pb^{2+}, the probe forms a stable hairpin structure such that fluorescence is completely quenched by intra-molecular linkage. However, in the presence of Pb^{2+} ion,

the substrate sequence is cleaved, and the strand containing the fluorophore is released by lack of sufficient binding affinity that is otherwise required to maintain the duplex. It is the strong quenching combined with high hydrolysis efficiency that allows the high sensitivity for the detection of Pb^{2+}. While this probe design utilizes intramolecular hybridization/dehybridization, it does not change the catalytic core of the DNAzyme, which maintains ribonucleotide cleavage efficiency and simplifies probe optimization. Theoretically, this probe design, which relies on intramolecular interaction, can therefore be used to engineer a prototype DNAzyme/substrate probe for any two given strands. In this paper, we report the design, molecular engineering, and optimization of the probe in terms of substrate length and linker, and we characterize the performance of the Pb^{2+} probe, challenging its detection limit down to the single Pb^{2+} ion.

Experimental Section

Chemicals and Reagents

All DNA synthesis reagents, including 6-fluorescein (FAM) phosphoramidite, 5′-4-(4-dimethylaminophenylazo)benzoic acid (Dabcyl) phosphoramidite, and 2′-*O*-triisopropylsilyloxymethyl-protected RNA monomers were purchased from Glen Research. Lead acetate and all reagents for buffer preparation and HPLC purification were from Fisher Scientific. The buffer used for the experiment contained 50 mM Tris-acetate at pH 7.2 and 100 mM NaCl.

Synthesis and Purification of Fluorescent-Labeled Oligonucleotides

To optimize the design of the hairpin probe, multiple candidates were designed and prepared (Table 2-1). All of them were synthesized using an ABI 3400 DNA/RNA

synthesizer (Applied Biosystems) at 1 μmol scale with the standard phosphoramidite chemistry.[96, 97] After complete cleavage, deprotection, and ethanol precipitation, the precipitates were dissolved in 0.5 mL of tetrabutylammonium fluoride solution, with shaking for 6 h at 35 °C. Then, desalting was performed with the 0.1 M triethylammonium acetate (TEAA, pH 7.0) as elution buffer. The HPLC analysis was performed on a ProStar HPLC Station (Varian Medical Systems) equipped with a fluorescence detector and a photodiode array detector. A C_{18} reverse-phase column (Alltech, C18, 5 μm, 250 mm × 4.6 mm) was used.

Determination of the Melting Temperature

Using a BioRad RT-PCR thermal cycler, thermal denaturizing profiles of each probe were measured to study the thermo stability of the designed probes. The substrate and enzyme molecular beacon chimer was used in the fluorescence-based method to determine the melting temperature. D_{10}, D_7, and D_5 were dissolved to the final concentration of 50 nM each in 50 nM Tris-acetate buffer, pH 7.2, with 100 mM NaCl, then annealed by heating to 90 °C for 5 min and subsequently cooled to 4 °C in intervals of 1 °C. The sample was kept at target temperature for at least 1 minute after the temperature was reached to ensure that the sample was at the stated temperature. Upon melting, the leaving substrate fragment was dissociated from the 8-17 DNAzyme strand, resulting in an increased fluorescence signal. The fluorescence intensity of each MB was measured and plotted against the temperature from 90 °C to 4 °C to generate the melting temperature curve.

Hybridization Assay

The mechanism of applying hairpin sequences to monitor DNA cleavage is shown schematically in Figure 1. D_{10} was annealed to a final concentration of 200 nM using the same procedure performed in the melting temperature determination. The annealed sample was then taken to room temperature for subsequent assays. A 90-μL aliquot of the 100 nM hybridized DNAzyme/substrate solution was loaded into each well of a 96-well plate. A 10-μL aliquot of concentrated metal ion stock solution was then added to the DNA solution using an eight-channel pipette to initiate the cleavage reaction. The fluorescence intensity was recorded for 100 μL of buffer containing 50 mM Tris-acetate (pH 7.2), 100 mM NaCl, the 200 nM DNAzyme/substrate solution without lead, and the 100 nM DNAzyme/substrate solution with 100× concentrated lead contamination. The excitation and emission wavelengths were set to 473 and 520 nm, respectively. Signal enhancement was calculated using the equation $(F_{\text{cleaved}} - F_{\text{buffer}})/(F_{\text{annealed}} - F_{\text{buffer}})$, where F_{cleaved} corresponds to fluorescence signals from the dissociation of this fluorescence strand in the presence of Pb^{2+}, F_{annealed} stands for the fluorescence signals from the hairpin probes without cleavage, and F_{buffer} represents the fluorescence signals of buffer.

Data Acquisition and Quantification

Substrate fluorescence detection was performed with a Tecan Safire microplate reader with 96-well plates. The excitation laser wavelength was set at 473 nm, and the emission wavelength was set at 520 nm, respectively, to monitor the fluorescence of FAM. Data quantification was performed in the XFluor program. For each experiment, 90 μL of the D_{10} solution was placed in the well, and the fluorescence of the sample was

measured immediately as $F_{annealed}$. Then, 10 µL of concentrated Pb^{2+} solution was added, followed by a 10-min incubation at room temperature. The fluorescence was taken, and then the solution in the well was collected and heated to 90 °C for 5 min. The fluorescence was measured again as $F_{cleaved}$. RNase free water was used as the internal standard to minimize the difference between each scan. Other metal salts used included the following: Mg^{2+}, Ca^{2+}, Sr^{2+}, Ba^{2+}, Mn^{2+}, Fe^{2+}, Co^{2+}, Ni^{2+}, Cu^{2+}, Zn^{2+}, Cd^{2+}, and Hg^{2+}.

Single Pb^{2+} Reaction

We applied Nuclepore polycarbonate membranes (Fisher Scientific), which are used in filtration, to form reactors of femtoliter volumes. We used membranes with pore diameters of 5 µm. These pore sizes were uniform, and the material was confirmed in bulk studies to be chemically inactive for the enzymatic reaction in this work. The thickness was 6 µm, producing volumes between 110 and 200 fL for each vial. Liquid filling of nanoscopic volumes has been a difficult technological problem in many fields, including biological studies where micromanipulators coupled with microinjection have been employed. No less a problem in this study, it was impossible to fill the vials one-by-one since we were simultaneously studying more than 100 vials. Therefore, the techniques applied here combined ultrasonic vibration with vacuum degassing.[98] We used rhodamine 6G dye solution to test this procedure. From the fluorescence image, we concluded that this procedure ensured that this surface was filled with the desired solution. The membrane was put onto a glass slide, and a small drop of the D_{10}/Pb^{2+} solution was added onto the top of the membrane. A very thin quartz coverslip (0.08

mm) was placed on the top to cover the liquid-filled vials. The polycarbonate was sandwiched between two quartz plates to create the vials. A tight seal was expected to form between the glass slides and the quartz coverslip. The quartz coverslip prevented any evaporation from these small vials and prevented mixing among the vials during the monitoring of the enzyme reactions.

Results and Discussions

Design and Optimization of Unimolecular Probe

Lead-dependent, site-specific cleavage of RNA has been the focus of many research endeavors.[99] We have designed a new probe for the Pb^{2+}-initiated catalytic reaction. We analyzed the 8-17 DNAzyme profile and designed a hairpin-structured Pb^{2+} probe. This 8-17 DNAzyme preformed the catalytic cleavage reaction with a two-step mechanism. Product analysis by MALDI-MS demonstrated that Pb^{2+} first catalyzed the cleavage reaction of the 8-17 DNAzyme by the formation of a product containing 2′,3′-cyclic phosphate. In a second catalytic reaction, Pb^{2+} further hydrolyzed the 2′,3′-cyclic phosphate. To increase the cleavage reaction efficiency, we constructed a hairpin structure lead probe with the substrate in close proximity to the DNAzyme, ensuring hybridization efficiency. With this design structure, the lead binding pocket was well formed before the target Pb^{2+} was added, thus increasing the apparent cleavage efficiency.

To maximize probe performance, the design of the probes needed to be optimized, including the length of linker between the catalytic and substrate domains and the design of the leaving substrate fragment. The design of the leaving substrate fragment is especially critical because it requires a sequence that is long enough to

form a stable duplex with the 8-17 DNAzyme sequence domain, but short enough to be dissociated well after the hydrolysis reaction. To accomplish this, we investigated varying the substrate sequences by measuring background fluorescence and melting temperature of the hairpin structures to compare hybridization efficiency and by using gel electrophoresis to compare hydrolysis efficiency (Figure 2-4).

To implement this plan, we designed probes containing 5, 7, and 10 base-paired leaving sequences, termed D_5, D_7 and D_{10}, respectively. No probe was designed containing a longer substrate because dissociation with a base pair in excess of 10 would, most likely, not have been favorable by its strong binding effect.[100] As shown in Figure 2-3, the fluorescence background of the probes without Pb^{2+} was significantly reduced with increasing numbers of base pairs. The low background is explained by the fact that probes can have quenched fluorescence signal only when they form stable hairpin structures. In the presence of Pb^{2+}, the stable hairpin structures bind the ions, switching into active state to catalyze the hydrolysis reaction. Thus, D_{10}, which had the lowest fluorescence background, still possessed the maximum efficiency in catalytic reaction, giving an approximate 16-fold signal enhancement when the Pb^{2+} was added. This signal enhancement is outstanding and much higher than the previously reported 4-fold enhancement with single quencher design or the 6-fold with a dual quencher design. The reduced background can be easily explained by the enhanced duplex stability resulting from intramolecular hybridization. As noted above, such duplex stability is achieved if fluorophore and quencher are in close proximity, and, in our design, quenching efficiency is well correlated to duplex stability, as defined by thermo denaturing profile. The T_m of D_5 was only 45 °C, while that of D_{10} is increased to 54 °C

(Table 2-2). The T_m of unlinked DNAzyme and its substrate is only 34 °C, which is slightly above room temperature. Since, as just noted, our design correlates quenching efficiency to duplex stability, this enhanced stability is quite significant because, at room temperature, a stable duplex of DNA would not be formed with such a high percentage if the two DNA probes were not linked in this novel unimolecular design.

This enhanced stability of duplex also resulted in improved hydrolysis reaction. This was first demonstrated by the cleavage reaction, which was detected within 2 min through fluorescence measurement, much faster than the previous design. Second, increased turnover numbers were calculated from the kinetics study. This result indicates the presence of a large amount of well-formed lead binding pockets, which, in turn, helped improve metal ion binding to D_{10}. Therefore, the increased hybridization efficiency, which naturally accompanies intramolecular interaction positively, correlates to the apparent increase in reaction rate. According to the result obtained from denaturing PAGE-gel electrophoresis (Figure 2-4), only D_{10} could show an efficient cleavage reaction over the others.

Characterizing the Probe with Analytical Parameters

To further obtain the full profile of the performance of D_{10}, we determined the dose response, reaction kinetics, calibration curve, and limit of detection. Figure 2-5 shows the full profile of dose-dependent fluorescence signal enhancement and the linear response in the presence of a low concentration of Pb^{2+}. According to the full profile (Figure 2-3), D_{10} can have up to a 20-fold signal enhancement with canalization of Pb^{2+} ions over the background with no Pb^{2+} canalization. This large signal enhancement

allows us to detect Pb^{2+} within a large dynamic range of nanomolar concentration with excellent detection limit, approximately 3 nM (3σ/slope). Such a low limit of detection is about 167 times better than that previously reported and 1600 times greater compared to the Pb^{2+} detection limit obtained from atomic spectroscopy, which was 4.8 μM.[101] Using the EPA standard for maximal lead contamination of drinking water at levels higher than 15 ppb Pb^{2+}, D_{10}, with its dynamic sensitivity range, can easily function well within that metric. In addition to the excellent sensitivity of D_{10}, this probe also showed fast kinetics in cleavage reaction (Figure 2-4). According to our investigation, it took much longer to reach this plateau (more than 30 min (data not shown)) in the case of the bimolecular approach (8-17 DNAzyme and its substrate). The superior performance of D_{10} can be attributed to several factors associated with the molecular beacon-based sensing strategy, i.e., where an intramolecular interaction, as opposed to an intermolecular interaction, is brought between DNAzyme sequence and leaving substrate fragment. First, since D_{10} mostly remains in the binding-active state, the probe itself binds Pb^{2+} very strongly in a short period of time. Second, the probe design allows very low background fluorescence or background variation, which produces high signal increases. Finally, and probably most unique, the signal can be amplified through fast turnovers of Pb^{2+} to react with multiple D_{10}, thus driving sensitivity up with fast dynamic response.

One of the most significant features of the DNAzyme-based metal probe is the excellent selectivity. This selectivity of artificial nucleic acid sequences to their targets derives from the unique secondary configurations enabling the probes to discriminate

nontargets. 8-17 DNAzyme also possesses the selectivity needed to distinguish Pb^{2+} out of nine competing bivalent ions. Thus, to demonstrate the excellent selectivity of D_{10} for Pb^{2+} against other metal ions, the fluorescence signal changes of nine competing divalent metals at concentrations of 10, 5, and 1 μM were obtained (Figure 2-5). As expected, they induced little to no fluorescence change, whereas some metals induced strong quenching to FAM, such as Cu^{2+}, Fe^{2+}, and Hg^{2+}. This result indicates that the intramolecular engineering of D_{10} did not affect the selectivity of Pb^{2+}.

Single Pb^{2+} Ion Reaction

According to the preliminary investigation, D_{10} is a highly sensitive and selective probe for Pb^{2+}-participating reactions. To further challenge the limit of D_{10}'s detection capability, we designed a single Pb^{2+} detection scheme using a femtoliter-well reactor. When a single Pb^{2+} remains inside such a reactor long enough to catalyze the cleavage reaction, a significant amount of fluorescent product can be produced for sensitive detection. We used membrane holes of approximately 5 μm in diameter, which contained a volume of 120 femtoliter. When it contained a single Pb^{2+}, the concentration was about 14 pM, which was well below the limit of detection of D_{10}. We employed a Pb^{2+} concentration (3.5 pM) by an amount statistically filling only 25% of the vials to minimize the chance that there would be more than 2 Pb^{2+} per single vial. The fluorescence signal was recorded using D_{10} only as a negative control (200 nM). We recorded the signal enhancement using D_{10} with Pb^{2+} as the sample. The obtained result is summarized in Figure 2-7. Single-ion reaction was monitored every 10 s for

1400 s. Since each image contained about 30−60 vials in most of the experiments, the fluorescence signal of each vial was analyzed, and a reaction rate curve was constructed. When the membrane vials were filled with only the D_{10} solution, we did not observe any significant fluorescence intensity change during the monitoring. This means that the D_{10} can form a stable hairpin structure without significant surface interaction. The probe was still stable, and no fluorescence increase was observed over a short period of time. After that, we added the desired amount of Pb^{2+} and continued to monitor the fluorescence. In contrast to the blank sample containing only D_{10}, we could now observe three typical patterns of fluorescence increases from the Pb^{2+}-treated samples in membrane holes: negligible, slight, and large fluorescence changes (blue, red, and black, respectively). By the distribution of such different reaction rates, it was demonstrated that most fluorescence enhancement originated from the least number of membrane pores. However, most of the fluorescent pores showed only limited fluorescence enhancement. We also performed the single-ion reaction kinetics inside polycarbonate membrane vials. By fluorescence enhancement real-time monitoring in specific holes, Figure 2-8 shows that the negligible increase of fluorescence came from the fluctuating fluorescence of the D_{10} probe, most likely as a result of local heating by the laser. The slight increase of fluorescence was from hydrolysis reaction by single Pb^{2+} in vials. We therefore concluded that the differences in fluorescence enhancement must have been correlated to the presence or absence of Pb^{2+} in the holes. We believe that the fluorescence increase was from hydrolysis reaction upon the addition of Pb^{2+}. Interestingly, despite the low concentration of Pb^{2+} ion, D_{10} was still able to bind the

single target referring to 14 pM and, as a result, generate a detectable fluorescence signal under the microscope. In addition, the fluorescence signal reached a plateau in a relatively short amount of time (less than 15 min).

Summary

We have demonstrated a highly sensitive and selective DNAzyme-based Pb^{2+} probe with DNA hairpin structure for Pb^{2+}-catalyzed reaction, leading to the ability to monitor a single Pb^{2+} in solution by means of fluorescence detection. Specifically, in our system, the leaving substrate fragment is labeled with a fluorophore, and an 8-17 DNAzyme sequence is labeled with a quencher. The hairpin structure links these two strands using poly T, which brings the quencher into close proximity with the fluorophore in the inactive state. The intramolecular linkage of the two strands assures efficient quenching of the fluorophore's fluorescence, surpassing the background. Upon reaction with Pb^{2+}, however, the leaving substrate fragment is cleaved at the RNA site by the enzyme, releasing a fluorescent fragment for detection. We have achieved a 16-fold increase of fluorescence intensity. This intramolecular design maintains a quantifiable detection range from 3 nM to 20 μM. We further demonstrated that this probe can be used to detect single Pb^{2+} by having one Pb^{2+} in a femtoliter reactor with sufficient substrate and about 15 min of reaction time. We believe that this probe could provide a simple and cost-effective, yet rapid and sensitive, measurement tool for Pb^{2+} detection. Given this degree of sensitivity and selectivity, our molecular engineering design may prove useful in the future development of other nucleic acid based probes for toxicological and environmental monitoring.

Table 2-1 Names and sequences used in Chapter 2. a rA is the RNA monomer. All synthesis was done with ABI synthesizer. The DNA/RNA chimers were purified by HPLC.

Name	Sequences
D_{10}	5′-/Dabcyl/-TATCTCTTCTCCGAGCCGGTCGAAATAGTGAGTTTTTTTTTTACTCACTATrAGGAAGAGATA-/FAM/-3′
D_7	5′-/Dabcyl/-ATCTTCCGAGCCGGTCGAAATAGTGAGTTTTTTTTTTACTCACTATrAGGAAGAT-/FAM/-3’
D_5	5′-/Dabcyl/-ATTCCCCGAGCCGGTCGAAATAGTGAGTTTTTTTTTTACTCACTATrAGGAAT-/FAM/-3’

Table 2-2 Comparison of melting temperature and fluorescence enhancement. D_5 shows the lowest melting temperature and signal-to- background ratio. D_{10} has the highest melting temperature and is therefore the most stable.

Hairpin Sequences	Tm (°C)	Signal/Background ratio
D_5	45	4
D_7	48	7
D_{10}	54	16

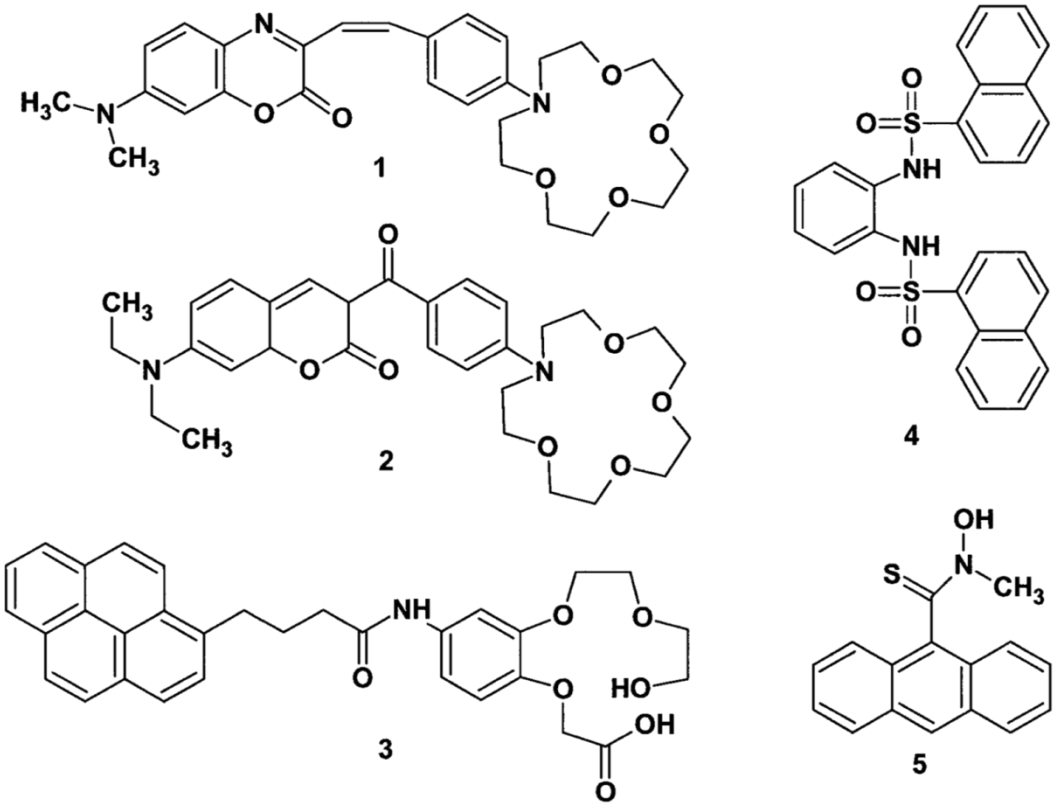

Figure 2-1. Examples of fluorescent organic chelator-based Pb^{2+} sensors.

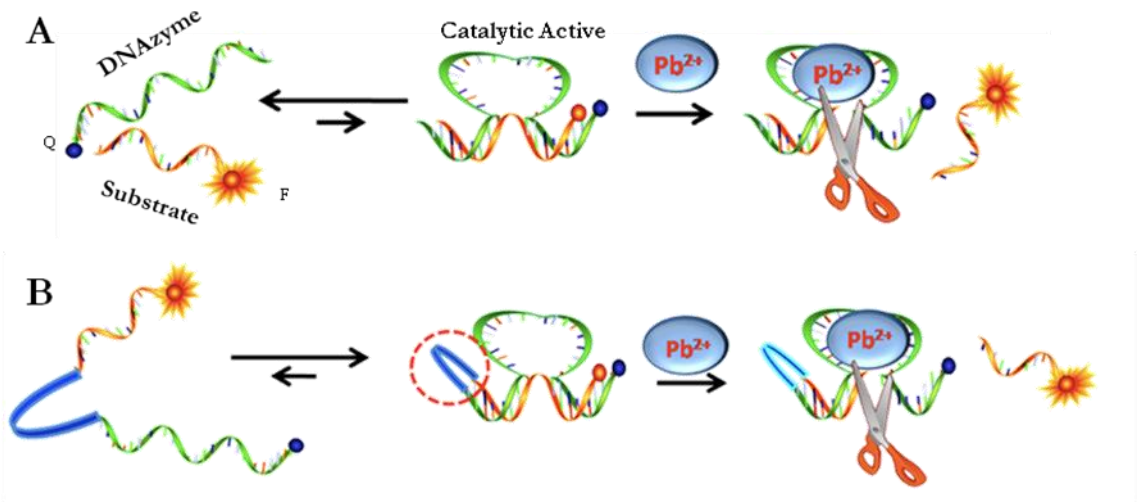

Figure 2-2. Schematic of the hairpin-structured unimolecular probe working principle. DNAzyme-based Pb^{2+} probe and its working principle. A) the 8-17 DNAzyme strand, which is labeled with a quencher, and substrate, which is labeled with a fluorophore, hybridized together in Tris-acetate buffer. After lead-induced cleavage, a 10-mer ssDNA is released which induces the fluorescence enhancement. B) The original substrate and enzyme were linked together as a hairpin structure by poly-T linker. The hairpin structure tends to maximize the hybridization efficiency.

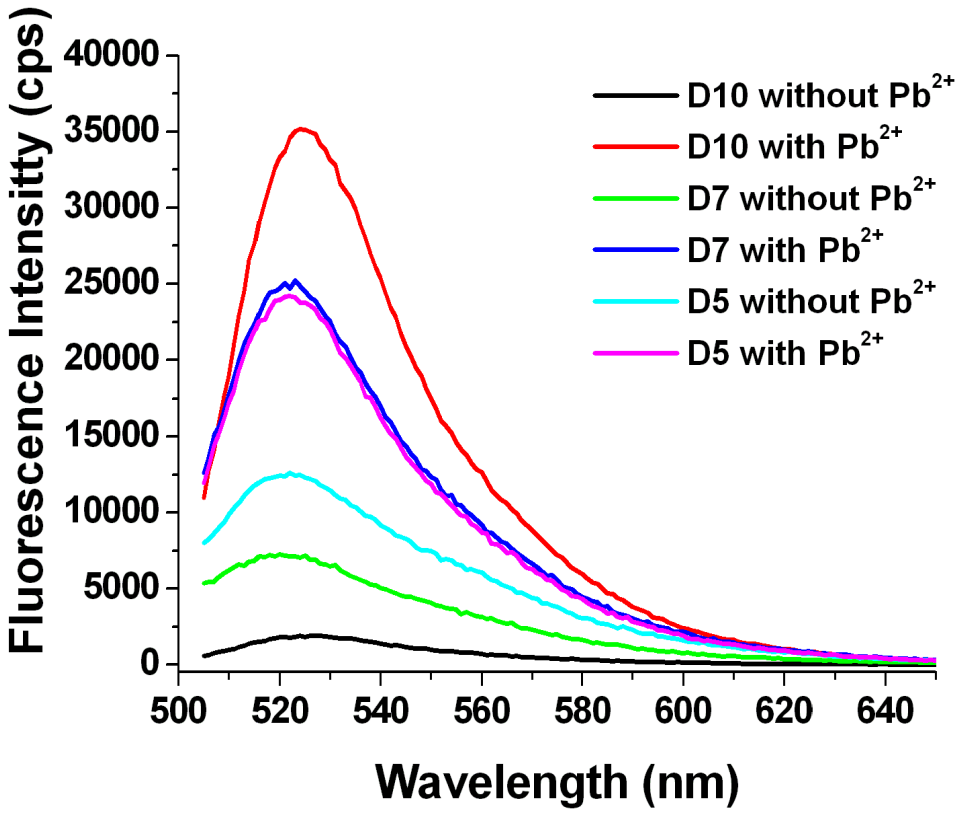

Figure 2-3. Fluorescence signal comparison for probe optimization.The Pb^{2+} sensor was in tris acetate buffer (pH 7.2) with 100 mM NaCl; the image was scanned 10 min after addition of metal ions. The five base-paired D_5 (green) gave the highest background fluorescence; meanwhile, the D_{10} (black) showed the lowest background. After a 10 min incubation, D_{10} showed a higher fluorescence signal (red) than either D_7 or D_5.

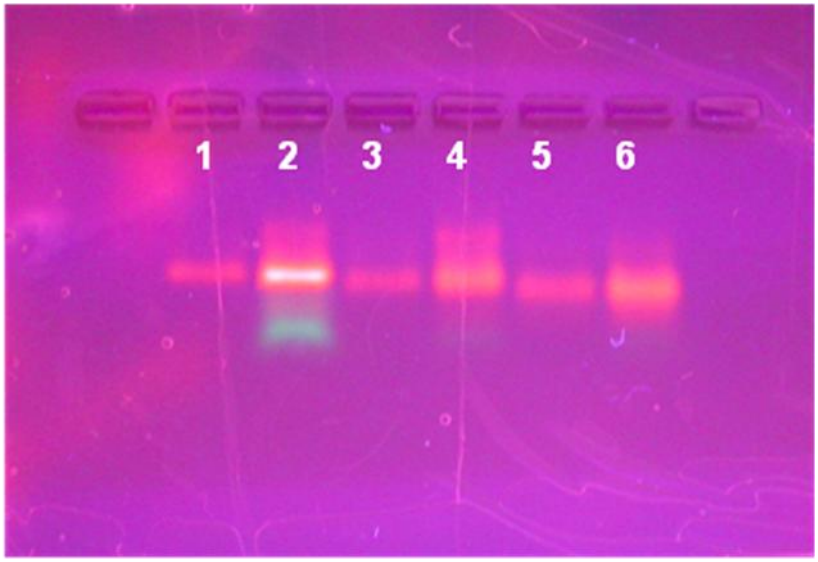

Figure 2-4. Characterization of substrate cleavage by DNAzyme using agarose gel.The Pb^{2+} sensor was in Tris acetate buffer (pH 7.2) with 100 mM NaCl; the image was scanned 10 min after addition of metal ions. Biochemical assay of the D_5, D_7, and D_{10} DNAzymes. Lanes 1, 3, 5: D_{10}, D_7, and D_5, respectively; lanes 2, 4, 6: 10 min after adding Pb^{2+} to the D_{10}, D_7, and D_5, respectively. The upper and lower bands are uncleaved and cleaved product, respectively.

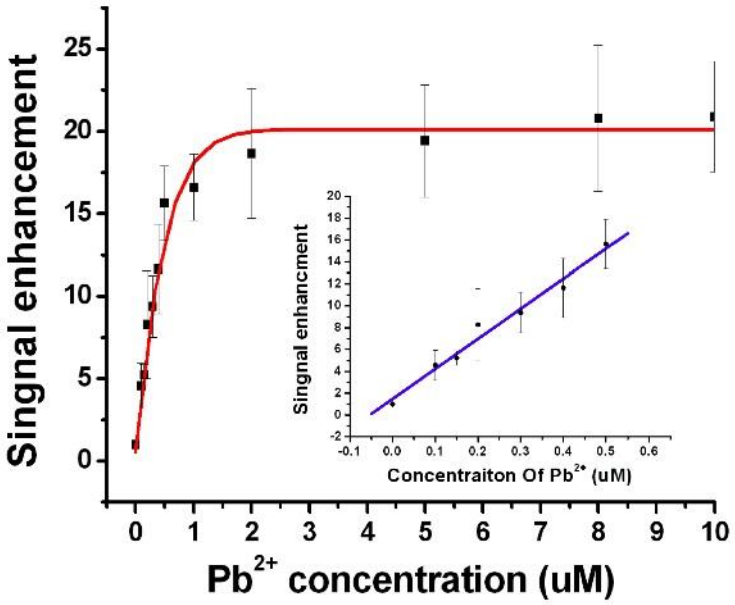

Figure 2-5. Fluorescence enhancement over background fluorescence at varying Pb^{2+} concentrations. The DNAzyme sensor concentration was 200 nM, and the buffer contained 50 mM Tris-acetate (pH 7.2) and 100 mM NaCl. (Inset) Probe responses to low concentrations of Pb^{2+}. The data was calculated from 3 parallel sets of measurement, error bar was calculated as standard derivation.

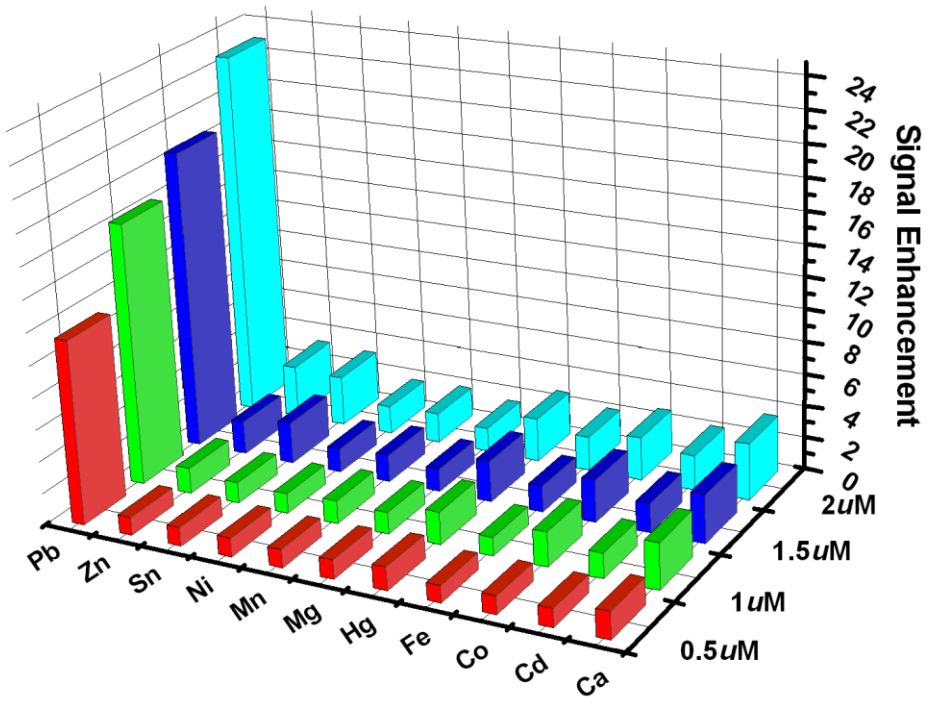

Figure 2-6. Selectivity of the Pb^{2+} probe sensor. Sensor responses to all competing metal ions at four concentrations (10, 5, 2, and 0.5 μM) were tested. The reaction time was 10 min.

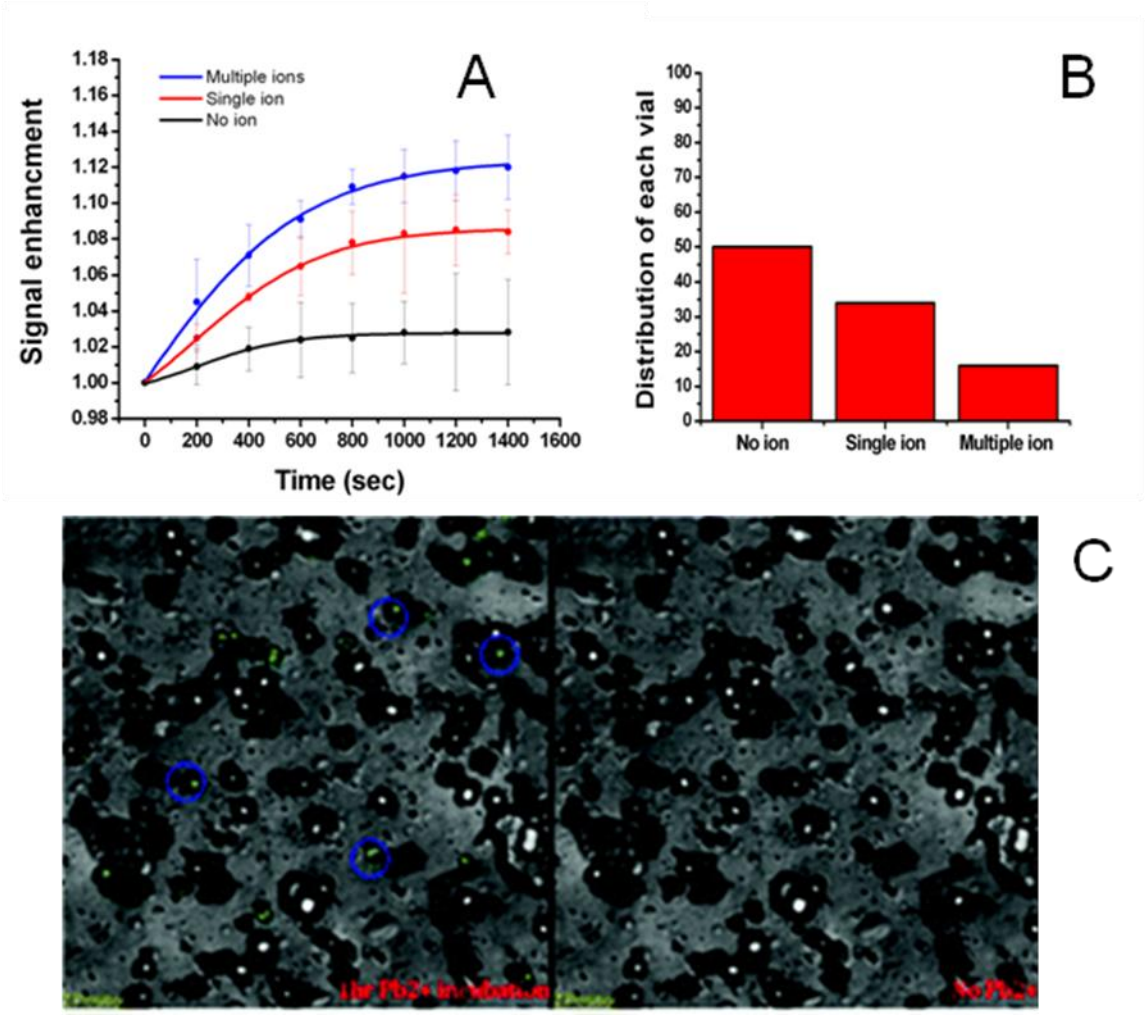

Figure 2-7. Single-ion reaction kinetics inside polycarbonate membrane vials. A and B) Individual Pb^{2+} ions were trapped inside membrane holes with the D_{10} solution. C) The membrane picture after 1 h Pb^{2+} incubation and the membrane picture without Pb^{2+} incubation. The blue line in (A) represents the dots in the blue circle in (C). All the other bright dots in (C) were recorded to the red line in (A). All the dark dots are represented by the black line in (A). The fluorescence enhancement was monitored over time. The background-corrected intensity in each vial has been normalized.

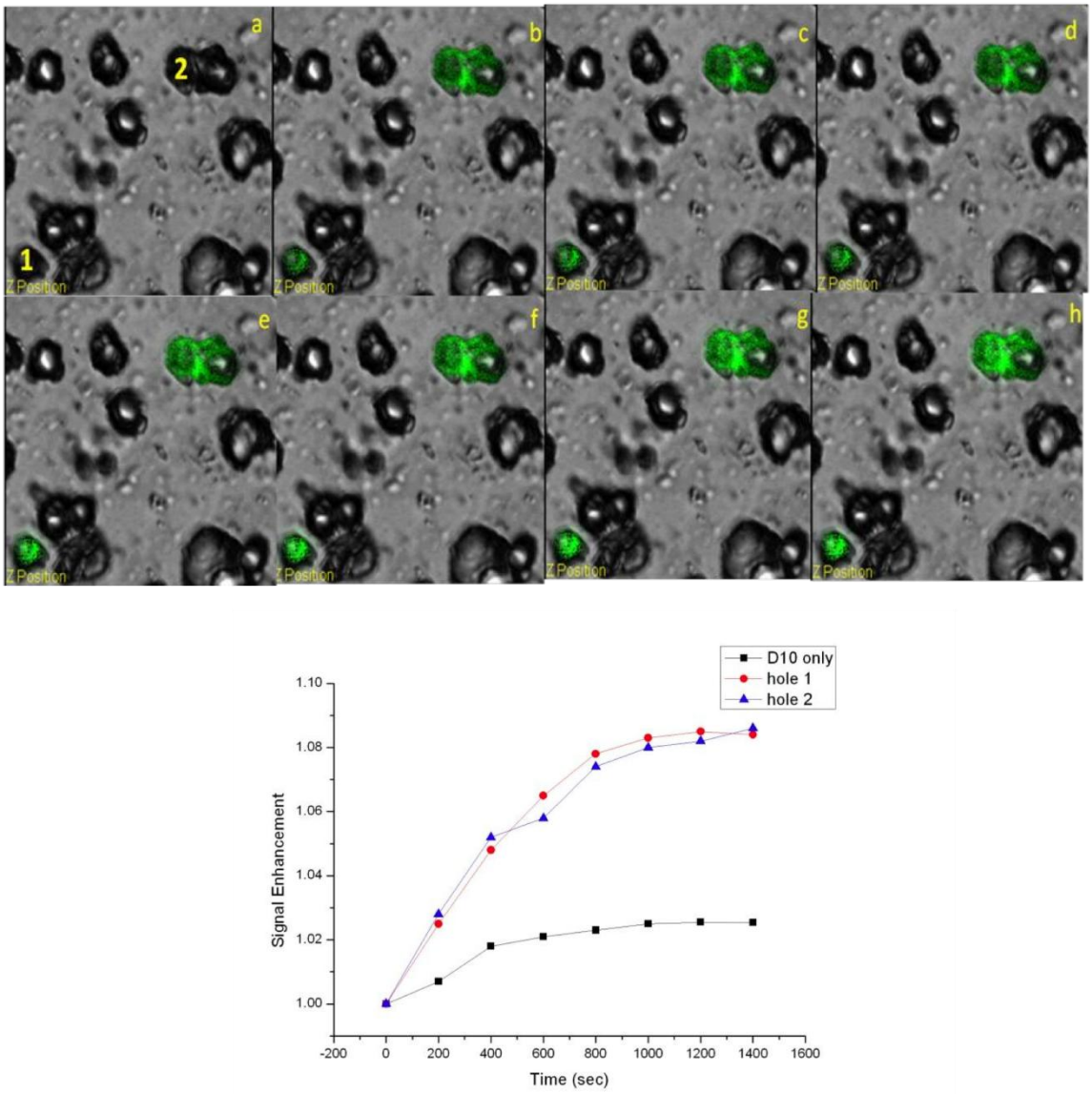

Figure. 2-8 Single-ion reaction kinetics inside polycarbonate membrane vials. A-H: Individual Pb^{2+} ions were trapped inside membrane holes with the D10 solution at different time interval: 0sec, 200sec, 400sec, 600sec, 800sec, 100sec, 1200sec, 1400sec. Hole 1 & Hole 2 fluorescence enhancement were recorded and plotted.

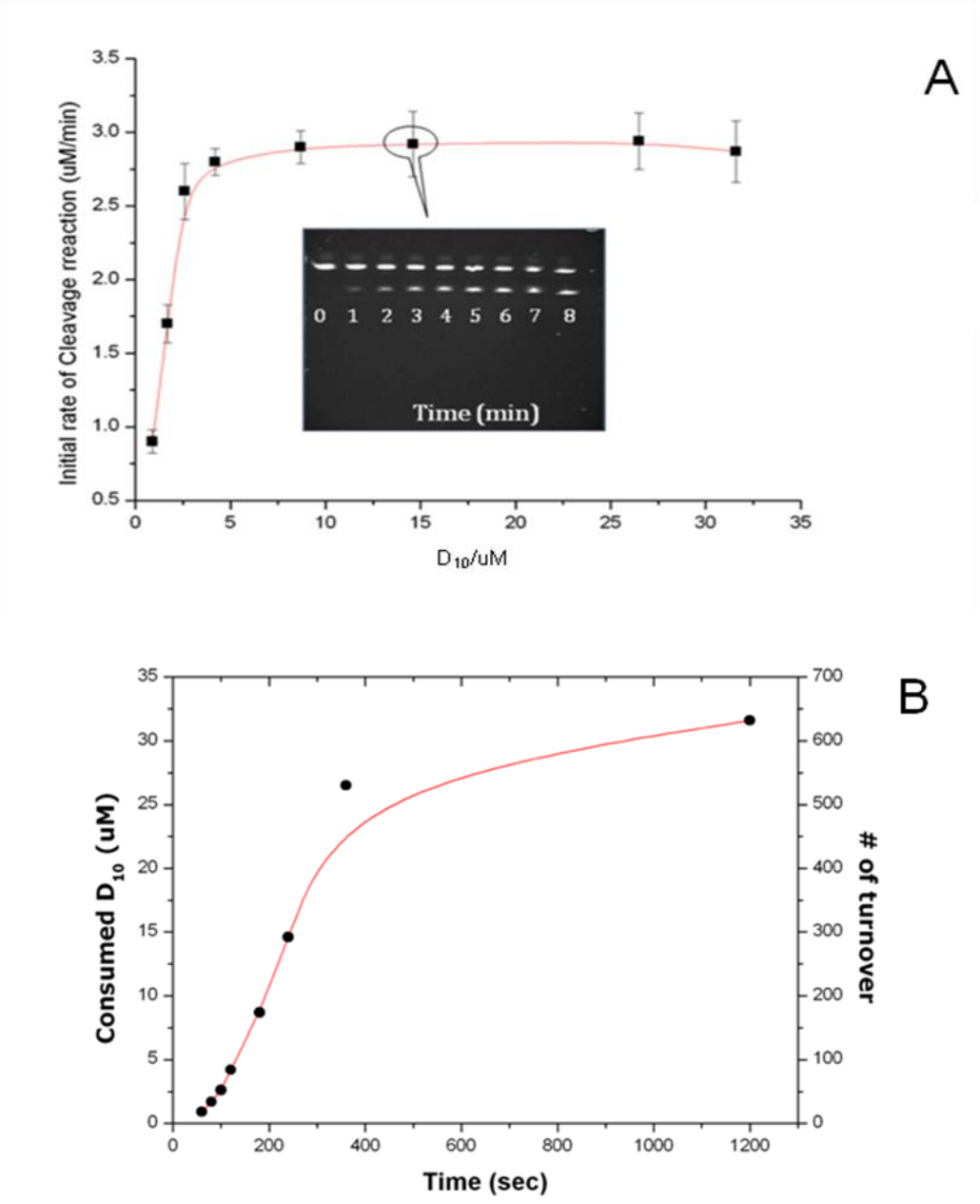

Figure 2-9. Catalytic activity of Pb^{2+} on D_{10} cleavage,A)The initial rate of cleavage of substrate D_{10}. a: [Enzyme]active = 0.02 μM. The line represents a nonlinear fit to the data using the Michaelis−Menten expression. (Inset) Analysis of extent of conversion of fluorescently labeled substrate DNA (20 μM) by PAGE. The upper band represents uncleaved substrate DNA, and the lower band represents the cleaved fragment containing the fluorescent label. B) Catalytic activity of Pb^{2+} on D_{10} cleavage. Confirmation of multiple turnovers by the catalysis reaction at room temperature. The line represents the calculated substrate consumption based on the integrated Michaelis−Menten equation

using the values obtained from (a), showing that the maximal turnover numbers could reach over 600.

CHAPTER 3
DNAZYME FOR TELOMERASE STUDY: A NEW WAY FOR EARLY CANCER DIAGNOSIS.

Telomerase

Telomerase is a unique ribonucleoprotein reverse transcriptase that catalyzes the synthesis of specific DNA sequence repeats ("TTAGGG" in all vertebrates) to the 3’ ends of eukaryotic chromosomes to protects linear ends of chromosome against constant loss of important DNA. Telomerase is a reverse transcriptase, uses its own RNA template when elongating telomeres, which are shortened after each cell division. As a result, every time the chromosome is copied, only 100-200 nucleotides are lost, which causes no damage to the organism's DNA.

Targeting Telomerase as a Unique Cancer Marker

Short telomeres and high expression of telomerase has been demonstrated in most of human cancer cells, compared to the absence of telomerase in most normal somatic cells.[102] With the infinite elongation of telomere by telomerase, the chromosome ends will never be shorten enough no matter how many cell divisions. Therefore, the cell death is prevented as long as all the conditions for telomere duplication are favorably met. Cancer cells keep immortal life because telomerase allow them to divide literally forever, which is the reason that they form tumors. In past decades, telomerase has gained growing interests as a potentially sensitive biomarker for early cancer diagnosis, prognosis or in monitoring as an indication of residual disease. For the discovery of how chromosomes are protected by telomeres and the enzyme telomerase, the Nobel Prize in Physiology or Medicine was awarded to Elizabeth Blackburn, Carol Greider and Jack Szostak in 2009.

As important cancer biomarker, telomerase activity has been observed in ~90% of human tumor,[103] suggesting that the immortality conferred by telomerase plays a key role in cancer development. In detail, telomerase protein has been found in 80% of lung cancers,[104] 75% of oral carcinomas,[105] 84% of prostate cancers,[106] 93% of breast cancers,[107] 85% of liver cancers,[108] 94% of neuroblastomas,[109] 95% of colorectal cancers,[110] and 98% of bladder cancers.[111, 112] Moreover, telomerase activity was recently confirmed in exfoliated cells found in the urine of bladder cancer patients.[113]

Several commercial available research assays such as telomeric repeat amplification protocol (TRAP) were applied to evaluate telomerase activity in vitro.[114] Only with few exceptions, these assays have shown that reactivation or upregulation of telomerase activity and its template RNA (hTR) and catalytic protein component (hTERT) are associated with all cancer types investigated. TRAP has been used extensively to study telomerase activity in uncultured and cultured samples of normal and tumor tissue from many cell types. After the first development of TRAP by Kim et al., Hirose and coworkers described a new quantitative and non-radioactive method, transcription mediated amplification (TMA), in conjunction with the hybridization protection assay (HPA), for telomerase activity.[115] Recent studies have focused on analyzing the expression level of telomerase components after the cloning[116] of genes encoding the components of the human telomerase complex including the telomerase RNA component (hTERC) that acts as a template to add telomeres to the ends of the chromosomes, telomerase reverse transcriptase (hTERT) and telomerase protein component 1 (hTEP1).[117] Fletcher et al. also developed a modified TRAP assay system in which telomerase in intact nuclei catalyses primer extention.[118]

DNAzyme-Based Catalytic Beacon for Telomerase Activity Study

To date, the most widely used and most sensitive telomerase detection assay is the polymerase chain reaction (PCR)-based telomeric repeat amplification protocol (TRAP). [119] [120] Although quite powerful, TRAP requires the use of DNA polymerases and is therefore susceptible to PCR-derived artifacts, [121] especially when screening compounds for telomerase inhibition. A number of PCR-free assays for telomerase activity, either based on direct probing [122] [123] or forming a sandwiched structure to the elongated strands, [124] have been developed over the past decade; however, the lack of an amplification mechanism has hindered most from achieving a sensitivity comparable to TRAP.

Here we report the development of a molecular sensor based on DNAzyme enzymatic cleavage function. We used a Pb^{2+}-specific DNAzyme as an active component for the analysis of telomerase activity. This hairpin molecule is engineered by an intramolecular assembly method and consists of four functional domains: 1) a DNAzyme catalytic sequence, 2) a primer with the ability for telomere elongation with trace amount of telomerase, 3) a poly thyme linker, and 4) a leaving substrate fragment generated through telomerization by telomerase enzyme, forming a dynamic G-quadruplex with the catalytic sequence. In the absence of Pb^{2+}, the probe forms a stable hairpin structure such that the reporter (molecular beacon) fluorescence is completely quenched by its intramolecular linkage between fluorophore and quencher. However, in the presence of Pb^{2+} ion, the telomere product sequence is cleaved, and the cleavage cascade will induce the fluorescence signal from its complementary reporter molecule (molecular beacon), while the fluorophore is released by lack of sufficient binding affinity that is otherwise required to maintain the beacon structure.

Theoretically, this probe design, which relies on intramolecular interaction, can be used to engineer a prototype DNAzyme/substrate probe for any two given strands. In this paper, we report the design, molecular engineering and optimization of the probe in terms of substrate length and linker, and we characterize the performance of the telomerase detection probe, challenging its detection abilities compared to the conventional TRAP assay.

Therefore, based on the ability of DNAzymes to initiate catalysis of lead ion (Pb^{2+}), we designed a unimolecular probe with DNA hairpin structure to monitor telomerase in solution by fluorescence detection. Upon reaction, DNAzyme will cleave its substrate at RNA site, releasing a fragment for detection with repetitive cycling for signal amplification. The resulting high sensitivity was achieved without losing selectivity of the intramolecular probe which maintains a quantifiable detection range from 0.1 μg to 20 μg and a selectivity of over 200-fold for cells containing telomerase over other normal cells. Based on these results, this probe could provide a simple, yet rapid and sensitive, measurement for telomerase detection.

Experimental Section

Chemicals and Reagents

All DNA synthesis reagents, including 6- Fluorescien (FAM) phosphoramidite, 5′-4-(4-dimethylaminophenylazo) benzoic acid, (Dabcyl) phosphoramidite, and 2’-O-Triisopropylsilyloxymethyl-protected RNA monomers were purchased from Glen Research. Lead acetate and all reagents for buffer preparation and HPLC purification were from Fisher Scientific. The buffer used for the experiment contained 50 mM Tris-Acetate at pH 7.2 and 100 mM NaCl.

Synthesis and Purification of Oligonucleotides

To optimize the design of the hairpin probe, multiple candidates were designed and prepared (Table 1). All of them were synthesized using an ABI 3400 DNA/RNA synthesizer (Applied Biosystems) at 1-μmol scale with the standard phosphoramidite chemistry. HPLC was performed on a ProStar HPLC Station (Varian Medical Systems) equipped with a fluorescence detector and a photodiode array detector. A C_{18} reverse-phase column (Alltech, C18, 5 μm, 250 × 4.6 mm) was used.

Determination of the Melting Temperature

Using a BioRad RT–PCR thermal cycler, thermal denaturizing profiles of each probe were measured to study the thermostability of the designed probes. The substrate and enzyme molecular beacon chimer was used in the fluorescence-based method to determine the melting temperature. $TeloD_{12}$, $TeloD_8$ and $TeloD_6$ were dissolved to the final concentration of 50 nM each in 50 nM Tris-acetate buffer, pH 7.2, with 100 mM NaCl, then annealed by heating to 90 °C for 5 min and subsequently cooled to 4 °C in intervals of 1 °C. The sample was kept at target temperature for at least 1 min after the temperature was reached to ensure that the sample was at the stated temperature. Upon melting, the leaving substrate fragment was dissociated from the 8-17 DNAzyme strand, resulting in an increased fluorescence signal. The fluorescence intensity of each MB was measured and plotted against the temperature from 90 °C to 4 °C to generate the melting temperature curve.

Cell Extraction

One normal cell line, HBE135, and two different liver carcinoma cell lines, M7617 and LH86, were used in experiments. LH 86, a novel human hepatoma cell line, is from a well-differentiated hepatocellular carcinoma tissue. HBE135, LH86 and M7617 cells

were cultured in Dulbecco's modified Eagle medium (DMEM) supplemented with 10% fetal bovine serum (FBS) (heat- inactivated) and 100 IU/mL penicillin-streptomycin at 37ºC in a humid atmosphere with 5% CO_2. Cells were harvested and washed twice with ice-cold phosphate-buffered saline (10 mM KPO_4, pH 7.5, 140 mM NaCl). Then cells were lysed in NP-40 lysis buffer (150 mM NaCl, 1% NP-40, 50 mM Tris-HCl, pH 8.0, and 5 mM EDTA) in the presence of proteinase inhibitor cocktail (Sigma) for 30 min on ice. Lysates were centrifuged at 14,000 rpm for 20 min at 4°C. The supernatant was stored at −80 °C in 20% glycerol and 100 mM NaCl. The protein content in the supernatant was measured using the Bio-Rad protein assay.

Telomerase-Mediated Primer Elongation

The reaction buffer was modified from [125], consisting of 20 mM Tris-HCl, 1.5 mM $MgCl_2$, 60 mM KCl, 1 mM EGTA, 0.05% Tween, and 50 μM nucleotide. To the reaction buffer, 0.15 nmol of probe and 1 μg of cell extract (protein) are added to generate the final reaction mixture. This reaction mixture is then diluted to a final volume of 50 μl and incubated for 1 h at 37°C in a PCR thermal cycler. Thereafter, the temperature is increased to 94°C for 5 min to deactivate telomerase and to terminate the elongation.

TRAP Assay

Telomerase extracts were prepared and analyzed as described.[126] Briefly, cells were washed in PBS and then lysed in ice-cold lysis buffer (10 mM Tris-HCl, pH 7.4,1 mM $MgCl_2$, 1 mM EGTA, 0.1 mM phenylmethylsulfonyl fluoride, 5 mM 2-mercaptoethanol, 0.5% CHAPS, 10% glycerol). All cell extracts were immediately frozen and stored at -80°C. Usually the whole-cell extracts were thawed immediately prior to the TRAP assay. First, extracts were centrifuged at 14000g for 30 min at 4°C,

then supernatants were transferred to a clean tube, and protein concentrations were measured by using the Bio-Rad protein assay kit. Finally, TRAP, which is a one-tube PCR-based assay, was performed,[102] as described below.

Briefly, the TS oligonucleotide (5'-AATCCGTCGAGCAGAGTT-3') served as both the telomerase template and the forward primer for the PCR. Telomerase activity in 5g of protein was measured by using incubation 1 hour at room temperature (25°C) for telomere extension followed by 34 cycles of PCR amplification (90°C, 90 sec; 50°C, 30 sec; 72°C, 45 sec; 94°C, 30 sec). Each TRAP assay included the following controls. Because telomerase contains a critical RNA template, a sample of each extract was treated with 1 unit of RNase A as a control for telomerase specificity. Every assay included a telomerase-positive and a telomerase-negative control extract. Each assay also contained an extract-free lane that contained only the reaction mixture to detect PCR amplification of primer dimers. Only assays in which all control lanes showed the expected results were included in this study. To test for inhibitors of Taq DNA polymerase that might be present in negative samples, mixtures of negative and positive extracts were tested for telomerase activity, by using a 1:1 ratio. Controls were done in which telomerase-positive extracts were mixed with lysis buffer also at a 1:1 ratio. As another approach to test for the presence of inhibitors, serial dilutions of the positive samples were done. Lysis buffer was used for dilution and the final volume was the same for all samples. There was no evidence of Taq DNA polymerase inhibitors. All telomerase reactions were done in a total volume of 50 µl, and was loaded on a 10% nondenaturing polyacrylamide gel, which was then electrophoresed for 1 hour min at 110 V followed by 85 min at 250 V. Gels were stained for 45 min in SYBRGreen I

(Molecular Probes) and analyzed by a Fluorimager SI (Molecular Dynamics). Usually telomerase signals were visible after 45 min. However, gels that were negative were stained longer and tested at different Fluorimager exposure ranges to increase sensitivity. Telomerase activity was manifested in this assay by the presence of a characteristic 6-bp ladder.[127]

Hybridization Assay

The mechanism of applying the TeloD9 hairpin sequence to monitor telomerase is shown schematically in Figure 3-1. TeloD9 was annealed to a final concentration of 200nM using the same procedure performed in the melting temperature determination. The annealed sample was then taken to room temperature for subsequent assays. An 80-µL aliquot containing 100 nM hybridized DNAzyme/substrate solution and 10X molecular beacon M_9 was loaded in each well of a 96-well plate. A 10-µL aliquot of concentrated telomerase stock solution was then added to the DNA solution using an eight-channel pipette to initiate the telomerization reaction, incubated at 37C for 30 minutes. Afterwards, a 10-µL aliquot of concentrated lead metal ion stock solution was added to the DNA solution to initiate the cleavage reaction. The fluorescence intensity was recorded for 100 µL buffer containing 50 mM Tris–acetate (pH7.2), 100 mM KCl, 100nM D9, 1µM M9 solution as three types: without telomerase, with telomerase, and telomerase with 50X concentrated lead contamination. The excitation and emission wavelengths were set to 473 nm and 520 nm, respectively. Signal enhancement was calculated using the equation $(F_{cleaved} - F_{buffer})/(F_{annealed} - F_{buffer})$, where $F_{cleaved}$ represents fluorescence signals from the dissociation of this fluorescence strand in the presence of Pb^{2+}; $F_{annealed}$ represents the fluorescence signals from the hairpin probes without cleavage; and F_{buffer} represents the fluorescence signals of buffer. Other metal

salts used included the following: Mg^{2+}, Ca^{2+}, Sr^{2+}, Ba^{2+}, Mn^{2+}, Fe^{2+}, Co^{2+}, Ni^{2+}, Cu^{2+}, Cd^{2+} and Hg^{2+}.

Gel-Based Activity Assay

Two μL TeloD9 samples were annealed in 50 mM Tris-acetate buffer containing 100 mM NaCl (pH 7.2). After taking a 5-μL aliquot out as a zero time point, Pb^{2+} was added to the remaining solution with a final concentration of 50 nM, and aliquots were periodically taken out at 60-second intervals. The TeloD9-only sample was also loaded on the gel to see the effect in the absence of telomerase alone, Pb^{2+} alone, and telomerase with Pb^{2+}. The cleaved and uncleaved substrates were separated by 20% denatured polyacrylamide gel electrofluorescence imaging, and the gel was analyzed by a fluorescence imager (FLA-3000G; Fuji, Tokyo, Japan) by exciting at 473 nm. Gels containing 20% polyacrylamide were run on a FB-VE10-1 electrophoresis unit (Fisher Biotech) at room temperature (200 V, constant voltage) for 50 minutes. The running buffer was TAE/Mg^{2+} buffer. After electrophoresis, the gels were scanned under a UV lamp.

Results and Discussion

Design and Optimization Probe for Catalytic Reaction for Telomerase Detection.

Several analytical procedures for the determination of telomerase activity were developed, including the TRAP that involves intensive PCR amplification or the functionalization of the telomeres with fluorescent labels.[128] We have designed a new probe for telomerase activity monitoring using Pb^{2+}-initiated DNAzyme catalytic reaction. Telomerase detection with this assay involves three basic steps (Figure 3-1). First, telomerase extracted from cancer cells are complexed onto their substrate oligonucleotides, which were annealed with 8-17 DNAzyme at 3’ end. These

oligonucleotide sequences serve as both the telomerase binding substrates (designated as TS) and the strands for partially helping 8-17 DNAzyme forming catalytic active tertiary structure. Using their intrinsic RNAs as templates, the bound telomerase can catalytically elongate the DNA strands in TTAGGG repeats in the presence of deoxyribonucleotide triphosphate (dNTP) monomers from a solution of the four dNTPs (i.e., dATP, dCTP, dGTP, and dTTP). The elongation product was able to recognize its complementary target (flanking binding arm at 5' end of 8-17 DNAzyme), contributing in formation of 8-17 DNAzyme catalytic active structure, followed by the cleavage of elongation substrate, while this probe went back to its initial state waiting for next round elongation. After the bound telomerase was removed with a sodium dodecyl sulfate (SDS) solution, we analyzed the cleavage product generated from above enzymatic amplification procedure using molecular beacon signal transduction mechanism. The molecular beacon would be opened upon cleavage product complementary hybridization, therefore released fluorescence signal. To increase the cleavage reaction efficiency, we constructed a hairpin structure telomerase probe with the substrate in close proximity to the 8-17 DNAzyme, ensuring total hybridization efficiency. With this design structure, the lead binding pocket was well formed, thus increasing the apparent cleavage efficiency.

To maximize probe performance, several design features must be considered. First, the length of the linker must be with appropriate length that once the primer is elongated, the product will reach a range that allows rapid hybridization with the DNAzyme and, hence, cleavage and release. Second, the primer must have higher binding affinity with telomerase than with 8-17 DNAzyme binding arm, which allows this

primer to be quickly recognized by the telomerase, easily dissociated from the DNAzyme binding arm in the presence of telomerase so that elongation can resume. Third, optimizing the length of 5'-end binding arm of DNAzyme depends on the nature of the telomere, which is fixed sequence (TTAGGG). To achieve suitable optimization by these requirements, we investigated varying the probe sequences (Table 3-2) by measuring background fluorescence and melting temperature of the hairpin structures to compare efficient structure formation by catalytic activity and by using gel electrophoresis to compare cleavage efficiency (Figure 3-2).

To implement this plan, we designed probes containing 6, 9, and 12 nucleotides telomere primer sequences, termed $TeloD_6$, TeloD9, and $TeloD_{12}$, respectively. No probe was designed containing a longer substrate because dissociation with a base pair in excess of 12 would, most likely, not have been favorable by its strong binding effect [129]; therefore, as a primer, it could not easily be dissociated for recognition by the complementary telomerase RNA template, resulting low efficiency of elongation. As shown in Figure 3-3, the fluorescence background from the telomerase detection using TeloD9 probes without Pb^{2+} was significantly reduced. In the presence of Pb^{2+}, the elongated duplex structures bind the ions, switching into active state to catalyze the cleavage reaction. Thus, TeloD9, with moderate length of primer, possessed the maximum efficiency in catalytic reaction, giving an approximate 15-fold signal enhancement when the Pb^{2+} was added. This outstanding signal enhancement in comparison to other candidates can be easily explained by enhanced telomerization efficiency based on the flexibility between two binding events: 1) the intro-molecular hybridization between primer and DNAzyme and 2) the intermolecular binding between

primer and telomerase elongation template. As noted above, since such duplex stability is achieved while the primer is extended by telomerase enzyme, the product will soon recognize its complementary strand from DNAzyme 5' end biding arm, followed by forming the intramolecular duplex. In the presence of Pb^{2+} ions, the product will be cleaved by DNAzyme and dissociated from 5' end binding arm, and, in our design, signal transduction is well correlated to duplex stability, as defined by thermo denaturing profile.

Since the T_m of unlinked DNAzyme and its substrate is only 36°C, which is closer to room temperature compared to the T_m of TeloD9 (60.3ºC). Given the T_m of TeloD9 (60.3ºC) is much higher, the enhanced stability of duplex is quite significant because, at room temperature, stable duplex of DNA would not be formed with high percentage if the two DNA probes are not linked in a unimolecular design.

This enhanced stability of duplex also resulted in improved cleavage reaction. The used of DNAzymes for amplified analysis of telomerase also reveals several advantages. This was first demonstrated by the molecular beacon fluorescence signal, which was detected within 5 minutes through fluorescence measurement, much faster than a whole PCR process (several hours). Second, increased turnover numbers were calculated from the kinetic study. This result indicates the presence of a large amount of well-formed lead binding pockets due to amplified generating of initial state of TeloD9, which, in turn, helped improve metal ion binding to TeloD9. Third, this probe design provided a novel form of amplification for the potential of detecting trace amount of telomerase in biological sample. Therefore, this new assay rivals the sensitivity and convenience of the conventional PCR-based method of telomerase detection.

According to the result obtained from fluorescence enhancement through molecular beacon opening due to telomeric DNA cleavage (Figure 3-2), TeloD9, when compared to the other candidates, showed efficient cleavage reaction after telomerization. Unlike $TeloD_{12}$ and TeloD9, $TeloD_6$ showed low fluorescence enhancement due to the low telomerization efficiency, 6 nucleotides could be too short to produce telomerase polymerization product, the incomplete hybridization did not favor efficient hydrolysis reaction, therefore the cleavage couldn't be resumed.[130] Similarly, noticeable cleavage was not observed for $TeloD_{12}$, too. In contrast, TeloD9, in the absence of Pb^{2+}, showed low fluorescence background signal, and upon the addition of Pb^{2+} (10 μM), the fluorescence enhancement was observed within 5 minutes. This experiment shows that the increased fluorescence was indeed a result of DNAzyme-catalyzed cleavage with Pb^{2+} as a cofactor.

Characterizing the Probe with Analytical Parameters

To further obtain the full profile of the performance of TeloD9, we determined its dose response, reaction kinetics, calibration curve, and limit of detection (LOD). Figure 3-4 shows the full profile of dose-dependent fluorescence signal enhancement and the linear response in the presence of a low concentration of lead ion. According to the full profile (Figure 3-3), TeloD9 can have up to 16-fold signal enhancement. This large signal enhancement allows us to detect telomerase within a large dynamic range of microgram concentration with low detection limit, approximately 0.1ug protein in cell extracts. In addition to the excellent sensitivity of TeloD9 toward telomerase, this probe also showed fast kinetics in cleavage reaction. As shown in Figure 3-5, the signal reached a plateau within 20 min. According to our investigation, it took much longer to reach this plateau (more than 30 minutes (data not shown)) in the case of the

bimolecular approach (8-17 DNAzyme and its substrate (start with telomere primer)). The superior performance of D_9 can be attributed to several factors associated with the molecular beacon-based sensing strategy, i.e., bringing intramolecular, instead of intermolecular, interaction between the DNAzyme sequence and substrate fragment sequence. First, the design of probe TeloD9 results in very high efficiency of telomerization elongation, which prepares it for binding in the active state since the TeloD9 elongated sequence mostly remains in the binding-active state. Second, the probe binds strongly and rapidly to Pb^{2+}. Finally, and probably most unique, once the primer is elongated in the presence of telomerase enzyme, the signal can be amplified through fast turnovers of telomerase enzyme and Pb^{2+} to react with multiple TeloD9, thus driving sensitivity up with fast dynamic response.

One of the significant features of the DNAzyme-based telomerase sensor is its excellent selectivity, which derives from unique secondary configurations enabling the probes to discriminate non-targets. With this capability, TeloD9 also possesses the selectivity needed to discriminate between healthy normal cells and cancer cells. Thus, to demonstrate the excellent selectivity of TeloD9 for cancer cells against normal cells, the fluorescence signal changes of three types of cell lines at different concentrations were obtained (Figure 3-6). As expected, they induced little to no fluorescence change, indicating that the intramolecular engineering of TeloD9 did not affect the selectivity for telomerase enzyme.

Characterizing Probe Activity with PAGE-Based Assay.

To further demonstrate the advantages of our probe design, we used a PAGE-based assay to assess the performance of the fluorescent probe in the presence of telomerase with TeloD9 in Tris-acetate buffer at pH 7.2. For multiple turnover kinetics

analysis, 20 μM TeloD9 was incubated with 2 μg protein at room temperature for a total of 20 min in vitro reaction. In the assay, aliquots were periodically removed, and the reaction was terminated by the addition of formamide (90%, v/v) containing 15 mM EDTA [131]. The cleaved DNA fragments were separated by polyacrylamide gel electrophoresis, and the extent of conversion was quantified using fluorescence imaging. K_m and k_{cat} values were obtained by fitting velocity of cleavage against substrate concentration using the equation $V = k_{cat}\cdot[S]/(K_m + [S])$. All reactions were terminated and processed as described in the previous section.

The multiple turnover results demonstrated our probe with the advantage of enzymatic signal amplification ensuring the ability for low detection of telomerase protein, which has potential applied in early cancer diagnosis. The TeloD9 and telomerase observed Michaelis−Menten kinetics under conditions where [protein] ≫ [TeloD9], which was corresponding to multiple turnovers kinetics. Under these conditions, the calculated values of V_{max}= 0.97 μM/min and K_m is 0.71 μM, and the catalytic turnover ceased by complete consumption of TeloD9. Specifically, in the presence of 2 μg protein, 20 μM TeloD9 was cleaved, resulting in over 700 catalytic turnovers of the DNAzyme. In this experiment, Pre-hybridization of the TeloD9 probe structure is not required. Thus, there is no need to heat up or cool down TeloD9 before hybridization and subsequent cleavage by introduction of Pb^{2+}.

Summary

In conclusion, we demonstrated a PCR-free, yet highly sensitive and selective DNAzyme-based telomerase sensor, with the formation of duplex between Pb^{2+}-specific DNAzyme fragment and telomere primer, which causes efficient and specific cleavage

of telomere target after telomerase elongation. We demonstrated that this probe could provide a simple and cost-effective, yet rapid and sensitive, measurement tool for telomerase detection. Specifically, our data suggested that the existence of telomerase could be triggered by the growth of telomere, as indicated by cleavage product in the presence of trace amount of telomerase, and that this intramolecular design maintains a quantifiable detection range from 0.1ug-1ug protein from cancer cell lysis. In addition, doses of Pb^{2+}, probe sensor, and telomerase enzyme could trigger a telomerase profile in cancer cells. Based on these lines of evidence, this novel probe can be applied to both cancer studies and cancer biomarker discovery. Given this degree of sensitivity and selectivity, our molecular engineering design may prove useful in the future development of other nucleic acid-based probes for clinical toxicology and cancer therapeutics.

Table 3-1. Names and sequences of DNA used in the paper. rA is the RNA monomer. All synthesis was done with an ABI synthesizer. The DNA/RNA chimers were purified by HPLC.

Name	Sequences
$TeloD_{12}$	5'-TAGGGCCGAGCCGGTCGAAAACCCTAACCCTTTTTTTTTTGGGTTAGGGTTrA-3'
TeloD9	5'-TAGGGCCGAGCCGGTCGAAAACCCTAATTTTTTTTTTTTAGGGTTrA-3'
$TeloD_6$	5'-TAGGGCCGAGCCGGTCGAAAACCCTTTTTTTTTTGGGTTrA-3'

Table 3-2. Comparison of melting temperature and fluorescence enhancement among different design sequences. TeloD6 shows the lowest melting temperature and signal to background ratio. TeloD12 has the highest melting temperature and is therefore the most stable.

Hairpin sequence	Tm (℃)	S/B ratio
$TeloD_6$	53.2	5
TeloD9	57.3	8
$TeloD_{12}$	59.1	14

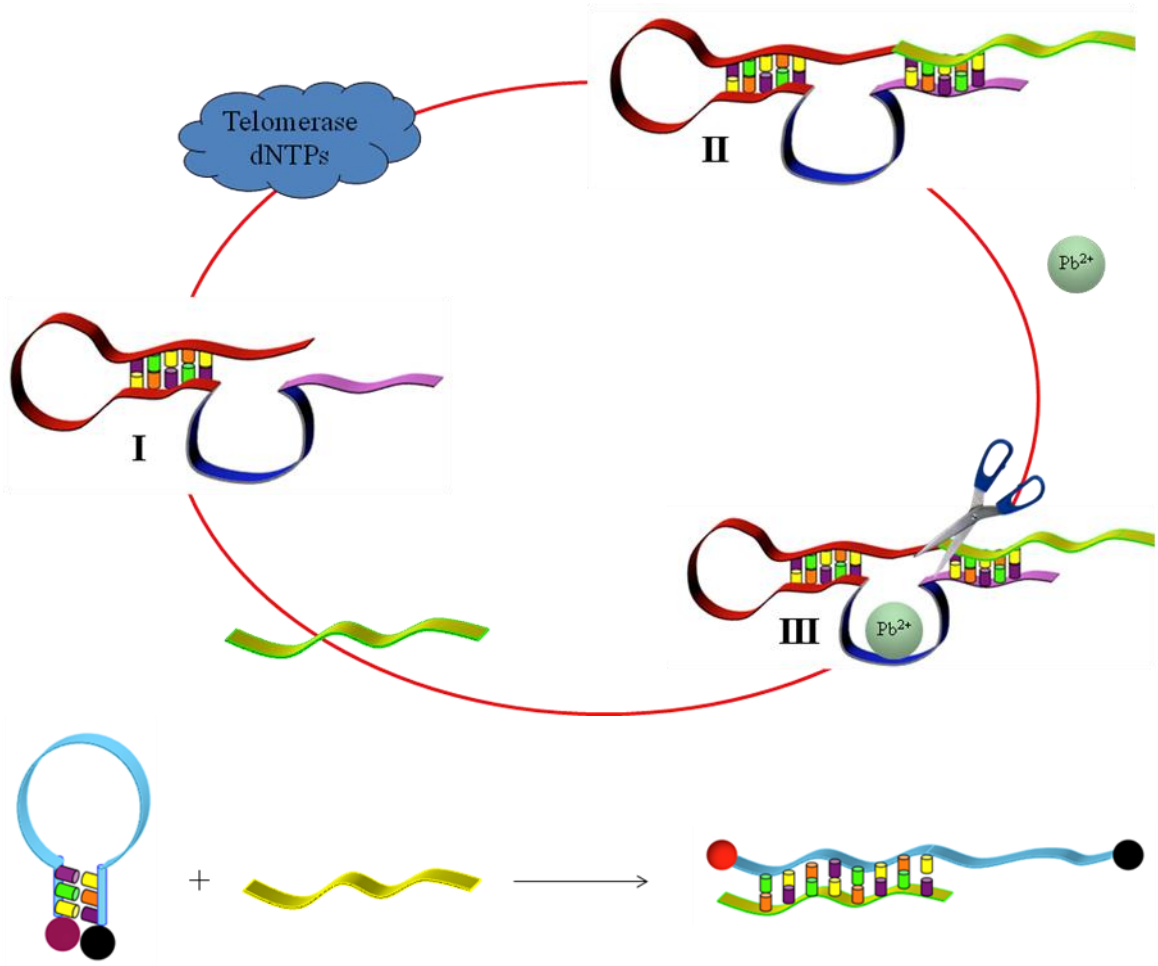

Figure 3-1. Schematic of the hairpin-structured, DNAzyme-based telomerase sensor and its working principle. I: the TeloD9 DNAzyme/substrate hybrid strand, which is composed of DNAzyme (8-17 DNAzyme, bottom), and pre-substrate (telomere primer, upper), hybridized together in Tris-acetate buffer, containing 60mM K+. After telomerase induced elongation, II: a elongation product is formed and hybridized to 8-17 DNAzyme, in which the 8-17 DNAzyme was forced to form its catalytic active structure. III: In the presence of 10 μM Pb^{2+}, the telomere product (yellow) will be cleaved and dissociated. This dissociated ssDNA will be caught by complementary Molecular Beacon report telomerase activity by fluorescence enhancement measurement.

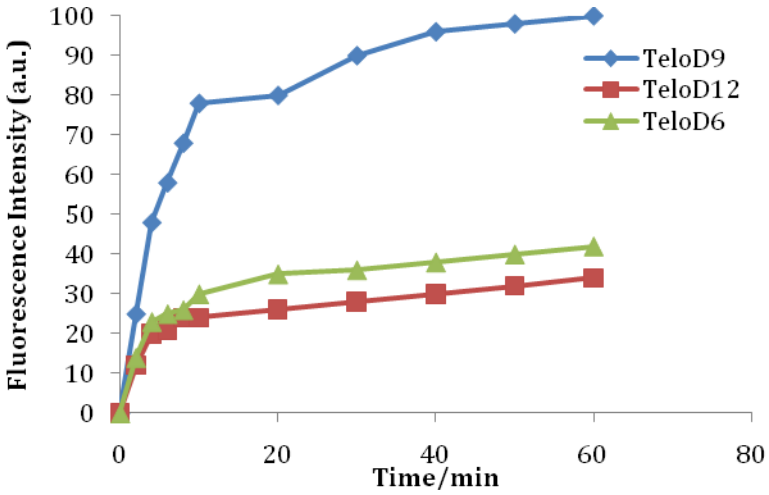

Figure 3-2. Optimization of synthesized probes using fluorescence signal comparison.Experiments were run in the presence of 2 µg protein after 10 min incubation with TeloD9, 6, and 12, respectively. Pb^{2+} was diluted to a final concentration of 10 µM

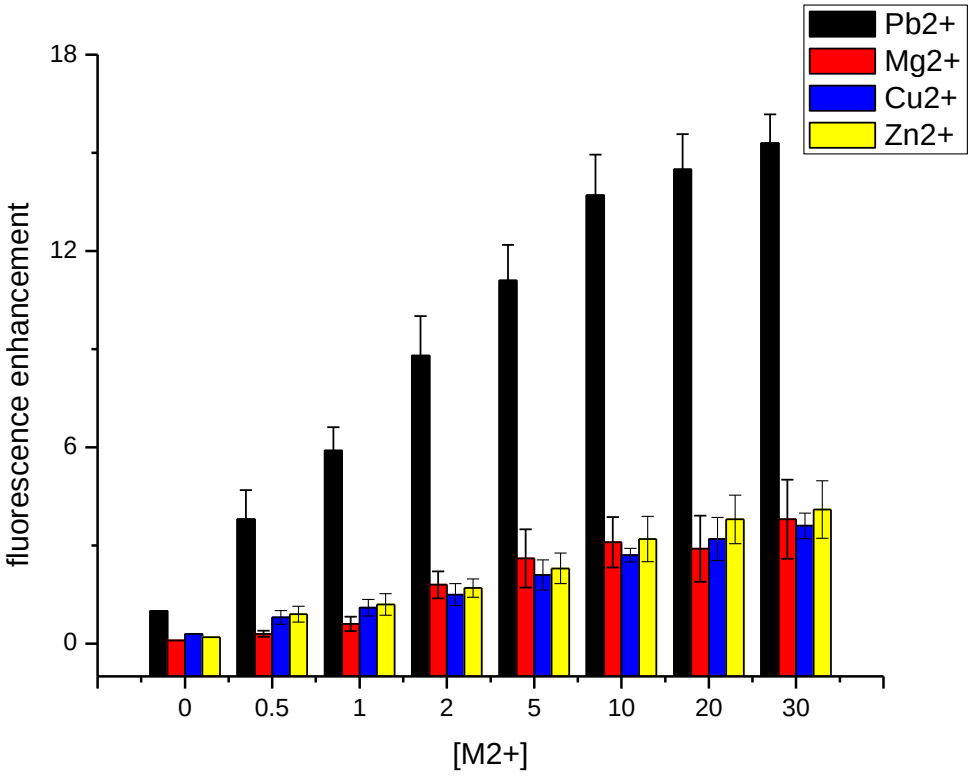

Figure 3-3. Selectivity of the TeloD9 probe sensor. Sensor responses to all competing metal ions at eight concentrations were tested. The reaction time was 10 min. The values indicated mean value from three experiments, and the error bars presented standard derivation from all three experiment.

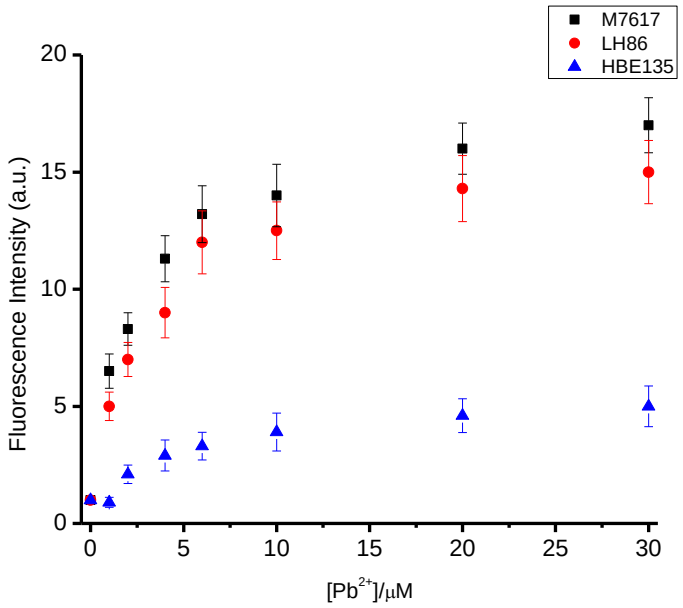

Figure 3-4. Fluorescence increase over background fluorescence at varying Pb^{2+} concentrations. The DNAzyme sensor concentration was 200 nM, and the buffer contained 50 mM Tris-acetate (pH 7.2) and 100 mM NaCl. The values indicated mean value from three experiments, and the error bars presented standard derivation from all three experiment.

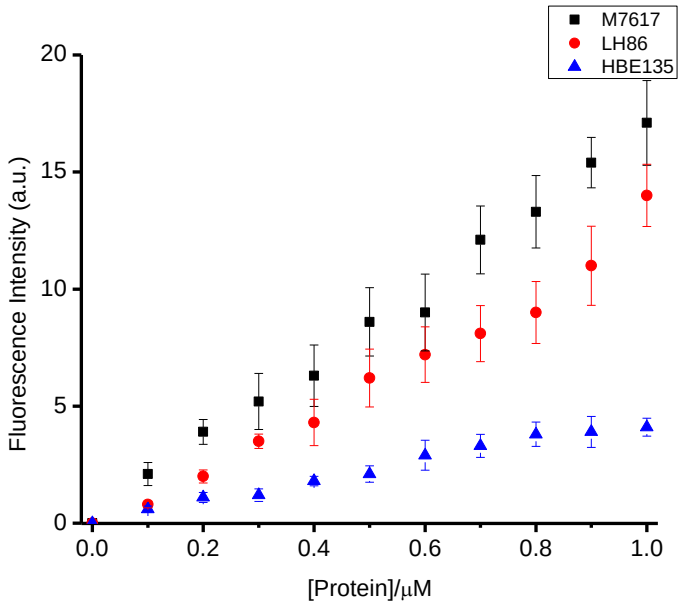

Figure 3-5. Dose-dependent telomerase elongation monitoring along with different total protein concentration. The background-corrected intensity in each cell type has been normalized. The values indicated mean value from three experiments, and the error bars presented standard derivation from all three experiment.

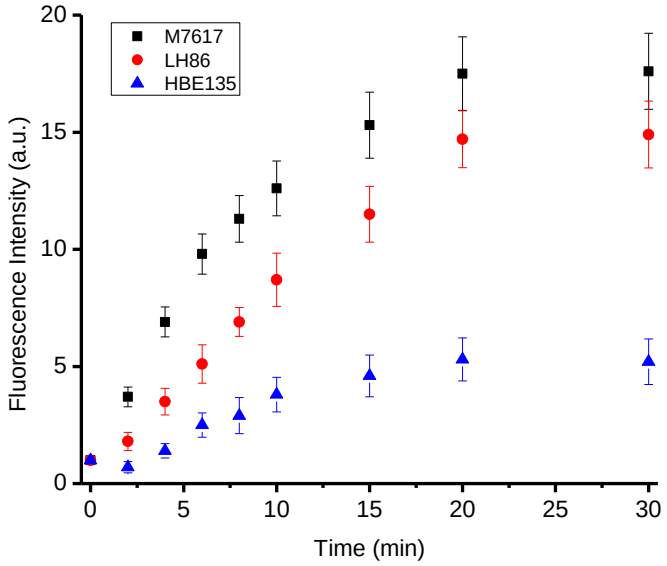

Figure 3-6. Analysis of DNAzyme cleavage reaction for different Pb^{2+} incubation times. M7617 and LH86 are cancer cells, and HBE135 is normal cell line. The values indicated mean value from three experiments, and the error bars presented standard derivation from all three experiment.

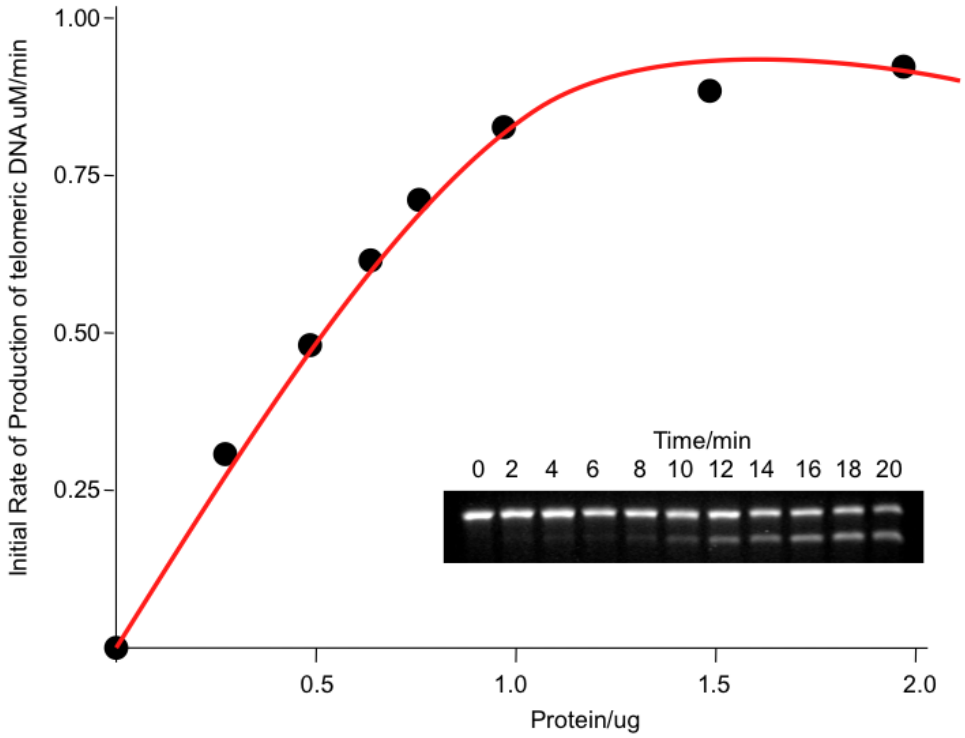

Figure 3-7. Catalytic activity of Pb^{2+} on D_{10} cleavage. The line represents a nonlinear fit to the data using the Michaelis−Menten expression. (Inset) The upper band represents uncleaved TeloD9, and the lower band represents the cleaved fragment.

CHAPTER 4
TARGETED DELIVERY OF TELOMERASE MRNA-CLEAVING DNAZYME TO TUMOR CELLS

Telomerase Biology

The telomerase enzyme, a ribonucleoprotein that functions as a reverse transcriptase, is the main positive regulator of telomere length. This enzyme consists of 6 subunits, including human telomerase RNA (hTR), telomerase-associated protein 1, human telomerase reverse transcriptase (hTERT), heat shock protein 90, p23 and dyskerin.[132] The template region of hTR encompasses 11 nucleotides (5'-CUAACCCUAAC-3'), which is complementary to the human telomere sequence (TTAGGG)n.[116] Telomerase has been validated repeatedly as a valuable cancer biomarker for disease detection, diagnosis, and prognosis across a broad spectrum of malignancy types and stages. Similarly, the cancer-specificity of telomerase (hTERT) expression has been exploited therapeutically as a homing beacon for immune and virus-mediated strategies.

The RNA subunit hTR and the catalytic subunit hTERT are the essential components for telomerase activity. The RNA subunit of telomerase serves as the template for addition of short sequence repeats to the 3' end of chromosome. The catalytic subunit, telomerase reverse transcriptase, is the most important component in telomerase complex, which is responsible for catalytic activity of telomerase. Activation of telomerase activity is strongly correlated with hTERT mRNA expression, indicating that hTERT is a major regulator of telomerase activity, thereby plays a critical role in cancer development.[133]

The expression of telomerase activity is regulated at different levels, including transcription, mRNA splicing, and maturation and modification of hTERT and hTERC. Positive and negative regulators of hTERT transcription were summarized in Table 4-1.

Telomerase as a Target for Cancer Therapy

Much evidence indicates that telomere maintenance confers an immortal phenotype to cancer cells. The loss of telomere sequences, on the other hand, may prevent it by inducing apoptosis.[134] Telomerase and telomeres thus offer a variety of potential targets for the development of anticancer therapies. Over the past decade, several experimental approaches has been developed aiming at disrupting telomerase function. For instance, inhibited telomerase enzymatic activity by various telomerase inhibitors, with induction of senescence and cell death; delivery of mutation of telomerase RNA template to interfere telomere function and induce cell death.[135]

Because of its potential usefulness for the development of novel anticancer therapies, telomere biology has been under intense investigation. Further research and a better understanding of the structure, function, expression, and regulation of telomeres and telomerase are essential before manipulation of this system approaches clinical applicability.

DNA-Base Micelle

The construction of complex supramolecular structures from simple amphiphilic molecules via molecular self-assembly has drawn much attention in recent years.[136-144] Amphiphilic peptides,[136-138] nucleic acids, lipids[139, 140] and polymers[141-144] have been shown to generate ordered supramolecular structures such as monolayers, micelles, vesicles, bilayers and nanotubes. For biomedical applications, micelle structures are of particular interest because of their small size, good biocompatibility, high stability both

In vitro and *in vivo*, and the ability to carry poorly soluble pharmaceuticals. An ideal self-assembled micelle would have: 1) well-defined and controllable size; 2) encoded biological functionalities; 3) high stability (low critical micelle concentration, CMC to prevent dissociation upon *in vivo* applications); 4) cell permeability and 5) easy synthesis. For these self-assembled materials to be most effective in applications, their size, shape, and chemical structure must be controlled precisely. While a variety of micelle systems have been demonstrated, the design of self-assembled systems in a controlled fashion, leading to stable and well-defined micelles with cell permeability, remains a fundamental challenge that has many applications in nanobiotechnology. Presumably, well-defined self-assembly requires precise molecular engineering of the corresponding building blocks, since all the information required for assembly must encoded in their molecular architecture. Dr.Haipen Liu has reported the design, construction, and self-assembly of a well-controlled amphiphilic DNA which meets the above criteria.[145]

In this oligonucleotides(Dons) micelle complex, a dactyl lipid tail was incorporated at the 5' end of Dons by solid-phase DNA synthesis. When dispersed in an aqueous solution, these amphiphilic DNA molecules spontaneously self-assembled into monodispersed micelle structures. In one application of this technology, a self-assembling aptamer–micelle nanostructure was formed of hydrophilic aptamers linked to hydrophobic lipids by poly(ethylene glycol) (PEG). In aqueous solution, these conjugate self-assembled into 3D spherical micelle structure with hydrophilic ODNs on the outside, and the lipid core on the inside (Figure 4-1). Yanrong Wu et al. constructed aptamer (ODNs that can recognize target molecules with specificity and selectivity)

based micelles, in their work, the presence of more than one aptamer on the micelle surface provides an approximately 750-fold increase in target binding affinity. The aptamer-micelle assembly is also able to be internalized, indicating it is a promising strategy for clinical applications by increasing therapeutic effectiveness. Furthermore, after two days of incubation with the aptamer-micelle assembly, normal cells maintained over 80% viability.

The oligonucleotide–lipid conjugates consist of distinct and highly negatively charged DNA chains covalently linked with two hydrocarbons. With unique properties such as excellent cell permeability, low critical micelle concentration (CMC), and nontoxicity, DNA-micelles may lead to revolutionary applications in drug delivery and cell biology. The size of the micelles can be fine tuned by changing the length of the DNA sequence and the micelles have been shown to be taken up across cell membranes, probably by endocytosis.

Micelle structures are of particular interest in biomedical applications because of their small size, good biocompatibility, high stability both ***In vitro*** and in vivo, and their ability to carry poorly soluble pharmaceuticals into intracellular regions.

Finally, we demonstrated that these DNA–micelles disintegrate themselves when incubated with biological cells, permeating the cell membrane by a process of endocytosis. Thus, it is additionally interesting to discover that the permeability of our DNA–micelles is size-dependent.

DNAzyme for Cancer Treatment

DNAzymes have come a long way from being just another analytic tool available to molecular biologists. Recent studies have shown the potential DNAzymes to serve as drugs both in cell-based assays and preclinical models of cancer. It is anticipated that

with the development of smart delivery systems for DNAzymes, better pharmacokinetics and pharmacodynamics will be possible, expediting DNAzyme march toward the clinic.

Sequence-Specific Cleavage of RNA by DNAzyme

The most well-characterized DNAzyme called 10-23 DNAzyme contains a cation-dependent catalytic core of 15 deoxyribonucleotides [12] that cleaves its target RNA between unpaired purine and pyrimidine through a de-esterification reaction. Sequence conservation in the border regions of the catalytic core is important for the maintenance of catalytic activity [146]. This core is flanked by complementary binding arms of 6 to 12 nucleotides, which, via Watson-Crick hybridization, confer specificity for the targeted mRNA. Once the target is bound, catalysis proceeds and the mRNA strand is cut into two. DNAzymes are purported to be just as efficient as protein enzymes at cleaving RNA [15].

In vitro cleavage experiments have shown that the 10-23 DNAzyme is highly specific [147]. Imperatively, DNAzyme activity is dependent on the prevailing secondary structure of long target RNA at the cleavage site [147]. For this reason, it is important to test a range of synthesized molecules to identify those that display a high level of activity against biologically relevant target molecules. The journey from *in vitro* cleavage kinetics to down-regulation of the target gene to evaluation *in vivo* can be arduous and is usually accompanied by a large attrition rate of candidate molecules.

Activities of DNAzymes Against Tumor Cells

Demonstrating cleavage kinetics with DNAzymes in a cell-free system is a valuable way to narrow the choice of molecules one needs to test in *in vitro* assays, mainly for successful down-regulation of the specific mRNA target. Having successfully

done this, one needs to screen the DNAzymes through selective cell-based assays that help identify the effects of such down-regulation on cell physiology.

The first usage of a DNAzyme against a target in cancer cells was by Wu and colleagues [148] who used three DNAzymes against the two variants of the p210 *bcr-abl* gene (splice 1, b3a2; splice 2, b2a2) and the p190 variant (ela2). The cleaving DNAzymes specifically inhibited p210bcr-abl protein expression by chronic myeloid leukemia K562 cells by ~40%, and inhibited cell growth by >50% over a 6-day assay period. The DNAzymes specifically inhibited the growth of *bcr-abl*–positive colonies by up to 80% using freshly isolated $CD34^+$ bone marrow cells from patients with chronic myeloid leukemia. .

Interaction between DNAzymes and transfection reagents were also examined using a panel of human cancer cell lines [149]. Based on those results, cell uptake was not significantly affected by DNAzyme size, or chemical modification.

Cieslak and coworkers [150] designed DNAzymes partially modified with phosphorothioate and with 2′-*O*-methyl groups at both the 5′ and 3′ ends indicated similar kinetics as unmodified DNAzyme toward mRNA cleavage, however, they were significantly more potent than the unmodified DNAzymes because of their greater stability. These DNAzymes inhibited microvascular endothelial cell capillary tube formation in fibrin and Matrigel, signaling their usefulness against tumor-induced angiogenesis.

DNAzymes were also designed to inhibit the growth of epidermal growth factor receptor–overexpressing A431 cancer cells in a dose-dependent manner when delivered with cationic lipids. [151]

These studies in cell culture show that different cancer gene targets can be successfully down-regulated whether they are endogenous (cell-expressed) or exogenous (virus-expressed) in a variety of cancer cell lines. Some of the effects in fact lead to anticancer activity as judged by phenotypical changes in cells. DNAzymes are amenable to chemical modification, allowing them to be made more resistant against nuclease degradation and can be made to different arm lengths. These findings have helped pave the way for the *in vivo* evaluation of DNAzymes.

Activation of telomerase and the stable of telomere length are essentially required for cellular immortalization and genetic alterations. Telomerase is thought to be necessary for cellular immortality and carcinogenesis hTERT is a catalytic subunit of telomerase and its expression is the rate-limiting factor of the enzymatic activity of human telomerase. According to studies, the most of examined tumors showed telomerase activity correlating with the expression of the activity-limiting component hTERT. hTERT was found in nearly all types of cancer but not in most normal somatic cells. So it is thought the target of anticancer strategy. DNAzyme is a kind of DNA molecule with enzyme activities. It can pairs with specific target mRNA and inactivate target mRNA by cutting. At present, most researches focus on 10-23 DNAzyme. The structure of 10-23 DNAzyme is like hammer ribozyme, containing a highly conserved catalyzing domain and two variable side arm domains. It was shown that transfection with 10-23 DNAzyme specifically reduces the expression of target genes. By use of antisense strategy, 10-23 DNAzyme complementary to hTERT mRNA could be used to inhibit hTERT gene expression and telomerase activity and induce tumor cell apoptosis.

DNAzyme targeting the telomerase mRNA

In an attempt to use DNAzyme to inhibit telomerse activity that is expressed in most cancer cells, and considered a target for cancer therapeutics (Shay and Wright, 2002), we designed 10-23 DNAzyme micelle nanostructure targeting the mRNA of the catalytic subunit of hTERT. Which is illustrated in Figure 4-4. The amphiphilic building block can be divided into three distinct segments. 1) 10-23 DNAzyme, which is highly hydrophilic. 2) Two C18 hydrocarbon tails, which is highly hydrophobic. 3) PEG linker which connected lipid tails and DNAzymes together, while enhanced plasmid half life of the nanostructure.[152] We hypothesized that due to the amphiphilic nature of our design, the DNAzyme-lipid molecules are able to self-assemble into micelles as a result of hydrophobic effect. We also modified binding arm of 10-23 DNAzyme using 2'-O-methyl-RNA (2'-O-meRNA) oligomers, which was reported to bind more tightly to complementary RNA sequences than do analogous DNA oligomers and have improved resistance to degradation by nucleases, reducing the need for phosphorothioate linkages and improving the selectivity of antisense effects.[153] 2'-O-meRNA oligomers inhibited telomerase in prostate cancer cells with potencies superior to those possessed by analogous peptide nucleic acids.[154] Additionally, 2'-O-methyl-RNA oligomers inhibited telomerase, leading to progressive telomere shortening and causing immortal human breast epithelial cells to undergo apoptosis with increasing frequency until no cells remain.[155] These results indicate the feasibility of using 2'-O-methyl-RNA oligomers for the treatment of telomerase-positive tumors.

Cleavage of target mRNA involves at least two processes, that is hybridization of DNAzyme with RNA substrate and cleavage of substrate in the DNAzyme-substrate duplex. The nanostructure was generated by the attachment of a lipid tail onto 5’ end of

DNAzymes, provides these unique nanostructures with an internalization pathway. Other merits include: extremely low off rate once bound with target cells, rapid recognition ability with enhanced sensitivity, low critical micelle concentration values, and dual-drug delivery pathways. In this type of DNAzyme assembly, the DNAzyme strand would not only act as the building block for the nanostructure, but also perform a recognition function to its specific target, and most important, the therapeutic function of preventing mRNA translating into protein. Furthermore, densely packing DNAzymes on such an assembly could create a multivalent effect, leading to greatly improve binding affinity of the DNAzymes to target mRNA. Engineering this type of DNAzyme micelle can be simple and could result in enhanced binding capability to its specific targets. Micelles are also considered to be dynamic and soft materials. Because the cell membrane is basically a dynamic lipid bilayer, a “soft” nanomaterial might produce some interesting interactions with it, particularly where such interactions involve cell permeability and drug delivery.

In summary, we have created a triple-threaten weapon killing cancer specifically targeting telomerase, thus paving the way for the construction of DNAzyme micelles with applications in diagnosis and targeted therapy.

Experimental Section

Oligonucleotides Synthesis.

All DNA and RNA oligomers were synthesized on an ABI3400 DNA/RNA synthesizer (Applied Biosystems, Foster City, CA) in our laboratory. All DNA oligonuclease bases were purchased from Glen Research, Sterling, VA. 5’-lipid phosphoramidite was synthesized by Dr.Haipeng Liu. The hybrid lipid-PEG-10-23 DNAzyme called LTM1023 (Lipid, Telomerase and 2’-O-Methyl) was synthesized with

extreme caution. A DNA library containing a randomized sequence was labeled with a 5'-lipid modifier and used as a control comparison. All sequences were further purified by reverse phase HPLC (ProStar, Varian, Walnut Creek, CA) on a C-8 column. A Cary Bio-300 UV spectrometer (Varian, Walnut Creek, CA) was used to measure absorbance to quantify the manufactured sequences. DNA and RNA sequences are summarized in Table 4-2. Keeping catalytic core in 10-23 DNAzyme (GGCTAGCTACAACGA) conserved, the 10-23 DNAzyme was designed to recognize hTERT sequence (gi: 4507438 from GenBank). Underline: catalytic core of 10-23 DNAzyme; Bold: 2'-O-methyl modified RNA binding arm for recognition of hTERT mRNA.

LTM1023: 5'-**CCACGGYCA** GGCTAGCTACAACGA **UCGGUCCAC**-3';

All the sequences used are summarized in Table 4-2. The cleavage site of hTERT mRNA is between G797 and U798. Primer design was using Primer3 online design tool, the designed forward primer (FP) and reverse primer (RP) are the sequences locate aside of mRNA cleavage site, providing amplification of a DNA segment of 222 bps.

***In vitro* cleavage of 19-mer RNA substrate**

Cleavage of fluorescently labeled 19-mer RNA substrate (named RS19) was performed to study the kinetics. Prior to mixing enzyme and target RNA, both solutions were denatured separately for 5 minutes at 90°C. An aliquot of 10 nM Dabcyl-labeled DNAzyme (named LTM1023-Dab) and 1 μM RS19 were mixed in 100 μL of ribozyme buffer (10 mM $MgCl_2$, 50 mM Tris–HCl pH 7.5) and incubated at 37°C for 20min in humid chamber. After 20 min, the cleavage reactions were stopped by addition of EDTA to a final concentration of 83 mM and cooling on ice. Samples were denatured for 5 min at 65°C, and substrate RNA and cleavage products were separated on a 20% denaturing polyacrylamide gel, the band intensity was analyzed by ImageJ.

Cell Culture and Treatment.

Human cervical cancer HeLa cells were grown in 5% CO_2 atmosphere at 37°C in DMEM (Invitrogen) containing 10% fetal bovine serum (FBS) in 10-cm dishes (Nunc). Cells were lysed in ice cold CAHPS lysis buffer (0.5% 3-[(Cholamidopropyl)dimethylammonio]-1-propanesulfonate, 10 mmol/L Tris (pH 7.5), 1 mmol/L $MgCl_2$, 1 mmol/L EGTA, 0.1 mmol/L benzamidine, 5 mmol/L β-mercaptoethanol, and 10% glycerol), in the presence of complete mini protease inhibitors (Roche Diagnostic). Clarified cell lysates were normalized for total protein concentrations by the Bradford protein assay (Bio-Rad). Semi-quantitative reverse transcription-PCR (RT-PCR) for gene expressions, telomerase activity assay, was indicated in individual experiments.

Telomerase Activity Assay

The TRAP assay was performed using a TRAP^{EZE} Non-isotopic Telomerase detection kit (Millipore). In brief, 2 µl of cell lysate and 48 µl of TRAP reaction mixture consisting of the 1 µl TS Primer (5′-AATCCGTCGAGCAGAGTT), 1 µl of 50 µM dNTP mix, 1 µl of TRAP primer mix (RP primer, K1 primer, and TSK1 template), and 0.4 µl of 2 IU Taq DNA polymerase in 20 mM Tris–HCl, pH 8.3, 1.5 mM $MgCl_2$, 63 mM KCl, 1 mM EGTA, 0.05% Tween 20, and 0.01% BSA[1] were mixed and incubated at 30 °C for 30 min. PCR was then performed as follows: 94 °C, 30 s; 59 °C, 30 s; 72 °C, 60 s, 30 cycles. PCR products were electrophoresed in 12% acrylamide gel for 6 hours at 250V.

hTERT mRNA Isolation

Cultured cells were washed once with phosphate-buffered saline and then scraped into a buffer (10 mM Hepes–KOH, pH 7.5, 1.5 mM $MgCl_2$, 10 mM KCl, and 1 mM dithiothreitol). The cells were washed in the buffer and then homogenized in 200 µl of a

cell lysis buffer (10 mM Tris–HCl, pH7.5, 1 mM $MgCl_2$, 1 mM ethylene glycol-bis (β-aminoethyl ether)*N*,*N*,*N*′,*N*′-tetraacetic acid (EGTA), 0.1 mM benzamidine, 5 mM β-mercaptoethanol, 0.5% 3-((3-cholamidopropyl)dimethylammonio)-1-propanesulfonate (Chaps; WAKO Chemical Industries, Osaka, Japan), and 10% glycerol) and incubated on ice for 30 min. Cell homogenates were then centrifuged at 12,000*g* for 20 min at 4 °C. The supernatant was added 0.2 mL of chloroform per 1 mL of TRIzol® Reagent used for homogenization. With 15 seconds shaking, the sample was incubate for 2–3 minutes at room temperature, followed by a centrifuge at 12,000×g for 15 minutes at 4°C. The aqueous phase was then poured into a new tube and proceeds to the RNA Isolation Procedure. After centrifuge, the supernatant was removed, leaving only the RNA pellet. The pellet was washed with 1 mL of 75% ethanol per 1 mL of TRIzol® Reagent used in the initial homogenization. We vortexed the sample briefly, then centrifuged the tube at 7500 × g for 5 minutes at 4°C. The sample was finally vacuum dried.

RT-PCR of hTERT mRNA.

hTERT mRNA was quantified before and after the cleavage by a reverse transcriptase-PCR assay using ThermoScript RT-PCR kit following the manufacturer's instruction (Invitrogen), for 35 cycles of 30 s at 72°C as the optimized annealing temperature and 64°C extension. Primers specific for different genes were as follows: hTERT ---- Forward Primer (FP): 5′-CTG GAA CCA TAG CGT CAG G-3′ and Reverse Primer (RP): 5′-GCA GGT GAC ACC ACA CAG AA-3′.

Each PCR reaction contained 10 μl of the reverse transcriptase reaction mixture, 0.5 μM primers, 10 mM dNTP, in 1 mM $MgCl_2$, 40 mM KCl, 8 mM Tris-HCl (pH 9.0), and 0.1% Triton X-100 in 50 μl. The products of the PCR reaction were electrophoresed in

12% nondenaturing polyacrylamide gel in 1× TBE (tris/borate/EDTA buffer) at 40 V for 18 h and stained with ethidium bromide (EB), photographed in a gel UV documentation system (Bio-Rad), and analyzed by ImageJ. PCR parameters are 32 cycles consisting of 95 °C for 45 s, 60 °C for 45 s and 72 °C for 2 min, followed by one cycle of 72 °C for 5 min.

***In vitro* cleavage of hTERT mRNA by LTM1023**

Each of the reactions was performed including: 10 μg total RNA, 10 μM LTM1023/or LTM0000/or LTM1111, 150mM KCl, 2mM MgCl2 at 37°C for 2 hours. After 2 hours, the cleavage reactions were stopped by addition of EDTA to a final concentration of 83 mM and cooling on ice. Samples were denatured for 5 min at 65°C, and substrate RNA and cleavage products were separated on a 20% denaturing polyacrylamide gel, the band intensity was analyzed by ImageJ. LTM0000 is the control of LTM1023 with random sequences at catalytic core. LTM1111 is the control of LTM1023 with random sequences at binding arms.

LTM1023 induces inhibition of telomerase activity in Hela cells

HeLa cells were incubated with different concentrations of LTM1023 as indicated for 72 h in cell cultures, and then subjected to telomerase activity analysis. Telomerase activity was determined by measuring telomerase activity in cell lysates after each treatment. Delivery of LTM1023 into HeLa cells was performed under 37 °C. Briefly, cells were digested with trypsin and transferred into a 24-well plate at 5×10^4 cells/well. After 12 h of incubation, medium was removed and cells were washed with PBS. 0.2 nmol of LTM1023 was suspended in PBS buffer to a final volume of 50 μl and incubated at room temperature for 15 min for an efficient self assembly (into micelle). The LTM1023 solution was then suspended in 200 μl serum- and antibiotics-free culture

medium, mixed gently and added to the cells. After incubation at 37 °C for 6 h, 750 μl normal serum-containing medium was added to the cells without removing the transfection mixture. Cells were exposed to such transfection every 24 h for three more times, harvested at 96 h after the first exposure and subject to hTERT mRNA analysis and telomerase activity assay. Treatment with LTM0000 and LTM1111 was used as control. LTM0000 and LTM1111 were also treated with Hela cells for control experiment.

Results and Discussion

In the present study, we demonstrated that LTM1023 represses telomerase activity in Hela cells through down-regulation of hTERT transcription. In our assays, we used Hela cells with high telomerase activity to evaluate the effects of LTM1023, a DNAzyme based telomerase inhibitor targeting the catalytic subunit of human telomerase.

Delivery of DNAzyme-based LTM1023 to Action Sites

The most challenging part for delivery of LTM1023 to play its pharmaceutical role in vivo is to survival from degradation in cytoplasm or nucleus before hybridize to its target mRNA. Delivery requires that the oligonucleotide survive local or systemic administration long enough to bind to the target cells, cross the cytoplasm membrane or become released from an endosomal/lysosomal vesicle, pass through the nuclear membrane (or cross the endoplasmic reticulum), and be able to functionally hybridize to the target RNA. This represents a long chain of events that are at best unlikely for a typical conventional drug let alone a large, labile, highly charged molecule. Liposome was the common cargo used for oligonucleotide delivery in vivo, however, it has the drawbacks such as low efficiency due to non-specificity binding. It is the first time using

lipid-anchored 10-23 DNAzyme for target-driven specifically drug delivery to hTERT mRNA in Hela cells.

From the worked done by Dr.Haipeng Liu on lipid-oligonucleotide cell surface anchoring, we were confident to conjugate lipid with 10-23 DNAzyme for Hela cell transfection. In Figure 4-6, telomerase activity was inhibited on a time course of 2 days, indicating that the LTM1023 was delivered into Hela cells, and catalytically cleaved the mRNA

Micelle Formation

Agarose Gel was used to identify micelle formation. Gel electrophoresis is a powerful technique in biology and is the standard method to separate, identify and purify nucleic acid with different sizes. We hypothesized that in the gel matrix, the micelle aggregation will lead to slow moving bands, however, if the aggregations are disrupted, only fast moving bands can be observed. In addition, a sharp or condensed band is consistent with uniform size and unique conformation. As shown in Figure 4-5, in TBE buffer, each DNA assemblies migrated as a single, sharp band with expected mobility, suggesting the micelle aggregations were formed and were stable. The mobility of our DNA amphiphilies solely depends on the length of the DNA, generally, shorter DNA assemblies migrate faster in the gel. It is important to point out that, the self-assembled structures exhibit single sharp bands for all of the assemblies (Figure 4-5), which indicates all the micelles have, uniform aggregation number. Attempts to estimate the aggregation number by reported method[6] yield inconclusive results, which, most likely due to the interference of the highly charged DNA. To further prove the slow mobility was a result of aggregation, we added 0.8% (w/v) Sodium dodecyl sulfate (SDS) to the gel, at this concentration, SDS can disrupt micelles resulting in a loss of hydrophobic

interactions. As expected, under UV illustration, all the DNA migrates as faster single violet (monomeric pyrene) bands.

Although some of the oligonucleotides by themselves lack an internalization pathway, the introduction of this unique lipophilic micelle structure formation allows the 10-23 DNAzyme to first spontaneously inserted into cell membrane, ultimately, penetrate the cells. For amphiphilic DNA uptake, it is not clear at this stage, that whether the micelles dissemble themselves and then insert into the cell membrane or the micelles cross the membrane as a structure. From Dr.Haipeng Liu's results, either way, the fact that fluorescence was accumulated in endosome strongly suggests an endocytic pathway. This approach applied here conjugate hydrophilic oligonucleotide with hydrophobic lipid, making it convenient for assemble therapeutic reagent 10-23 DNAzyme, and cell permeability of this class of micelles is a plus to efficient delivery of 10-23 DNAzyme into telomerase positive cells.

Kinetics Analysis of Cleavage of *In vitro* Transcribed RNA Substrate

For single turnover experiment, 1 pmol of *In vitro*-transcribed RNA substrate was incubated at 37 °C with 10 pmol DNAzyme. Reactions were stopped at various time points by the transfer of reaction aliquots to an equal volume of ice- cold stop buffer (90% formamide, 20 mM EDTA and loading dye). At completion, the uncleaved substrate and products were resolved by electrophoresis on a 16% denaturing polyacrylamide gel. First-order rate constant k_{obs} was obtained from single turnover experiments, a curve was fitted to the data using the equation $\%P = \%P_{\infty} – C \exp[–kt]$. In this equation %P is the percentage product, $\%P_{\infty}$ is the percentage product at $t = \infty$, C is the difference in %P between $t = \infty$ and $t = 0$, and k is the first-order rate constant. The results in Figure 4-10 showed that LTM1023 has a kcat/Km value at 3.2×10^{5} min^{-}

$^{1}M^{-1}$, which is much lower that many of the reported values that can be, for instance, about 3.2×10^{5} $min^{-1}M^{-1}$ for the original 10-23 DNAzyme. We believe this improvement was contributed from 3 aspects: 1, the high density of LTM1023 using micelle structure, 2, lipid modification of 10-23 DNAzyme has been proved to be able internalized into cells within 2 hours, and 3, the modification of 10-23 binding arms with 2'-O-methyl RNA.

A substrate has to form Watson–Crick base-pairing with DNAzyme before it is cleaved. This requires that both DNAzyme and RNA substrate adopt proper conformation to facilitate the formation of DNAzyme–RNA duplex. Particularly the two target recognition domains on the DNAzyme have to get close in order to hybridize with the substrate. The probe nuclease stability was enhanced by modified with 2'-O-Methy ribonucleotide. Compared to LTM1111, LTM1023 displayed sustained intracellular activity; however, only LTM1023 maintained specificity to target hTERT mRNA. Our results indicated that and 2'-O-methyl RNA modification was reported to improve binding affinity to complementary RNA sequences than do analogous DNA oligomers and have improved resistance to degradation by nucleases, reducing the need for phosphorothioate linkages and improving the selectivity of antisense effects.[153] 2'-O-me RNA oligomers inhibited telomerase in prostate cancer cells with potencies superior to those possessed by analogous peptide nucleic acids.[154] Additionally, 2'-O-methyl-RNA oligomers inhibited telomerase, leading to progressive telomere shortening and causing immortal human breast epithelial cells to undergo apoptosis with increasing frequency until no cells remain.[155] These results indicate the feasibility of using 2'-O-methyl-RNA oligomers for the treatment of telomerase-positive tumors.

For multiple turnover kinetics analysis, RNA substrate at various concentrations was incubated with 20 nM LTM1023 at 37 °C for 30 min in reaction buffer. K_m and k_{cat} values were obtained by fitting velocity of cleavage against substrate concentration using the equation $V = k_{cat}\cdot[S]/(K_m + [S])$. All reactions were terminated and processed as described in the previous section.

Taken together all these results, we concluded that the enhanced binding and cleavage kinetics through micelle design does take place and imply, in turn, that LTM1023 micelle is a unique telomerase therapeutic candidate for *in vitro* telomerase inhibition study.

DNAzyme-Based LTM1023 Micelles Decreases hTERT mRNA Abundance *in Vivo*.

For DNAzymes to cleave RNA under in vivo conditions, we transfected HeLa cells with the LTM1023 and examined their effect on the level of hTERT mRNA and telomerase activity using TRAP assay. As mentioned in previous section, chemical modification of the lipid and 2'-O-methyl group in LTM1023 binding arms have improved the drug performance ***In vitro***, and according to literature, the chemical modifications to the nucleotides (e.g. 2'-O-Me) have been used successfully to enhance nuclease stability and prolong oligonucleotides half-life in serum while still enabling their function. The drug-induced inhibition of telomerase activity was shown by testing cleavage reaction at different concentration of LTM1023. Time course studies demonstrating that LTM1023 inhibition of telomerase activity occurs within 24 hours of treatment, further confirmed the successfully delivery of LTM1023 into Hela cells by lipid micelle assembly. We identify that the effect of LTM1023 on cancer cell apoptosis is mediated by a mechanism involving repression of the hTERT gene and thereby, inhibition of telomerase activity. Although future studies are required to investigate the mechanisms

underlying LTM1023-induced hTERT gene repression and telomere shortening, the finding that LTM1023 had dramatically reduced the hTERT mRNA content in time-dependent experiment (Figure 4-12) demonstrated that, the hTERT mRNA reduction from treatment with drug LTM1023 was accomplished with high percentage of LTM1023 transfected into Hela cells within 24 hours, and the cleavage of mRNA was catalytically processed with a fast kinetics.

Summary

Telomerase remains an attractive target for cancer therapy because telomerase is present in most malignant cells but undetectable in most normal somatic cells [156]. Thus an agent effectively inhibiting telomerase could be active against many forms of malignancy yet spare most types of normal cells [157]. Nucleic acid agents hold the promise of a degree of specificity that may be difficult to achieve with small molecules. Here we reported that *in vitro* cleavage of hTERT gene using DNAzyme based micelles could down-regulate the telomerase activity, leading to an inhibition of the malignant phenotype of HeLa cells. In conclusion, by assembling micelle structure with 10-23 DNAzyme-lipid hybrid, we have constructed a multifunctional nanostructure that enables anticancer therapy by inhibition telomerase activity. Further, we demonstrated that DNAzyme-loaded micelles are able to kill target cancer cells effectively, suggesting target-specific drug delivery. We anticipate that the present DNAzyme micelle system could be applied to the design of similar multifunctional nanostructures for bioanalytical and therapeutical functions.

Table 4-1. Positive and negative regulators of hTERT transcription.[158]

Positive	oncogene *cMyc*
	transcription factor Sp1
	human papillomavirus 16 protein E6
	steroid hormones
Negative	transcription factor Mad1
	p53
	pRB
	E2F
	myeloid cell-specific zinc finger protein 2
	interferon-gamma
	Wilms' tumor 1 tumor suppressor protein
	transforming growth factor-beta

Table 4-2. Summary of probe sequences.

Name	DNA Sequences
LTM1023	5'-Lipid-$(HEG)_6$-CCACGGUCA GGCTAGCTACAACGA UCGGUCCAC-3'
LTM1023-Dab	5'-Lipid-$(HEG)_6$-Dabcyl-CCACGGUCA GGCTAGCTACAACGA UCGGUCCAC-3'
LTM0000	5'-Lipid-$(HEG)_6$-GGUGCCAGU GGCTAGCTACAACGA AGCCAGGUC-3'
LTM1111	5'-Lipid-$(HEG)_6$-CCACGGUCA AGGCATCGAATTAGC UCGGUCCAC-3
RS19-FAM	5'-UGUGGACCGAGUGACCGUGGU-3'
RS19	5'-UGUGGACCGAGUGACCGUGGU-FAM-3'
FP	5'-CTGGAACCATAGCGTCAGG-3'
RP	5'-GCAGGTGACACCACACAGAA-3'

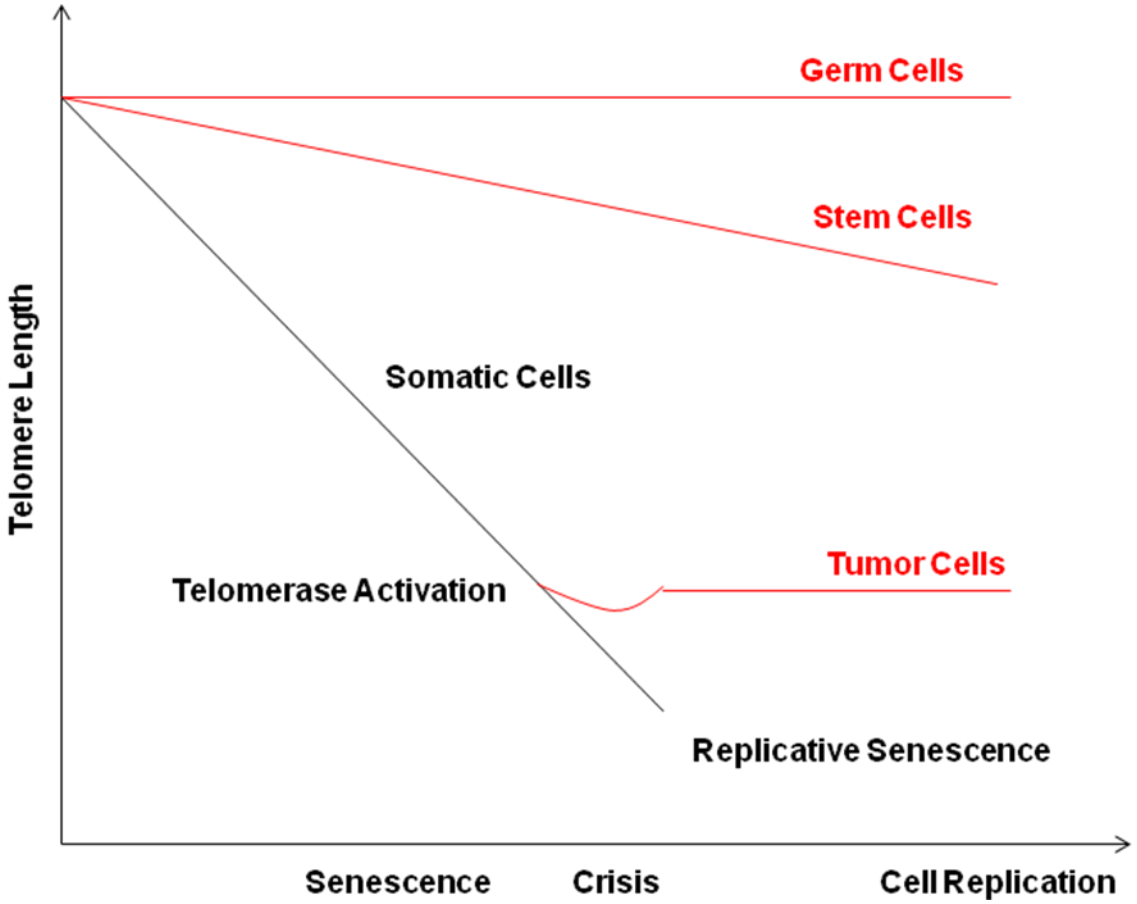

Figure 4-1. The telomere-telomerase hypothesis Changes in telomere length are detected in germ cells, stem cells, somatic cells, and tumor cells. Red: telomerase positive.

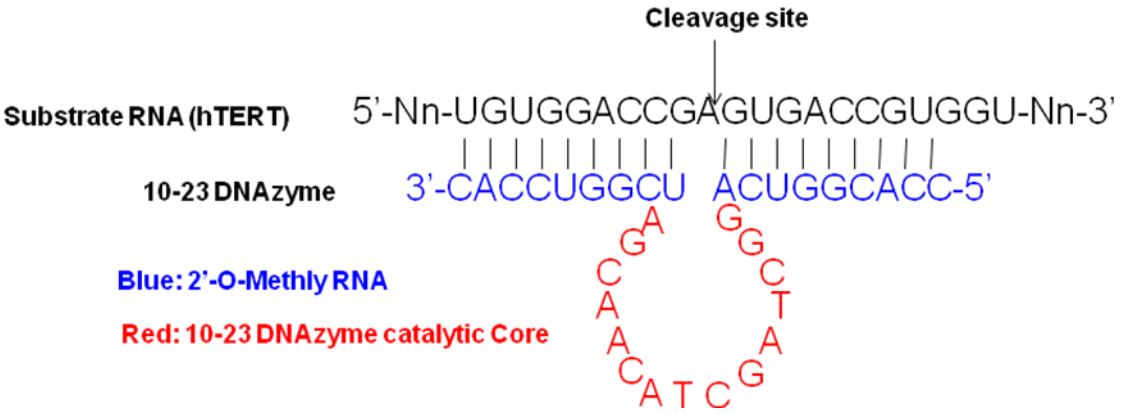

Figure 4-2. Secondary structure of the 10–23 DNAzyme–substrate complexe. The 10–23 DNAzyme consists of two variable binding domains, designed two binding arms, which flank a conserved 15 base unpaired motif that forms the catalytic domain. The only requirement of the RNA polynucleotide substrate is for a core sequence containing an R (A, G) and Y (C, U) junction.

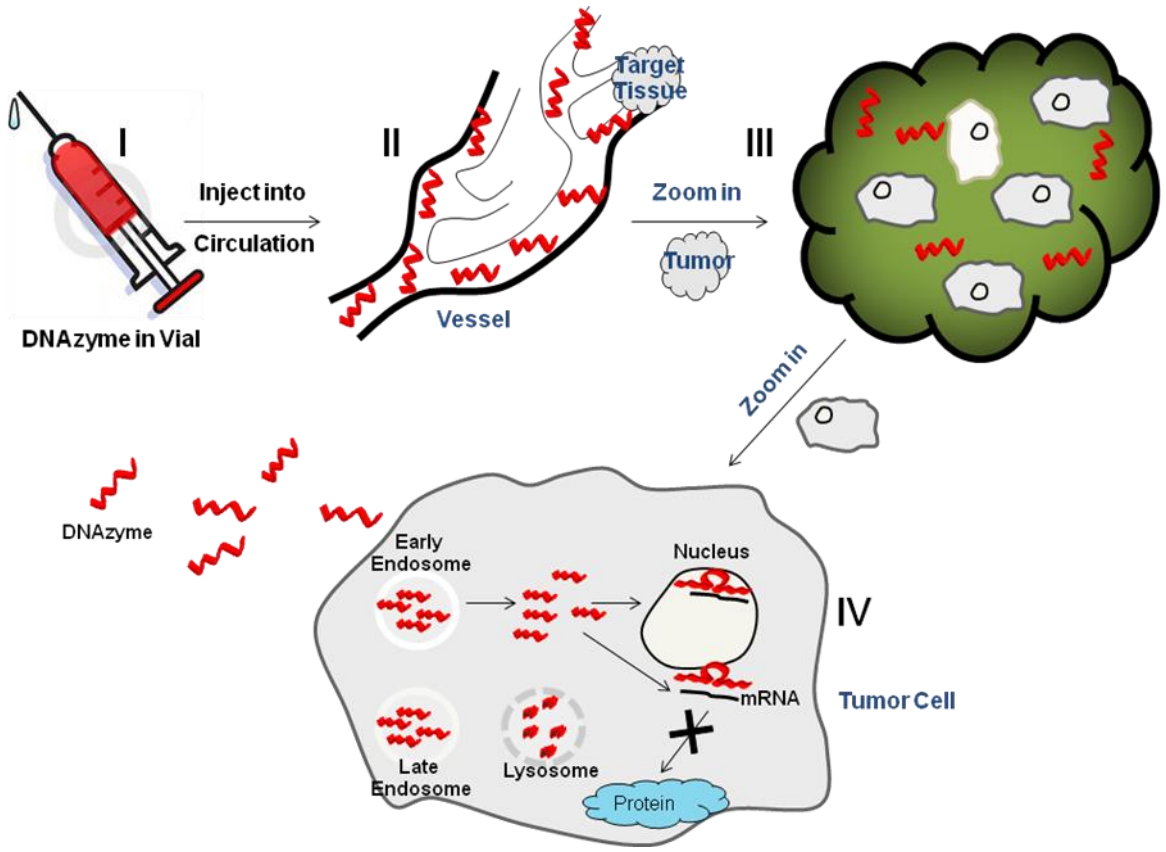

Figure 4-3.Route taken by free DNAzyme to down-regulate target gene in targeted cancer cells. I, DNAzyme is administered via the blood supply. II, DNAzyme is carried by blood circulation to the site of the lesion and other tissues. III, DNAzyme extravagates through the capillaries and moves toward the cancer cells. IV, DNAzyme neutralizes its targeted mRNA in the nucleus or in the cytoplasm.

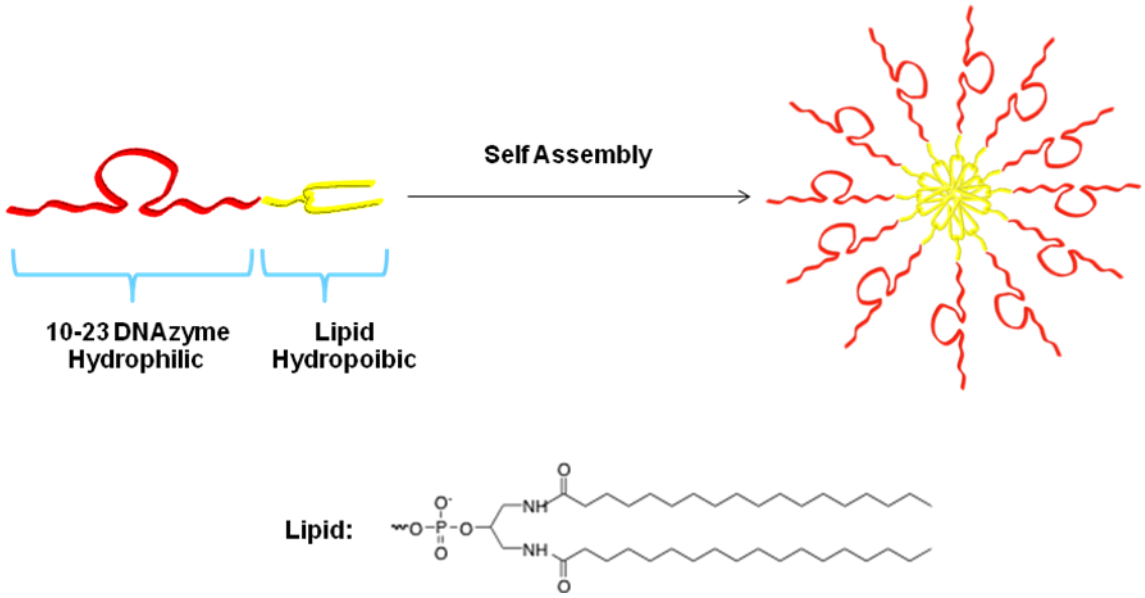

Figure 4-4.Schematic of the design and assembly of DNA micelles.The micelle contains a 10-23 DNAzyme, a PEG (Polyethylene glycol) unit and a lipid molecule. Molecular structure of lipid used for this study is shown.

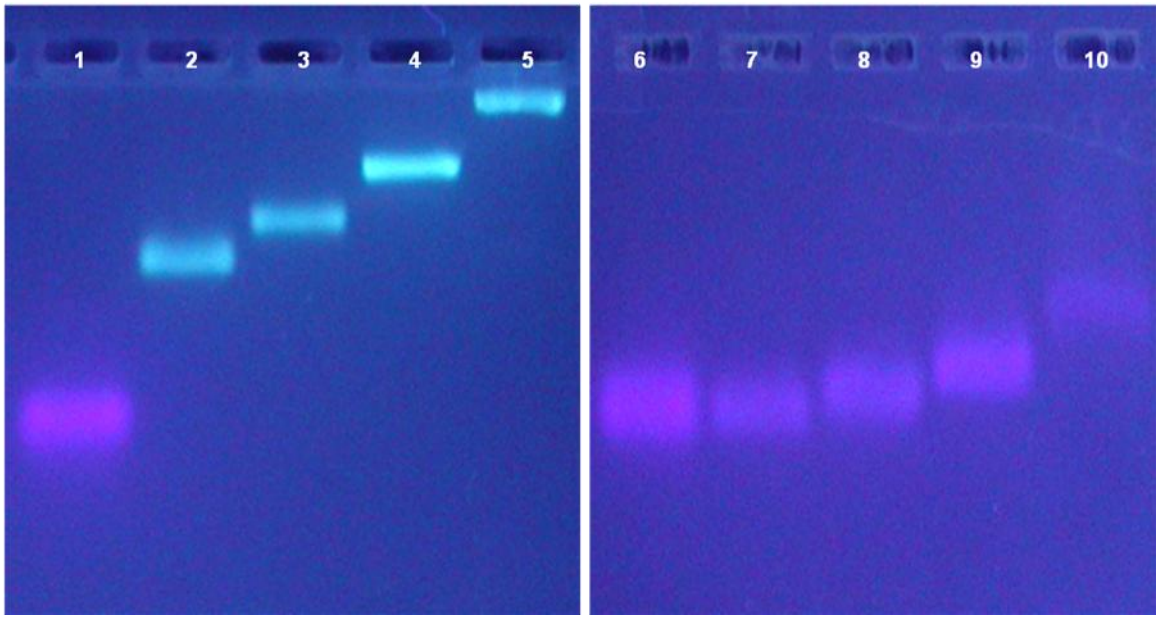

Figure 4-5. 4% agarose gel analysis of DNA micelle structure. From 1-5 &6-10: 1(or 6): 10-23 DNAzyme only, 2(or 7): lipo-5, 3(or 8): lipo-10, 4(or 9): LTM1023 and 5(or 10): lipo-50. The gel were illustrated under. Left: gel ran in 1xTBE buffer. right: Gel ran in 1xTBE buffer containing 0.8% SDS.

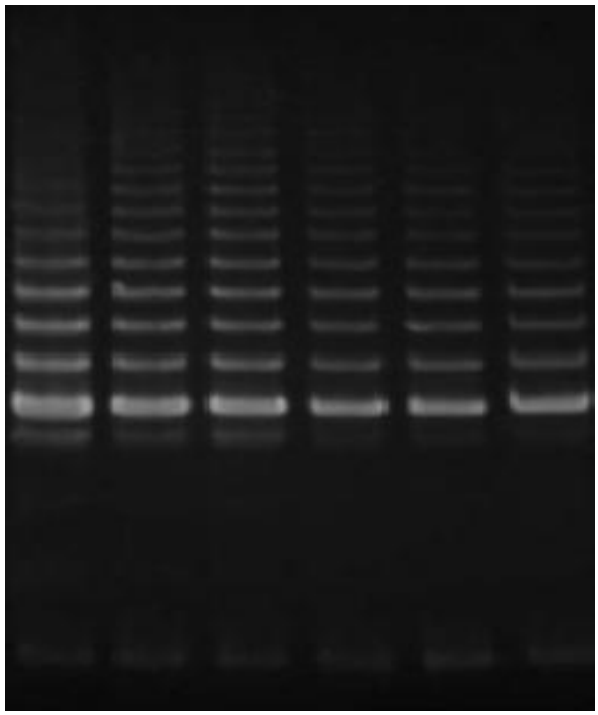

Figure 4-6. Telomerase activity by TRAP assay.

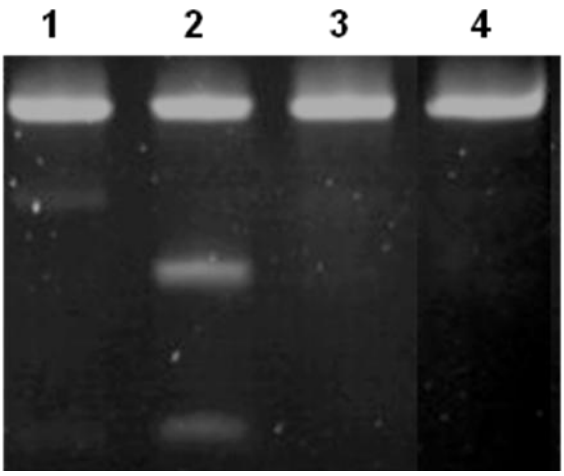

Figure 4-7. *In vitro* cleavage of the 19-mer in machine synthesized RNA.1: Control without substrate. 2: LTM1023 with RS19. 3: LTM0000 with RS19. 4: LTM1111 with RS19. All the sequences were annealed at 95 °C for 5 minutes and subsequently cooled down to room temperature within 1 hour. The mixture was then diluted into reaction buffer with a reaction time of 30 minutes.

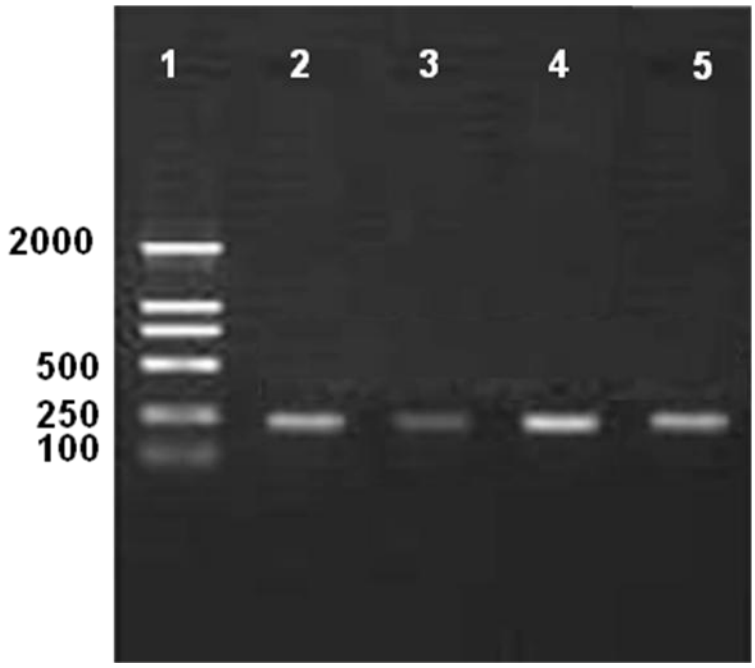

Figure 4-8. RT-PCR products of human telomerase transcriptase(hTERT) mRNA after *In vitro* cleavage with LTM1023.Lane 1:DL2000 DNA Marker; Lane 2:Control(without any oligodeoxynucleotide) Lane 3: LTM1023; Lane 4: LTM0000; Lane 5: LTM1111.

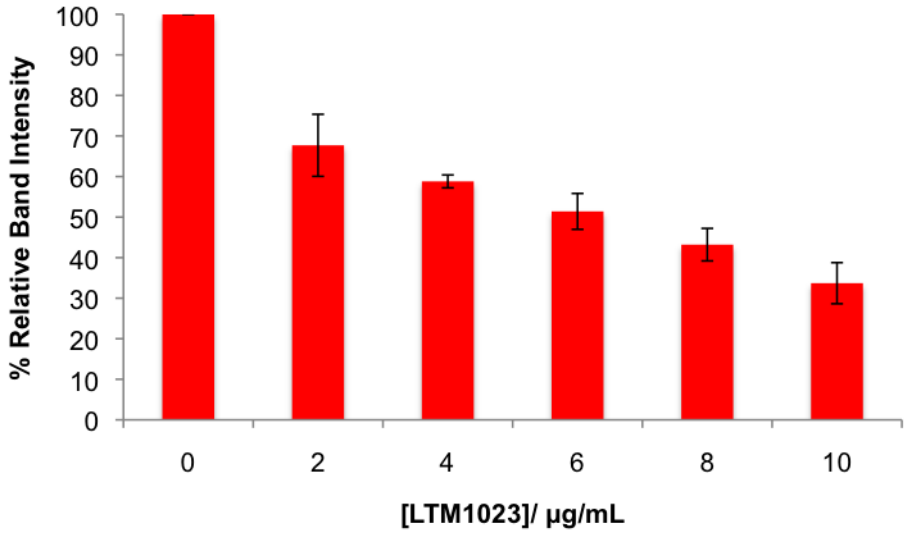

Figure 4-9 Dose dependent for cleavage of in vitro transcribed mRNA.10 µg total RNA, 10 µM LTM1023/or LTM0000/or LTM1111, 150mM KCl, 2mM MgCl2 at 37°C for 2 hours. After 2 hours, the cleavage reactions were stopped by addition of EDTA. Samples were denatured for 5 min at 65°C, and substrate RNA and cleavage products were separated on a 20% denaturing polyacrylamide gel. Error bars represent standard deviations from four independent measurements.

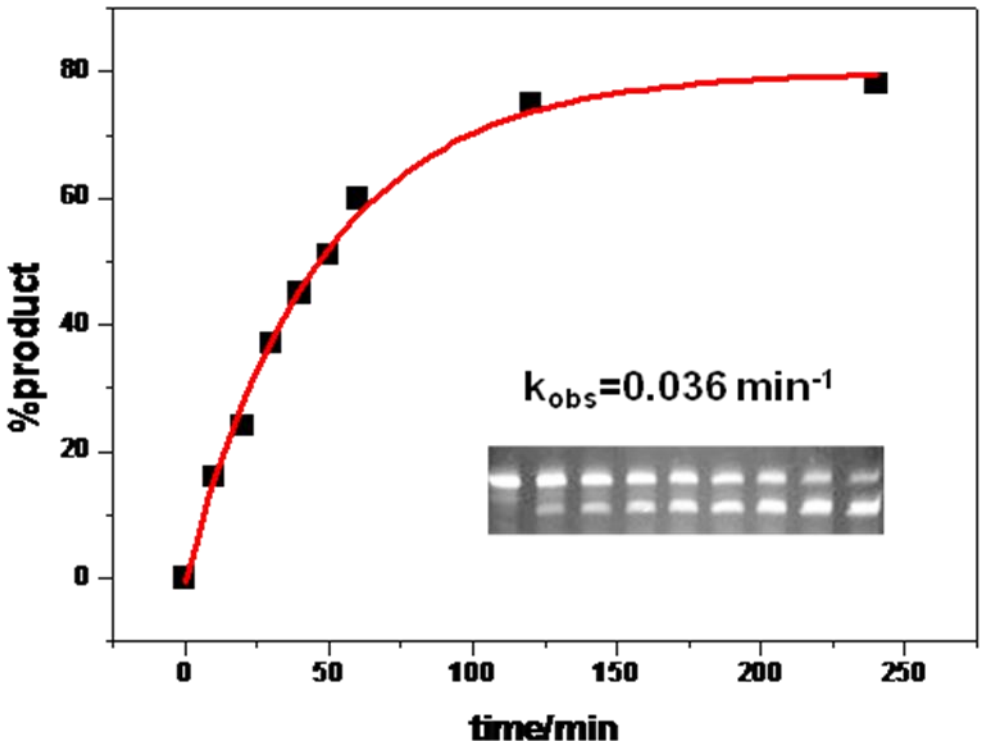

Figure 4-10. Single turnover of kinetics assay using PAGE.1 pmol of *in vitro*-transcribed RNA substrate was incubated at 37 °C with 10 pmol DNAzyme.

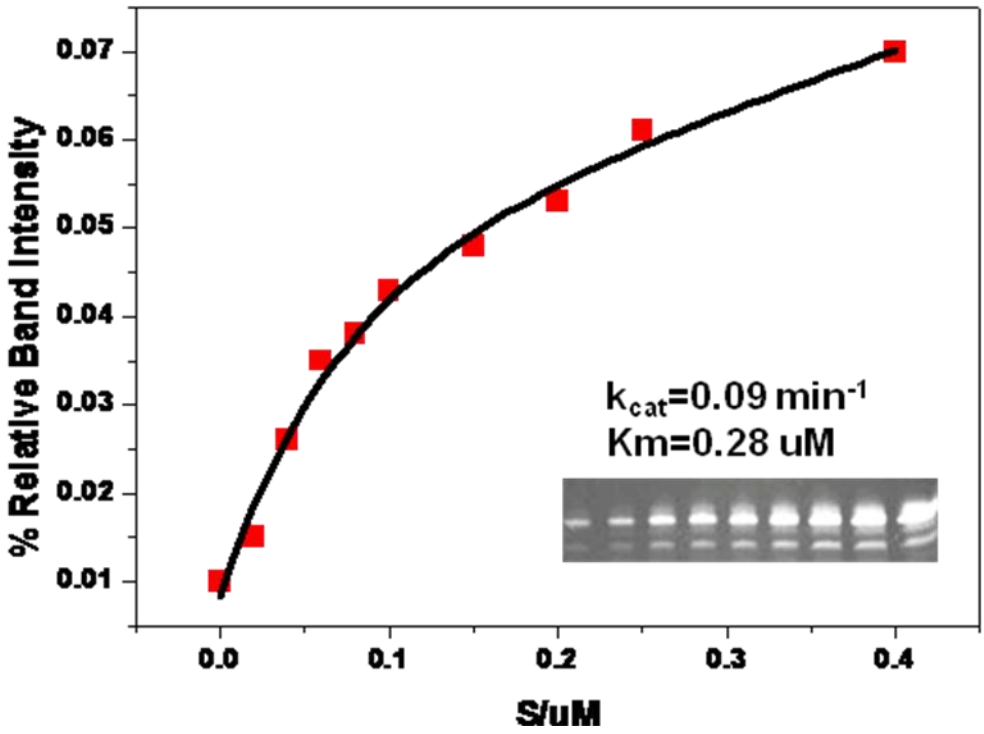

Figure 4-11. Multiple turnover kinetics analysis.Multiple turnover kinetics analysis of LTM1023 for *In vitro* RNA reaction, which was terminated at 30 min. Cleavage products were analyzed by PAGE. Inserted image shows representative PAGE used to quantify the cleavage.

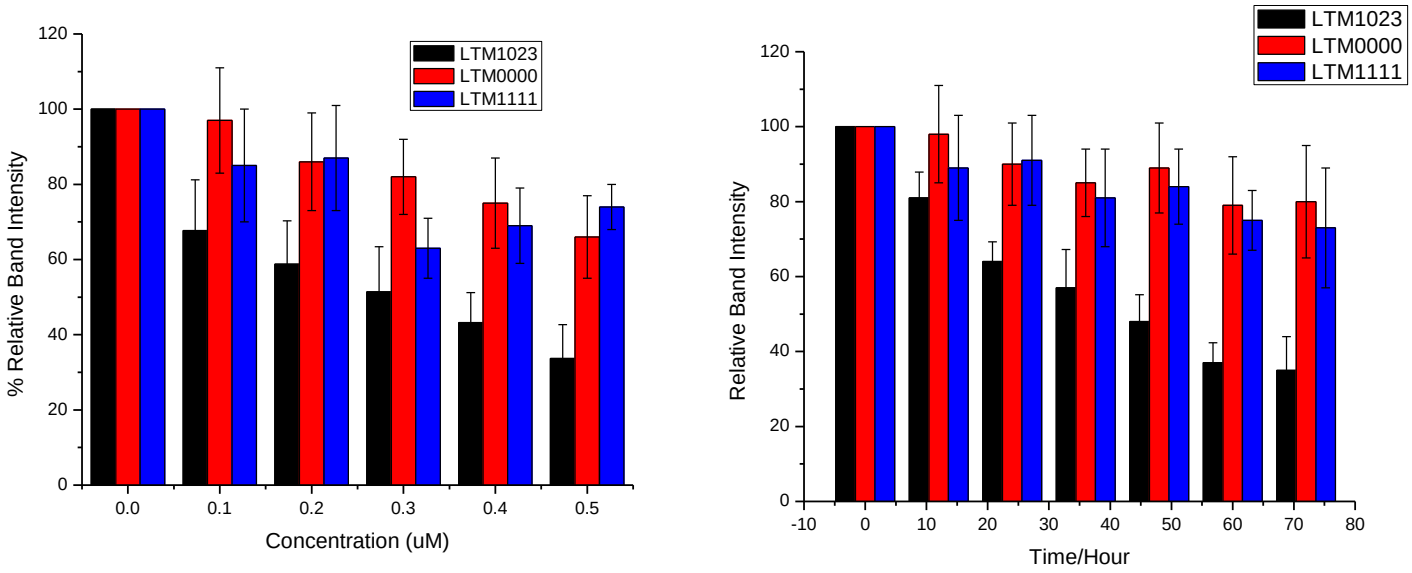

Figure 4-12. Time-dependent and dose-dependent studies *in vivo.*Hela cells were transfected by LTM1023/0000/1111 as described in text. After 2 days, the net growth of Hela cells was inhibited by more than 50% by LTM1023. The results represent the means of duplicate samples from three experiments. Error bars represent standard deviations from three independent measurements

CHAPTER 5
SUMMARY AND FUTURE DIRECTIONS

Molecular Engineering of DNAzymes for Bioanalytical and Biomedical Applications

Last decades, many different types of nucleic acid probes and architectures have been proposed and developed in recent years. Among them, DNA probes have served as a novel class of recognition elements to detect a wide variety of targets; for example, ions, small molecules, nucleic acids, proteins, and even living cells. These developments have been accelerated by advanced technologies for modifying DNA-based probes with different signaling mechanisms. The overall direction of this doctoral research has been dedicated to engineering catalytic nucleic acids with the goal of building novel molecular tools and devices for biological science, biomedical research and therapeutic applications. This work has encompassed three main avenues of research: development of molecular probes for improved detection of metal ions, engineering DNAzymes for target-driven early diagnostic, and molecular assembly DNAzymes to enhance inhibitory functions for cancer therapy.

Heavy metal contamination in the human body or environment is a significant problem, and there is a clear demand for ultrasensitive detection methods to monitor such a contamination for high throughput and rapid screening. To meet the goal, we have developed a Pb^{2+}-specific unimolecular ultrasensitive nucleic acid sensor using catalytic DNAzyme. The optimized sensor demonstrated detection limits in the nanomolar range (3nM) with superior sensitivity and excellent selectivity when used with a routine fluorospectrometer. Use of a confocal microscope and microwell array provided a clear positive report with only 2nM of Pb^{2+}, i.e., a single Pb^{2+} ion.

The second phase of this research was development of DNAzyme-based molecular tools for cancer early diagnostic. In most cancer cells, high level of telomerase were detected, which indicate that telomerase is considered as an important cancer biomarker. Currently, telomerase is mostly detected by using telomeric repeat amplification protocol (TRAP) that involves intensive PCR amplification. We designed a DNAzyme-based hairpin sensor for the enzymatic amplified analysis of telomerase activity. Treatment of the sensor with cancer cell extract in the presence of the dNTP nucleotide mixture results in the cleavage of elongation product, which was determined by complementary molecular beacon. Thus, the telomerase activity was monitored by fluorescent signal from molecular beacon opening.

Another research project involved the DNAzyme was the development of anti-cancer drug using 10-23 DNAzyme, which targeted hTERT mRNA preventing protein transcription. The process involves the assembly of lipid conjugated 10-23 DNAzyme into micelles for efficient in vivo drug delivery and enhanced localized drug density. The 10-23 DNAzyme was synthesized with modified binding arms with 2'-O-Me RNA in order to improve drug resistance in serum and binding ability to mRNA target. The time dependent experiment demonstrated that within 24 hours, the hTERT in Hela cells was dramatically inhibited. The in vitro experiment also indicated that this micelle design and base modification attributed for the unique drug performance.

In summary, this research has focused on the design, synthesis and investigation of catalytic nucleic acids for the biological sciences, biomedical research, and therapeutic and clinical applications. The successful outcome to these studies will lead

to a better understanding of biological processes and the development of advanced molecules for nucleic acid-based detections and medicines.

Future Direction: Developing High Throughput Metal-Screening Device using DNAzyme-based Logic Gate

So far, there are many DNAzymes already known, including those targeting Cu^{2+}, UO^{2+}, Pb^{2+}, and Zn^{2+}, and there is no doubt that more DNAzymes could be selected through the process introduced in Chapter 1 called in vitro selection. Thus, by smart engineering those DNAzyme, we would be able to develop a variety of sensitive sensors targeting different ions.

Logic gate has been attractive recently in biological applications, which perform a logical operation on one or more logic inputs and produces a single logic output. Logic gates operate in your bloodstream, collectively making medical decisions and taking action, ultimately serve as dissolved “doctors”—sensing molecules such as markers on cells and jointly choosing how to respond.

As we know, Cu^{2+} uptake could be significantly reduced in the presence of Zn^{2+} while Cu^{2+} absorption is increased in dietary Zn^{2+} deficiency, and, Zn^{2+} induces methallothionein(MT)-gene expression, which could be enhanced when liver Cu^{2+} concentrations exceed the value for Cu^{2+}.We constructed a model probe that can validate the existing of both ions or either of them in a complicated biological environment using Zn^{2+} and Cu^{2+} specific DNAzymes.

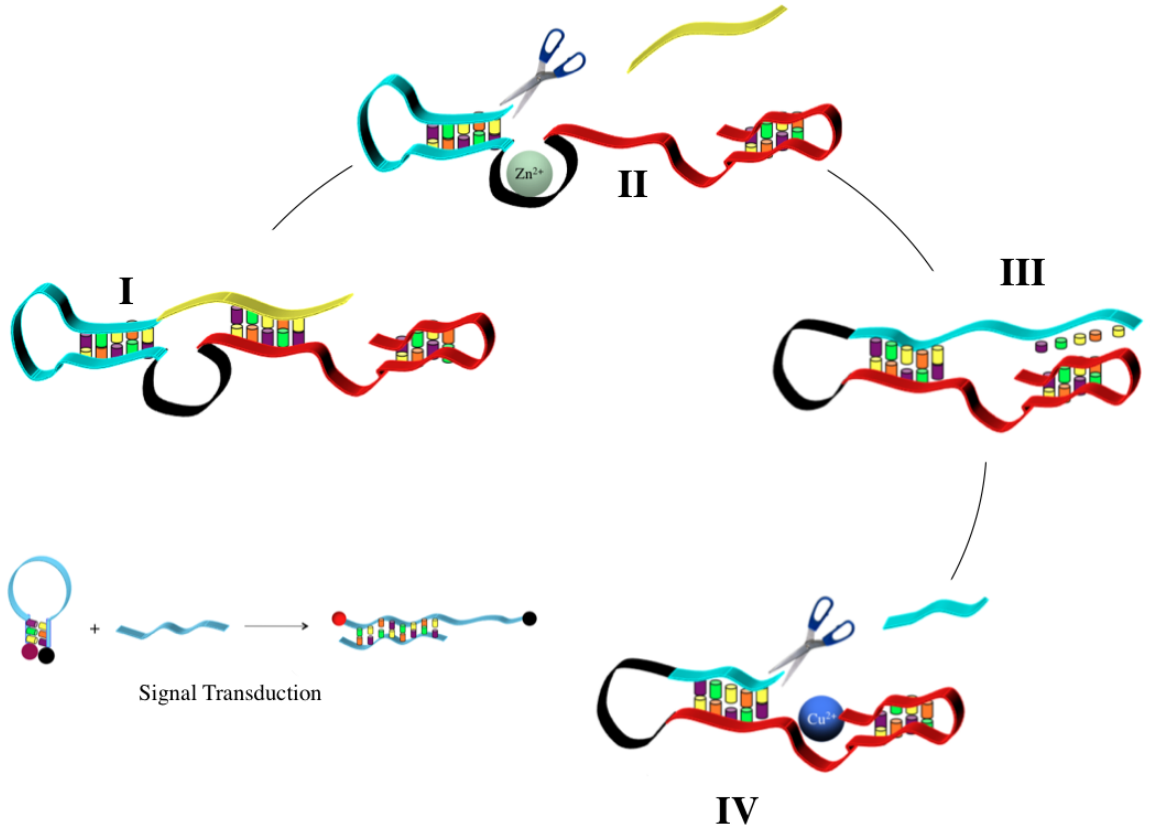

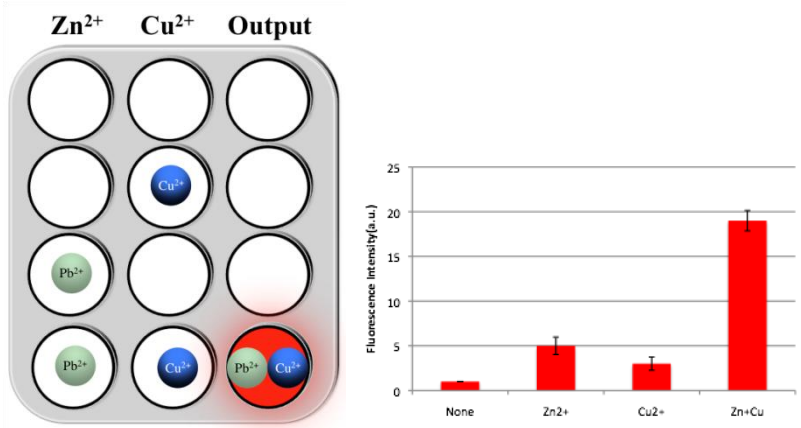

Figure 5-1. Molecular logic gates for multiple metal ions detection.(I) Design of "AND" logic gates for Cu^{2+} and Zn^{2+} using their specific DNAzymes. (II) In presence of Zn^{2+}, probe will be cut and rearranged into Cu^{2+} specific DNAzyme. (III) The existing of Cu^{2+} will cleave the substrate and detection of this leaving strand will be realized using molecular beacon.

LIST OF REFERENCES

1. Watson, J.D. & Crick, F.H. Molecular structure of nucleic acids; a structure for deoxyribose nucleic acid. *Nature* **171**, 737-738 (1953).

2. Ingle, J.D. & Crouch, S.R. Spectrochemical Analysis. (1988).

3. Lakowicz, J.R. Principles of fluorescent spectroscopy. Kluwer Academic /Plenum Publishers, New York. . (1999).

4. Tyagi, S. & Kramer, F.R. Molecular beacons: probes that fluoresce upon hybridization. *Nat Biotechnol* **14**, 303-308 (1996).

5. Tyagi, S., Bratu, D.P. & Kramer, F.R. Multicolor molecular beacons for allele discrimination. *Nat Biotechnol* **16**, 49-53 (1998).

6. Breaker, R.R. & Joyce, G.F. A DNA enzyme that cleaves RNA. *Chem Biol* **1**, 223-229 (1994).

7. Cuenoud, B. & Szostak, J.W. A DNA metalloenzyme with DNA ligase activity. *Nature* **375**, 611-614 (1995).

8. Breaker, R.R. Tech.Sight. Molecular biology. Making catalytic DNAs. *Science* **290**, 2095-2096 (2000).

9. Flynn-Charlebois, A., Prior, T.K., Hoadley, K.A. & Silverman, S.K. In vitro evolution of an RNA-cleaving DNA enzyme into an RNA ligase switches the selectivity from 3'-5' to 2'-5'. *J Am Chem Soc* **125**, 5346-5350 (2003).

10. Li, Y. & Breaker, R.R. Phosphorylating DNA with DNA. *Proc Natl Acad Sci U S A* **96**, 2746-2751 (1999).

11. Carmi, N., Balkhi, S.R. & Breaker, R.R. Cleaving DNA with DNA. *Proc Natl Acad Sci U S A* **95**, 2233-2237 (1998).

12. Santoro, S.W. & Joyce, G.F. A general purpose RNA-cleaving DNA enzyme. *Proc Natl Acad Sci U S A* **94**, 4262-4266 (1997).

13. Li, Y. & Sen, D. A catalytic DNA for porphyrin metallation. *Nat Struct Biol* **3**, 743-747 (1996).

14. Sheppard, T.L., Ordoukhanian, P. & Joyce, G.F. A DNA enzyme with N-glycosylase activity. *Proc Natl Acad Sci U S A* **97**, 7802-7807 (2000).

15. Silverman, S.K. In vitro selection, characterization, and application of deoxyribozymes that cleave RNA. *Nucleic Acids Res* **33**, 6151-6163 (2005).

16. Silverman, S.K. & Baum, D.A. Use of deoxyribozymes in RNA research. *Methods Enzymol* **469**, 95-117 (2009).

17. Turner, A.P., Chen, B. & Piletsky, S.A. In vitro diagnostics in diabetes: meeting the challenge. *Clin Chem* **45**, 1596-1601 (1999).

18. Kruger, K. et al. Self-splicing RNA: autoexcision and autocyclization of the ribosomal RNA intervening sequence of Tetrahymena. *Cell* **31**, 147-157 (1982).

19. Doherty, E.A. & Doudna, J.A. Ribozyme structures and mechanisms. *Annu Rev Biochem* **69**, 597-615 (2000).

20. Joyce, G.F. Directed evolution of nucleic acid enzymes. *Annu Rev Biochem* **73**, 791-836 (2004).

21. Breaker, R.R. DNA enzymes. *Nat Biotechnol* **15**, 427-431 (1997).

22. Lu, Y. New transition-metal-dependent DNAzymes as efficient endonucleases and as selective metal biosensors. *Chemistry* **8**, 4589-4596 (2002).

23. Faulhammer, D. & Famulok, M. The Ca2+ ion as a cofactor for a novel RNA-cleaving deoxyribozyme. *Angew. Chem., Int. Ed. Engl.* **35**, 2837-2841 (1997).

24. Li, J., Zheng, W., Kwon, A.H. & Lu, Y. In vitro selection and characterization of a highly efficient Zn(II)-dependent RNA-cleaving deoxyribozyme. *Nucleic Acids Res* **28**, 481-488 (2000).

25. Cruz, R.P., Withers, J.B. & Li, Y. Dinucleotide junction cleavage versatility of 8-17 deoxyribozyme. *Chem Biol* **11**, 57-67 (2004).

26. Santoro, S.W., Joyce, G.F., Sakthivel, K., Gramatikova, S. & Barbas, C.F., 3rd RNA cleavage by a DNA enzyme with extended chemical functionality. *J Am Chem Soc* **122**, 2433-2439 (2000).

27. Carmi, N., Shultz, L.A. & Breaker, R.R. In vitro selection of self-cleaving DNAs. *Chem Biol* **3**, 1039-1046 (1996).

28. Carmi, N. & Breaker, R.R. Characterization of a DNA-cleaving deoxyribozyme. *Bioorg Med Chem* **9**, 2589-2600 (2001).

29. Sen, D. & Geyer, C.R. DNA enzymes. *Curr Opin Chem Biol* **2**, 680-687 (1998).

30. Molek, P., Strukelj, B. & Bratkovic, T. Peptide phage display as a tool for drug discovery: targeting membrane receptors. *Molecules* **16**, 857-887.

31. Zuker, M. Mfold web server for nucleic acid folding and hybridization prediction. *Nucleic Acids Res* **31**, 3406-3415 (2003).

32. Stojanovic, M.N. & Stefanovic, D. A deoxyribozyme-based molecular automaton. *Nat Biotechnol* **21**, 1069-1074 (2003).

33. Stojanovic, M.N. & Stefanovic, D. Deoxyribozyme-based half-adder. *J Am Chem Soc* **125**, 6673-6676 (2003).

34. Chen, Y. & Mao, C. Reprogramming DNA-directed reactions on the basis of a DNA conformational change. *J Am Chem Soc* **126**, 13240-13241 (2004).

35. Chen, Y., Wang, M. & Mao, C. An autonomous DNA nanomotor powered by a DNA enzyme. *Angew Chem Int Ed Engl* **43**, 3554-3557 (2004).

36. Faulhammer, D. & Famulok, M. Characterization and divalent metal-ion dependence of in vitro selected deoxyribozymes which cleave DNA/RNA chimeric oligonucleotides. *J Mol Biol* **269**, 188-202 (1997).

37. Mei, S.H., Liu, Z., Brennan, J.D. & Li, Y. An efficient RNA-cleaving DNA enzyme that synchronizes catalysis with fluorescence signaling. *J Am Chem Soc* **125**, 412-420 (2003).

38. Liu, Z., Mei, S.H., Brennan, J.D. & Li, Y. Assemblage of signaling DNA enzymes with intriguing metal-ion specificities and pH dependences. *J Am Chem Soc* **125**, 7539-7545 (2003).

39. Roth, A. & Breaker, R.R. An amino acid as a cofactor for a catalytic polynucleotide. *Proc Natl Acad Sci U S A* **95**, 6027-6031 (1998).

40. Wang, Y. & Silverman, S.K. Characterization of deoxyribozymes that synthesize branched RNA. *Biochemistry* **42**, 15252-15263 (2003).

41. Hoadley, K.A., Purtha, W.E., Wolf, A.C., Flynn-Charlebois, A. & Silverman, S.K. Zn2+-dependent deoxyribozymes that form natural and unnatural RNA linkages. *Biochemistry* **44**, 9217-9231 (2005).

42. Sreedhara, A., Li, Y. & Breaker, R.R. Ligating DNA with DNA. *J Am Chem Soc* **126**, 3454-3460 (2004).

43. Chinnapen, D.J. & Sen, D. A deoxyribozyme that harnesses light to repair thymine dimers in DNA. *Proc Natl Acad Sci U S A* **101**, 65-69 (2004).

44. Li, Y., Liu, Y. & Breaker, R.R. Capping DNA with DNA. *Biochemistry* **39**, 3106-3114 (2000).

45. Burmeister, J., von Kiedrowski, G. & Ellington, A.D. Cofactor-Assisted Self-cleavage in DNA Libraries with a 3'-5'-Phosphoramidate Bond. *Angew Chem Int Ed Engl* **36**, 1321-1324 (1997).

46. Yang JM, L.K. Trace elements, vitamins, and nutrition. In: McClatchey KD, Ed. Clinical Laboratory Medicine. 2nd ed. Philadelphia, Pa.: Lippincott Williams and Wilkins; 2002:456–460. (2002).

47. (CEC), C.f.E.C. *Taking Stock 2002 North American Pollutant Releases and Transfers* (2005).

48. Needleman, H.L. *Human Lead Exposure* (1992).

49. (ATSDR), A.f.T.S.a.D.R. *Toxicological Profile for Lead* (1999).

50. Godwin, H.A. The biological chemistry of lead. *Curr Opin Chem Biol* **5**, 223-227 (2001).

51. Magyar, J.S. et al. Reexamination of lead(II) coordination preferences in sulfur-rich sites: implications for a critical mechanism of lead poisoning. *J Am Chem Soc* **127**, 9495-9505 (2005).

52. Lanphear, B.P. et al. Low-level environmental lead exposure and children's intellectual function: an international pooled analysis. *Environ Health Perspect* **113**, 894-899 (2005).

53. Bannon, D.I., Murashchik, C., Zapf, C.R., Farfel, M.R. & Chisolm, J.J., Jr. Graphite furnace atomic absorption spectroscopic measurement of blood lead in matrix-matched standards. *Clin Chem* **40**, 1730-1734 (1994).

54. Parsons, P.J. & Slavin, W. A Rapid Zeeman Graphite-Furnace Atomic-Absorption Spectrometric Method for the Determination of Lead in Blood. *Spectrochimica Acta Part B-Atomic Spectroscopy* **48**, 925-939 (1993).

55. Aggarwal, S.K., Kinter, M. & Herold, D.A. Determination of lead in urine and whole blood by stable isotope dilution gas chromatography-mass spectrometry. *Clin Chem* **40**, 1494-1502 (1994).

56. Bowins, R.J. & Mcnutt, R.H. Electrothermal Isotope-Dilution Inductively-Coupled Plasma-Mass Spectrometry Method for the Determination of Sub-Ng Ml(-1) Levels of Lead in Human Plasma. *Journal of Analytical Atomic Spectrometry* **9**, 1233-1236 (1994).

57. Feldman, B.J., Osterloh, J.D., Hata, B.H. & D'Alessandro, A. Determination of lead in blood by square wave anodic stripping voltammetry at a carbon disk ultramicroelectrode. *Anal Chem* **66**, 1983-1987 (1994).

58. Wang, J. *Stripping Analysis: Principle, Instrumentation and Application, VCH, Deerfield Beach* (1985).

59. Kim, S.K., Lee, S.H., Lee, J.Y., Bartsch, R.A. & Kim, J.S. An excimer-based, binuclear, on-off switchable calix[4]crown chemosensor. *J Am Chem Soc* **126**, 16499-16506 (2004).

60. Chen, C.T. & Huang, W.P. A highly selective fluorescent chemosensor for lead ions. *J Am Chem Soc* **124**, 6246-6247 (2002).

61. Metivier, R., Leray, I. & Valeur, B. A highly sensitive and selective fluorescent molecular sensor for Pb(II) based on a calix[4]arene bearing four dansyl groups. *Chem Commun (Camb)*, 996-997 (2003).

62. Addleman, R.S., Bennett, J., Tweedy, S.H., Elshani, S. & Wai, C.M. Response of a benzoxainone derivative linked to monoaza-15-crown-5 with divalent heavy metals. *Talanta* **46**, 573-581 (1998).

63. Hayashita, T. et al. Highly selective recognition of lead ion in water by a podand fluoroionophore/gamma-cyclodextrin complex sensor. *Chem Commun (Camb)*, 2160-2161 (2003).

64. Deo, S. & Godwin, H.A. A selective, ratiometric fluorescent sensor for Pb2+. *Journal of the American Chemical Society* **122**, 174-175 (2000).

65. Chen, P. et al. An exceptionally selective lead(II)-regulatory protein from Ralstonia metallidurans: Development of a fluorescent lead(II) probe. *Angewandte Chemie-International Edition* **44**, 2715-2719 (2005).

66. Blake, D.A. et al. Antibody-based sensors for heavy metal ions. *Biosensors & Bioelectronics* **16**, 799-809 (2001).

67. Khosraviani, M., Pavlov, A.R., Blake, R.C., Yu, H. & Blake, D.A. An ELISA immunoassay to measure lead-chelate complexes. *Faseb Journal* **12**, A464-A464 (1998).

68. Kim, Y.J., Johnson, R.C. & Hupp, J.T. Gold nanoparticle-based sensing of "spectroscopically silent" heavy metal ions. *Nano Letters* **1**, 165-167 (2001).

69. Li, J. & Lu, Y. A highly sensitive and selective catalytic DNA biosensor for lead ions. *Journal of the American Chemical Society* **122**, 10466-10467 (2000).

70. Kavallieratos, K., Rosenberg, J.M., Chen, W.Z. & Ren, T. Fluorescent sensing and selective Pb(II) extraction by a dansylamide ion-exchanger. *J Am Chem Soc* **127**, 6514-6515 (2005).

71. Chae, M.Y., Yoon, J. & Czarnik, A.W. Chelation-enhanced fluorescence chemosensing of Pb(II), an inherently quenching metal ion. *J Mol Recognit* **9**, 297-303 (1996).

72. Payne, J.C., ter Horst, M.A. & Godwin, H.A. Lead fingers: Pb2+ binding to structural zinc-binding domains determined directly by monitoring lead-thiolate charge-transfer bands. *Journal of the American Chemical Society* **121**, 6850-6855 (1999).

73. Chen, P. & He, C. A general strategy to convert the MerR family proteins into highly sensitive and selective fluorescent biosensors for metal ions. *J Am Chem Soc* **126**, 728-729 (2004).

74. Liu, J. & Lu, Y. Improving fluorescent DNAzyme biosensors by combining inter- and intramolecular quenchers. *Anal Chem* **75**, 6666-6672 (2003).

75. Brown, A.K., Li, J., Pavot, C.M. & Lu, Y. A lead-dependent DNAzyme with a two-step mechanism. *Biochemistry* **42**, 7152-7161 (2003).

76. Zivarts, M., Liu, Y. & Breaker, R.R. Engineered allosteric ribozymes that respond to specific divalent metal ions. *Nucleic Acids Res* **33**, 622-631 (2005).

77. Hartig, J.S., Gruene, I., Najafi-Shoushtari, S.H. & Famulok, M. Sequence-Specific Detection of MicroRNAs by Signal-Amplifying Ribozymes. *J. Am. Chem. Soc.* **126**, 722-723 (2004).

78. Pavlov, V., Shlyahovsky, B. & Willner, I. Fluorescence Detection of DNA by the Catalytic Activation of an Aptamer/Thrombin Complex. *J. Am. Chem. Soc.* **127**, 6522-6523 (2005).

79. Hartig, J.S. et al. Protein-dependent ribozymes report molecular interactions in real time. *Nat. Biotechnol.* **20**, 717-722 (2002).

80. Sokol, D.L., Zhang, X., Lu, P. & Gewirtz, A.M. Real time detection of DNA.RNA hybridization in living cells. *Proc Natl Acad Sci U S A* **95**, 11538-11543 (1998).

81. Abdelgany, A., Wood, M. & Beeson, D. Hairpin DNAzymes: a new tool for efficient cellular gene silencing. *J. Gene Med.* **9**, 727-738 (2007).

82. Liu, J. et al. A catalytic beacon sensor for uranium with parts-pertrillion sensitivity and millionfold selectivity. *Proc. Natl. Acad. Sci. U. S. A.* **104**, 2056-2061 (2007).

83. Lim, M.H. & Lippard, S.J. Metal-Based Turn-On Fluorescent Probes for Sensing Nitric Oxide. *Acc. Chem. Res.* **40**, 41-51 (2007).

84. Todd, A.V., Fuery, C.J., Impey, H.L., Applegate, T.L. & Haughton, M.A. DzyNA-PCR: use of DNAzymes to detect and quantify nucleic acid sequences in a real-time fluorescent format. *Clin. Chem. (Washington, D. C.)* **46**, 625-630 (2000).

85. Lu, Y. New transition-metal-dependent DNAzymes as efficient endonucleases and as selective metal biosensors. *Chem.--Eur. J.* **8**, 4588-4596 (2002).

86. Agency for Toxic Substances and Disease Registry, Toxicological Profile for Lead (Draft), Atlanta, U.S. Department of Health and Human Services, Public Health Service. (1992).

87. Levin, R. et al. Lead exposures in U.S. children, 2008: Implications for prevention. *Environ. Health Perspect.* **116**, 1285-1293 (2008).

88. Lancer, F. Environ. Health Perspect. **116** (2008).

89. Morbidity Mortality Weekly Report; Centers for Disease Control and Prevention: Atlanta, GA. **58**, 55-58 (2009).

90. Corrin, D. Identifying Lead in Your Home; Minnesota Extension Service, University of Minnesota. (1994).

91. Needleman, H. Lead poisoning. *Annu. Rev. Med.* **55**, 209-222 (2004).

92. Preventing Lead Poisoning in Young Children; Centers for Disease Control and Prevention: Atlanta, G. **34**, 66-68 (1985).

93. Nigg, J.T. et al. Low blood lead levels associated with clinically diagnosed attention-deficit/hyperactivity disorder and mediated by weak cognitive control. *Biol. Psychiatry* **63**, 325-331 (2008).

94. Riess, M.L. & Halm, J.K. Lead poisoning in an adult: lead mobilization by pregnancy? *J Gen Intern Med* **22**, 1212-1215 (2007).

95. National Primary Drinking Water Standards; U.S. Environmental Protection Agency: Washington, DC, . *EPA 816-F-01-001* (2003).

96. Beaucage, S.L. & Iyer, R.P. The synthesis of modified oligonucleotides by the phosphoramidite approach and their applications. *Tetrahedron* **49**, 6123-6194 (1993).

97. Beaucage, S.L. & Iyer, R.P. Advances in the synthesis of oligonucleotides by the phosphoramidite approach. *Tetrahedron* **48**, 2223-2311 (1992).

98. Tan, W. & Yeung, E.S. Monitoring the Reactions of Single Enzyme Molecules and Single Metal Ions. *Anal. Chem.* **69**, 4242-4248 (1997).

99. Scott, W.G. RNA structure, metal ions, and catalysis. *Curr Opin Chem Biol* **3**, 705-709 (1999).

100. Wolfrum, C. & Josten, A. Oligonucleotides as coding molecules in an anti-counterfeiting system. *Nucleosides, Nucleotides Nucleic Acids* **24**, 1069-1074 (2005).

101. Mao, X.L., Wu, J. & Ying, Y.B. [Applications of atomic emission spectrum from liquid electrode discharge to metal ion detection]. *Guang Pu Xue Yu Guang Pu Fen Xi* **30**, 537-542.

102. Kim, N.W. et al. Specific association of human telomerase activity with immortal cells and cancer. *Science* **266**, 2011-2015 (1994).

103. Argyle, D.J. & Nasir, L. Telomerase: a potential diagnostic and therapeutic tool in canine oncology. *Vet Pathol* **40**, 1-7 (2003).

104. Hiyama, K. et al. Alterations in telomeric repeat length in lung cancer are associated with loss of heterozygosity in p53 and Rb. *Oncogene* **10**, 937-944 (1995).

105. Kannan, S. et al. Telomerase activity in premalignant and malignant lesions of human oral mucosa. *Cancer Epidemiol Biomarkers Prev* **6**, 413-420 (1997).

106. Sommerfeld, H.J. et al. Telomerase activity: a prevalent marker of malignant human prostate tissue. *Cancer Res* **56**, 218-222 (1996).

107. Hiyama, E. et al. Telomerase activity in human breast tumors. *J Natl Cancer Inst* **88**, 116-122 (1996).

108. Tahara, H. et al. Telomerase activity in human liver tissues: comparison between chronic liver disease and hepatocellular carcinomas. *Cancer Res* **55**, 2734-2736 (1995).

109. Hiyama, E. et al. Correlating telomerase activity levels with human neuroblastoma outcomes. *Nat Med* **1**, 249-255 (1995).

110. Tahara, H. et al. Telomerase activity in preneoplastic and neoplastic gastric and colorectal lesions. *Clin Cancer Res* **1**, 1245-1251 (1995).

111. Kyo, S., Kunimi, K., Uchibayashi, T., Namiki, M. & Inoue, M. Telomerase activity in human urothelial tumors. *Am J Clin Pathol* **107**, 555-560 (1997).

112. Lin, Y. et al. Telomerase activity in human bladder cancer. *Clin Cancer Res* **2**, 929-932 (1996).

113. Kinoshita, H. et al. Detection of telomerase activity in exfoliated cells in urine from patients with bladder cancer. *J Natl Cancer Inst* **89**, 724-730 (1997).

114. Zendehrokh, N. & Dejmek, A. Telomere repeat amplification protocol (TRAP) in situ reveals telomerase activity in three cell types in effusions: malignant cells, proliferative mesothelial cells, and lymphocytes. *Mod Pathol* **18**, 189-196 (2005).

115. Hirose, M., Abe-Hashimoto, J., Tahara, H., Ide, T. & Yoshimura, T. New method to measure telomerase activity by transcription-mediated amplification and hybridization protection assay. *Clin Chem* **44**, 2446-2452 (1998).

116. Feng, J. et al. The RNA component of human telomerase. *Science* **269**, 1236-1241 (1995).

117. Nakamura, T.M. et al. Telomerase catalytic subunit homologs from fission yeast and human. *Science* **277**, 955-959 (1997).

118. Fletcher, T.M., Trevino, A. & Woynarowski, J.M. Enzymatic activity of endogenous telomerase associated with intact nuclei from human leukemia CEM cells. *Biochem Biophys Res Commun* **265**, 51-56 (1999).

119. Savoysky E, A.K., Tsuchiya M, Yamazaki T. *Nucleic Acids Res.* **24**, 1175-1176 (1996).

120. Herbert BS, H.A., Wright WE, Shay JW. *Nature Protoc.* **1**, 1583-1590 (2006).

121. Niemeyer, C.M., Adler, M., and Wacker, R. *Trends Biotechnol.* **23**, 208-216 (2005).

122. Weizmann, Y., Patolsky, F., Lioubashevski, O., and Willner, I. *J. Am. Chem. Soc.* **126**, 1073-1080 (2004).

123. Zheng, G., Patolsky, F., Cui, Y., Wang, W. U., and Lieber, C. M. *Nat Biotechnol* **23**, 1294-1301 (2005).

124. Schmidt, P.M., Lehmann, C., Matthes, E., and Bier, F. F. *Biosens. Bioelectron.* **17**, 1081-1087 (2002).

125. Kim NW, P.M., Prowse KR, Harley CB, West MD, Ho PLC, Coviello GM, Wright WE, Weinrich SL, Shay JW *Science* **266**, 2011-2014 (1994).

126. Kim, N.W. et al. Response. *Science* **268**, 1116-1117 (1995).

127. Morin, G.B. The human telomere terminal transferase enzyme is a ribonucleoprotein that synthesizes TTAGGG repeats. *Cell* **59**, 521-529 (1989).

128. Patolsky, F. et al. Lighting-up the dynamics of telomerization and DNA replication by CdSe-ZnS quantum dots. *J Am Chem Soc* **125**, 13918-13919 (2003).

129. C. Wolfrum, A.J. *Nucleosides, Nucleotides, and Nucleic Acids* **24**, 1069-1074 (2005).

130. Zhao, G. & Guan, Y. Polymerization behavior of Klenow fragment and Taq DNA polymerase in short primer extension reactions. *Acta Biochim Biophys Sin (Shanghai)* **42**, 722-728.

131. Tae-Jin Yim, J.L., Yi Lu, Ravi S. Kane, Jonathan S. Dordick *J. Am. Chem. Soc.* **127**, 12200-12201 (2005).

132. Chang, J.T., Chen, Y.L., Yang, H.T., Chen, C.Y. & Cheng, A.J. Differential regulation of telomerase activity by six telomerase subunits. *Eur J Biochem* **269**, 3442-3450 (2002).

133. Yokoyama, Y. et al. The 5'-end of hTERT mRNA is a good target for hammerhead ribozyme to suppress telomerase activity. *Biochem Biophys Res Commun* **273**, 316-321 (2000).

134. Armanios, M. et al. Haploinsufficiency of telomerase reverse transcriptase leads to anticipation in autosomal dominant dyskeratosis congenita. *Proc Natl Acad Sci U S A* **102**, 15960-15964 (2005).

135. Mergny, J.L., Riou, J.F., Mailliet, P., Teulade-Fichou, M.P. & Gilson, E. Natural and pharmacological regulation of telomerase. *Nucleic Acids Res* **30**, 839-865 (2002).

136. Hartgerink, J.D., Beniash, E. & Stupp, S.I. Self-assembly and mineralization of peptide-amphiphile nanofibers. *Science* **294**, 1684-1688 (2001).

137. Hartgerink, J.D., Beniash, E. & Stupp, S.I. Peptide-amphiphile nanofibers: a versatile scaffold for the preparation of self-assembling materials. *Proc Natl Acad Sci U S A* **99**, 5133-5138 (2002).

138. Lim, Y.B., Lee, E. & Lee, M. Controlled bioactive nanostructures from self-assembly of peptide building blocks. *Angew Chem Int Ed Engl* **46**, 9011-9014 (2007).

139. Jeong, J.H. & Park, T.G. Novel polymer-DNA hybrid polymeric micelles composed of hydrophobic poly(D,L-lactic-co-glycolic acid) and hydrophilic oligonucleotides. *Bioconjug Chem* **12**, 917-923 (2001).

140. Gosse, C. et al. Micelles of Lipid-Oligonucleotide Conjugates: Implications for Membrane Anchoring and Base Pairing. *J Phys Chem B* **108**, 6485-6497 (2004).

141. Alemdaroglu, F.E., Safak, M., Wang, J., Berger, R. & Herrmann, A. DNA multiblock copolymers. *Chem Commun (Camb)*, 1358-1359 (2007).

142. Chan, Y.H. & Boxer, S.G. Model membrane systems and their applications. *Curr Opin Chem Biol* **11**, 581-587 (2007).

143. Discher, D.E. & Eisenberg, A. Polymer vesicles. *Science* **297**, 967-973 (2002).

144. Torchilin, V.P., Lukyanov, A.N., Gao, Z. & Papahadjopoulos-Sternberg, B. Immunomicelles: targeted pharmaceutical carriers for poorly soluble drugs. *Proc Natl Acad Sci U S A* **100**, 6039-6044 (2003).

145. Liu, H. et al. DNA-based micelles: synthesis, micellar properties and size-dependent cell permeability. *Chemistry* **16**, 3791-3797.

146. Zaborowska, Z., Furste, J.P., Erdmann, V.A. & Kurreck, J. Sequence requirements in the catalytic core of the "10-23" DNA enzyme. *J Biol Chem* **277**, 40617-40622 (2002).

147. Cairns, M.J., Hopkins, T.M., Witherington, C., Wang, L. & Sun, L.Q. Target site selection for an RNA-cleaving catalytic DNA. *Nat Biotechnol* **17**, 480-486 (1999).

148. Wu, Y. et al. Inhibition of bcr-abl oncogene expression by novel deoxyribozymes (DNAzymes). *Hum Gene Ther* **10**, 2847-2857 (1999).

149. Dass, C.R., Saravolac, E.G., Li, Y. & Sun, L.Q. Cellular uptake, distribution, and stability of 10-23 deoxyribozymes. *Antisense Nucleic Acid Drug Dev* **12**, 289-299 (2002).

150. Cieslak, M. et al. DNAzymes to beta 1 and beta 3 mRNA down-regulate expression of the targeted integrins and inhibit endothelial cell capillary tube formation in fibrin and matrigel. *J Biol Chem* **277**, 6779-6787 (2002).

151. Beale, G. et al. Gene silencing nucleic acids designed by scanning arrays: anti-EGFR activity of siRNA, ribozyme and DNA enzymes targeting a single hybridization-accessible region using the same delivery system. *J Drug Target* **11**, 449-456 (2003).

152. Ambegia, E. et al. Stabilized plasmid-lipid particles containing PEG-diacylglycerols exhibit extended circulation lifetimes and tumor selective gene expression. *Biochim Biophys Acta* **1669**, 155-163 (2005).

153. Agrawal, S. et al. Mixed-backbone oligonucleotides as second generation antisense oligonucleotides: in vitro and in vivo studies. *Proc Natl Acad Sci U S A* **94**, 2620-2625 (1997).

154. Pitts, A.E. & Corey, D.R. Inhibition of human telomerase by 2'-O-methyl-RNA. *Proc Natl Acad Sci U S A* **95**, 11549-11554 (1998).

155. Herbert, B. et al. Inhibition of human telomerase in immortal human cells leads to progressive telomere shortening and cell death. *Proc Natl Acad Sci U S A* **96**, 14276-14281 (1999).

156. Hanahan, D. & Weinberg, R.A. The hallmarks of cancer. *Cell* **100**, 57-70 (2000).

157. Sharma, S. et al. Preclinical and clinical strategies for development of telomerase and telomere inhibitors. *Ann Oncol* **8**, 1063-1074 (1997).

158. Cong, Y.S., Wright, W.E. & Shay, J.W. Human telomerase and its regulation. *Microbiol Mol Biol Rev* **66**, 407-425, table of contents (2002).

BIOGRAPHICAL SKETCH

Hui Wang was born in Huainan, China in November of 1980. After graduating from Fengtai High School, she attended University of Science and Technology of China to pursue a degree in chemical physics. Following the strong interests in chemistry she relocated Gainesville, FL in the United States to attend the University of Florida in 2006. While at the University of Florida, she joined the research group of Dr. Weihong Tan for her Ph.D. work in the area of catalytic nucleic acid for analytical and therapeutic applications. She received her Doctor of Philosophy degree in Chemistry from the University of Florida in August of 2011.